

University of Nebraska - Lincoln

DigitalCommons@University of Nebraska - Lincoln

Industrial and Management Systems
Engineering -- Dissertations and Student
Research

Industrial and Management Systems
Engineering

6-2012

DEVELOPMENT AND VALIDATION OF A MODEL FOR GRANULAR MATERIAL VOLUME MEASUREMENTS

Pourya Fasounaki

University of Nebraska-Lincoln, Pourya1999@gmail.com

Follow this and additional works at: <https://digitalcommons.unl.edu/imsediss>



Part of the Industrial Engineering Commons, Mechanical Engineering Commons, Mechanics of Materials Commons, Mining Engineering Commons, Operational Research Commons, and the Other Operations Research, Systems Engineering and Industrial Engineering Commons

Fasounaki, Pourya, "DEVELOPMENT AND VALIDATION OF A MODEL FOR GRANULAR MATERIAL VOLUME MEASUREMENTS" (2012). *Industrial and Management Systems Engineering -- Dissertations and Student Research*. 28.

<https://digitalcommons.unl.edu/imsediss/28>

This Article is brought to you for free and open access by the Industrial and Management Systems Engineering at DigitalCommons@University of Nebraska - Lincoln. It has been accepted for inclusion in Industrial and Management Systems Engineering -- Dissertations and Student Research by an authorized administrator of DigitalCommons@University of Nebraska - Lincoln.

DEVELOPMENT AND VALIDATION OF A MODEL FOR GRANULAR
MATERIAL VOLUME MEASUREMENTS

by

Pourya Fasounaki

A THESIS

Presented to the Faculty of

The Graduate College at the University of Nebraska

In Partial Fulfillment of Requirements

For the Degree of Master of Science

Major: Industrial and Management System Engineering

Under the supervision of Professor Ram Bishu

Lincoln, Nebraska

May, 2012

DEVELOPMENT AND VALIDATION OF A MODEL FOR GRANULAR MATERIAL VOLUME MEASUREMENTS

Pourya Fasounaki, M.S.

University of Nebraska, 2012

Advisor: **Ram R. Bishu**

Commercial storage bins are a quintessential part of a grain supply chain. Having the advantage of taking up space in vertical rather than horizontal fields, cylindrical bins are very useful for grain production companies; As a result, various types of bins and silos are being constructed more often than ever, especially, as the expenses of acquiring and/or managing vast operation fields are skyrocketing while, even finding suitable fields for lease or purchase is a challenge for this matter.

Keeping inventory record of packed grains in silos poses challenges since the bulk material's different segments do not discharge uniformly, leading to formation of random peaks and valleys on the surface. To facilitate obtaining accurate volume measurement of the grains by taking into account this non-linear behavior on the surface, laser or plumb-bob level-sensing devices are employed at different part of the surface to probe the level of material under those regions. An acceptable estimation method commonly practiced is installing the sensors at the distance equal to $1/6$ of the diameter of bin from the side wall. However, since this method disregards other possible peak and valleys which might be present at other areas on surface in an unsystematic fashion, the accuracy of the results using this method is debatable. The main goals of this research is to study the behavior of granular material in silo while discharging downward and by doing so, differentiate

certain flow patterns formed during this process which could be important in predicting granular materials' behavior on the surface.

Since the numerical model needs the input parameter value to function, a couple of important mechanical properties such as normal/shear stiffness, friction coefficient, and *Young's modulus* were obtained by performing numerical triaxial tests in order to facilitate the validation of the parameters which had been previously taken from available literature. The slope of the stress-strain diagram for this particle at the linear region was calculated from the graphs needed to obtain the *Young's modulus* for the specific grain (polyethylene plastic). This value matched with the one that had been already chosen, hence validated the values as being suitable approximations. In order to conduct the study, three unique numerical discharge models were built with two types of granular material and assigned to these, were the material/mechanical properties of polyethylene plastic and corn kernels separately. Validation procedures were conducted (grain volume measurements) by setting up a physical silo in the lab and monitoring center and side discharge developments for real polyethylene and maize grains, sequentially. The differences in results of numerical and lab discharge were small and large, depending on the materials used, as well as the type of discharge process performed (center or side). At the end, reruns of models were carried out with improved input values.

ACKNOWLEDGMENTS

I have been indebted in the preparation of this thesis to my mentor and supervisor, professor Ram Bishu, whose patience, kindness, and support, as well as his far-reaching academic knowledge, have been invaluable to me. I am extremely grateful for having him as my advisor.

I would like to thank my committee members Dr. Michael Riley and Dr. Demet Batur for providing very helpful suggestions needed to improve my research. I greatly appreciate their feedback and guidance.

I extend my gratitude to Mr. McLain and Mr. Hartzell, who gave me the opportunity for the internship in their company and made available the instruments and space for performing experiments required for the thesis to be successfully performed.

Lastly, I would like to express my gratitude to my family for their unconditional support.

Table of Contents

List of Figures	X
List of Tables.....	XVI
Chapter 1- Introduction	1
1.1 Inventory Monitoring in Silos and the Related Issues	1
1.2 Scope of the Thesis.....	2
1.3 Chapter Details	3
Chapter 2- Literature Review	5
2.1 Level Sensors for Accumulated Material in Silos.....	5
2.2 Level Sensor Types.....	8
2.2.1 Admittance-type Sensors.....	8
2.2.2 Rotating-paddle Sensors.....	9
2.2.3 Vibrating Point Sensors.....	9
2.2.4 Ultrasonic Level Detectors	10
2.2.5 Capacitance Level Detectors.....	10
2.3 Granular Material Characteristics.....	10
2.3.1 Granular Material -General Description.....	10
2.3.2 Molecular Dynamics.....	11
2.3.3 Description of Bulk Material flow in Silos.....	12
2.3.4 Behavior of Bulk Solid in Silos.....	13

2.4 Janssen Theory.....	15
2.5 Micro and Macro Behaviors of Bulk Material.....	16
2.6 Granular Flow.....	17
2.7 Stress Analysis of Granular Material.....	17
2.8 Confined Granular Material Behavior.....	17
2.9 Bulk Material Volume Measurements.....	18
2.10 Review of a Number of Significant Granular Flow Parameter.....	26
2.10.1 Particle Size and Distribution Influences on Silo Discharge Process.....	33
2.10.2 Limitations in Simulating Large-Scale Models with DEM.....	34
Chapter -3 Objectives and Rationale of Research.....	35
3.1 Overview.....	35
3.1.1 Inadequacy of Preceding Silo DEM Simulations.....	36
3.2 Need for this Study.....	37
3.3 Objectives.....	40
Chapter-4 Methodology	42
4.1 Overview.....	42
4.2 Model Development.....	42
4.3 Description of Running the Simulation Package.....	44
4.4 Validating the Numerical Models by Lab Experiment Procedures.....	44
4.5 Actual Procedure.....	45
4.5.1 Brief Overview of Elements to Be Considered in <i>PFC3D</i> Model.....	46

4.5.1.1 Spherical Elements Resembling Granular Particles.....	46
4.5.1.2 Boundary Conditions of the Model	46
4.5.1.3 Initial Condition of the Models.....	47
4.5.1.4 Porosity Considerations.....	47
4.5.1.5 Contact Representation for the Models.....	48
4.5.2 Lab Experiment for Validation and Calibration Purpose.....	48
Chapter-5 Results	46
5.1 Development of Numerical Models-Background.....	49
5.1.1 Simulation Model Designs.....	51
5.1.2 Model 1.....	53
5.1.3 Model 2.....	54
5.2 Running of the Simulation Models.....	57
5.2.1 Specific Procedures.....	57
5.2.2 Specific Results from Three Simulation Models.....	58
5.2.2.1 Model 1- Center Discharge of Polyethylene Plastic pellets.....	58
5.2.2.2 Model 2- Side Discharge of Polyethylene Plastic Pellets.....	62
5.2.2.3 Model 3-Center Discharge of Corn with porosity of 0.50.....	65
5.3 Lab Study procedure.....	69
5.3.1 General Description.....	66
5.3.2 Discharging Process.....	72
5.4 Comparing Simulation and Lab Results.....	74

5.4.1 Model 1 (Center Discharge of Polyethylene Plastic Pellets).....	74
5.4.2 Model 2 (Side Discharge of Polyethylene Plastic Grains).....	75
5.4.3 Model 3 (Center Discharge of Maize).....	77
Chapter-6 Detailed Results.....	79
6.1 Chapter Summary.....	79
6.2 Investigation of Various Parameters in Models.....	79
6.2.1 Model 1-Center Discharge of Polyethylene Plastic Pellets.....	79
6.2.2 Model 2- Side Discharge of Polyethylene Plastic Pellets.....	84
6.2.3 Model 3- Center Discharge of Maize	90
6.3 Volume Measurement Validation.....	92
6.3.1 Model 1- Center Discharge of Polyethylene Plastic Pellets.....	92
6.3.2 Model 2 -Side Discharge of Polyethylene Plastic Grains.....	95
6.3.3 Model 3 (Center Discharge of Maize).....	97
6.4 General Comparison	98
6.5 Validation by Discharge Flow Rate Values.....	101
6.6 General Volume Measurement Results.....	103
6.7 Recommendations... ..	104
6.7.1 Calibration of the Simulation Parameters.....	104
6.8 Triaxial Shear Test Simulation.....	106
6.8.1 General Description.....	106
6.8.2 Sample Preparation for Triaxial Test for Polyethylene Plastic Pellets.....	108

6.8.3 Stress State Computation with Servo Control Process.....	108
6.8.4 Computation of Elastic Properties of the Sample.....	109
6.8.5 Test of Stress Failure for the Sample.....	111
Chapter-7 Discussions.....	115
7.1 Specific Discussions.....	115
7.1.1 Modeling.....	115
7.1.2 Simulation Models.....	116
7.1.2.1 Model 1.....	116
7.1.2.2 Model 2.....	118
7.1.2.3 Model 3.....	119
7.2 Laboratory Experiment for Validation	120
7.3 Limitations.....	124
7.4 Future Work and Extension /Recommendations.....	126
References.....	128
Appendix A Distinct Element Method (DEM).....	132
A.1 General Description.....	132
A.2 Boundary conditions in Simulation.....	136
A.3 Force-Displacement Law.....	138
A.4 Simplified Hertz-Mindlin Model.....	141
A.5 Slip Model.....	141
A.6 Rolling.....	142

A.7 Motion Law.....	142
A.8 Time-Step Establishment.....	144
A.9 Damping System Model.....	144
A.10 Contact Models.....	145
A.10.1 Linear Contact Model.....	146
A.10.2 Bonds.....	147
Appendix -B Codes Used for Simulation Model (partial).....	149
Appendix-C Codes Used for Numerical Triaxial Tests (Partial).....	166

List of Figures

Figure 2.1 Overview of a measurement system.....	5
Figure 2.2 Block diagram of a radar system	6
Figure 2.3 The SiloVis software interface.....	6
Figure 2.4 A display unit showing bulk material level.....	6
Figure 2.5. Multiple-point 3D bin volume measurement.....	7
Figure 2.6 Admittance-type sensors.....	9
Figure 2.7 An element of bulk solid under stress.....	14
Figure 2.8 Pressure developments in fluids and bulk solids	15
Figure 2.9 Camera-centered active triangulation geometry.....	20
Figure 2.10 Point cloud generation using triangulation with a laser stripe	20
Figure 2.11 Structured –light 3D scanner.....	20
Figure 2.12 Working principle of a structured-light 3D scanner	21
Figure 2.13 A NURBS Mesh.....	21
Figure 2.14 Stockpile shape characteristic and 3D scanning views.....	24
Figure 2.15 Experimental set-up: (A) schematically and (B) tomography	25
Figure 2.16 Possible paths of wall normal stress and implicit σ_1 directions	27
Figure 2.17 Possible paths of wall shear stress of σ_s during filling and discharge.....	27
Figure 2.18 Filling height h_f , vertical stress at the outlet s_v , and feeder force F_h vs. time	28
Figure 2.19 Evolution of kinetic energy during filling with various friction coefficients	29

Figure 2.20 Comparison of numerical and analytical values with $\mu=0.3$	29
Figure 2.21 Time variation of relative discharge mass for various inclination angles	30
Figure 2.22 A simulation model geometry and the representative pressures	31
Figure 2.23 Radial velocity profiles for maize model discharge from a hopper	32
Figure 2.24 Schematic of an ore pass which resembles a bulk storage system.....	33
Figure 2.25 Downward- sequential model for stress field construction	34
Figure3.1 Level sensor installed in 1/6 of the bin diameter.....	39
Figure 5.1 Cylindrical container model used in the study.....	51
Figure 5.2 Model 1, a cylindrical container filled with circular particles.....	53
Figure 5.3 Side-discharge point as seen from the bottom of the silo.....	53
Figure 5.4 Physical corn grain dimensions.....	54
Figure 5.5 Model 3, cylindrical container filled with circular particles.....	56
Figure 5.6 Initial contour state of center-discharge process	58
Figure 5.7 Contact forces as seen vertically from bottom	59
Figure 5.8 Initial velocity vectors and, displacement vectors –center discharge.....	59
Figure 5.9 Contour state of center-discharge process well into discharge process.....	60
Figure 5.10 Velocity vectors and, displacement vectors well into discharge.....	60
Figure 5.11 Contact forces as seen from below at the middle of discharge.....	60
Figure 5.12 Contour state of center-discharge process in the end of discharge.....	61
Figure 5.13.Velocity vectors and, displacement vectors in the end of discharge process.....	61
Figure5.14 Surface topography decrescence through center discharge process	62

Figure 5.15 Initial stages of side-discharge of the silo.....	62
Figure 5.16 Velocity and displacement vectors for initial stage of side discharge.....	63
Figure 5.17 Midway through side discharge process of plastic pellets.....	63
Figure 5.18 Velocity and displacement for half way through side discharge of PP	64
Figure 5.19 Final stages of side discharge of plastic pellets.....	64
Figure 5.20 Velocity and displacement vectors for final part of side discharge of PP.....	65
Figure 5.21 Surface topography decrease through side discharge process.....	65
Figure 5.22 Initial stages of maize center discharge course.....	66
Figure 5.23 Velocity and displacement vectors for initial stage corn discharge.....	66
Figure 5.24 Remaining maize particles in the bin halfway through discharge.....	67
Figure 5.25 Contact forces halfway through discharge of maize particles.....	67
Figure 5.26 Velocity and displacement vectors halfway through discharge.....	68
Figure 5.27 Contact forces for the final stage of maize discharge	68
Figure 5.28 Final stage of maize discharge simulation	69
Figure 5.29 Velocity and displacement vectors at the final stage of maize discharge.....	69
Figure 5.30 Model Silo used for validation.....	70
Figure 5.31 A picture of the silo model lid.....	71
Figure 5.32 Discharge gates at the bottom.....	71
Figure 5.33 Discharge mechanisms at the bottom of the model	71
Figure 5.34 Laser level sensor device.....	72
Figure 5.35 Polyethylene particles discharging out of the system.....	72

Figure 5.36 Random measurement of point levels of granular pack.....	74
Figure 5.37 Comparing numerical simulation with lab results in center discharge of PP.....	74
Figure 5.38 Comparing numerical results with lab side discharge results	76
Figure 5.39 Comparing numerical results with lab side discharge result.....	78
Figure 6.1 Vertical velocity charts of spheres vs. respective X-positions in the silo.....	80
Figure 6.2 Velocity charts of spheres vs. their respective Y-positions in the silo.....	81
Figure 6.3 X, Y, and Z positions of a collection of particles) vs. time.....	82
Figure 6.4 a) X-velocity of a ball vs. time b) Z-velocities of a couple of particles vs. time c) Z position of a ball vs. its Y position d) Z position of a ball vs. its X position and, e) Z velocity of a ball vs. its vertical	83
Figure 6.5 X and Y forces from particle movements on the cylindrical wall vs. time.....	84
Figure 6.6 Vertical velocity charts of particles vs. their respective X-positions in the silo.....	85
Figure 6.7 Vertical velocity charts of vs. their respective Y-positions in the silo.....	85
Figure 6.8 Vertical velocity charts of vs. their respective vertical positions	86
Figure 6.9 X path vs. vertical path and, Y path vs. vertical path of two particles.....	87
Figure 6.10 Vertical velocities and vertical positions of a collection of particles	87
Figure 6.11 Mean contact forces and mean unbalanced forces of the system	88
Figure 6.12 a:Y force of cylindrical wall vs. time, b: X force of cylindrical wall vs. time c: Z force of flat-bottom wall vs. time and, d: Y force of cylindrical wall vs. its X force.....	89
Figure 6.13 Porosity of grains for side discharge of plastic pellets.....	89
Figure 6.14 Vertical (z) velocities vs. X coordinate (a), vs. Y coordinate (b), and vs. height for maize center discharge simulation	90

Figure 6.15 X force and Z force endured by cylindrical and bottom flat walls vs. time.....	91
Figure 6.16 Mean unbalance forces and average stress	92
Figure 6.17 Porosity value of discharging maize in the silo.....	92
Figure 6.18 Initial sample of compact assembly prepared for the triaxial test	108
Figure 6.19 Axial deviatoric stress vs. axial strain for elastic load/unload test.....	110
Figure 6.20 Volumetric strain vs. axial strain for elastic load/unload test.....	110
Figure 6.21 Axial deviatoric and confining stresses vs. axial strain for grains without bond....	111
Figure 6.22 Axial deviatoric/ confining stresses vs. axial strain for bonded grains 0.05MN....	112
Figure 6.23 Axial deviatoric and confining stress vs. axial strain for bonded grains 0.1MN....	113
Figure 6.24 Volumetric strain vs. axial strain for bonded grains -0.05MN.....	113
Figure 6.25 Volumetric strain vs. axial strain for bonded material	114
Figure 7.1 Level sensor installed at 1/6 of the bin diameter.....	121
Figure A.1 Contact-only deformation and the contact forces between grains	136
Figure A.2 Calculation cycle in DEM simulation	138
Figure A.3 Ball-Ball contact.....	139
Figure A.4 Ball-Wall contacts	139
Figure A.5 Rolling resistance effect on particles.....	142
Figure A.6 Illustration of contact forces between two spheres.....	145
Figure A.7 Normal component of stiffness in a linear contact model	146
Figure A.8 Shear component of stiffness model in a linear contact model.....	147
Figure A.9 Contact bond	148

Figure A.10 Parallel bond.....148

List of Tables

Table 2.1 3D level sensing device benefits.....	8
Table 5.1 General spectrum of modeling situations.....	50
Table 5.2 Material Properties used in the numerical model for polyethylene plastic	52
Table 5.3 Material mechanical Properties used in the maize numerical model.....	56
Table 6.1 Volume calculations for center discharged PP-18 point measurements.....	93
Table 6.2 Volume calculations for center discharged PP 3 point measurements.....	93
Table 6.3 Volume calculations for center discharged PP 2 points (located at about 1/6 diameter of silo's side walls) measurement.....	94
Table 6.4 Volume calculations for center discharged PP 2 point measurements.....	94
Table 6.5 Volume calculations for center discharged PP –single point measurement.....	94
Table 6.6 Volume calculations for side discharged PP-18 point measurements.....	95
Table 6.7 Volume calculations for side discharged PP 3 point measurements.....	96
Table 6.8 Volume calculations for side discharged PP 2- point (1/6D) measurements.....	96
Table 6.9 Volume calculations for side discharged PP 2 point measurements.....	96
Table 6.10 Volume calculations for side discharged PP single point measurements	96
Table 6.11 Volume calculations for center discharged maize-18 point measurements.....	97
Table 6.12 Volume calculations for center discharged maize- 3 point measurements.....	97
Table 6.13 Volume calculations for center discharged maize 2- point (1/6D) measurements.....	98
Table 6.14 Volume calculations for center discharged maize 2 point measurements.....	98

Table 6.15 Volume calculations for center discharged maize single point measurements.....	98
Table 6.16 Average values for 18-point discharges.....	99
Table 6.17 Average values for 3-point discharges.....	99
Table 6.18 Average values for 2-point (1/6D) discharges.....	99
Table 6.19 Average values for 2-point discharges.....	99
Table 6.20 Average values for single-point discharges.....	100
Table 6.21 Average values for 18-point measurements for 3 models	100
Table 6.22 Average values for 3-point measurements for 3 models.....	100
Table 6.23 Average values for 2-point (1/6D) measurements for 3 models.....	100
Table 6.24 Average values for 2-point (random) measurements for 3 models.....	100
Table 6.25 Average values for single point (random) measurements for 3 models.....	100
Table 6.26 Comparing Discrepancies in volume (%) of center and side discharges.....	100
Table 6.27 Average and discrete discharge rate values for numerical models.....	102
Table 6.28 Average and discrete discharge rate values for physical model discharges.....	102
Table 6.29 Average and discrete percentage errors.....	102
Table 6.30 Volume measurement error value change comparisons to 18-point.....	104
Table 6.31 Volume measurement error comparison between three and single point.....	104
Table 6.32 Volume measurement results of calibrated simulation for three models.....	105
Table 6.33 Volume measurement results of calibrated simulation and lab results.....	106
Table A.1 Quantities in the balance equations of discrete and continuum system.....	135

Chapter-1

INTRODUCTION

1.1 Inventory Monitoring in Silos and the Related Issues

In the modern age of technology the inevitability of intense competition among companies in providing the fastest and the most efficient products to the customers, the importance of managing the existing inventory and continuous monitoring of its flow are more vital than it was in the past. The research has a focus on inventory that is non-liquid and stored in bulk quantities in silos

Companies are adopting the so-called lean production/supply management practices in order to survive as well as capture the attention of potential customers, while optimizing their limited resource utilization. Novel philosophies such as *JIT* (just-in-time) and *Lean Six Sigma* and many more, all place the biggest emphasis on competent management of the business's inventory so that, at any point during the process, the production line would be able to provide desired service from customers in as short a time as possible. Of course, keeping higher than required inventory level is not a resourceful solution since it costs money and contradicts the concept of *JIT*. Management in general, prefers to have access to the most accurate level of inventory in large silos at anytime for periodic and/ or continuous reviews and as a result, implementation of material level-sensors in silos is imperative.

Grain production companies are examples of companies that own many large silos in which they store corn, soybeans, wheat, and any other type of grains. It is common knowledge that silos are used for mass storage of grain, cement, and food products such

as flour, salt and also pharmaceutical materials. Silos are large structures (usually cylindrical), normally up to *100 ft* in diameter and *275 ft* in height. The wall materials of these structures are usually made from corrugated steel. These kinds of huge bins typically have multiple filling ports (top) and discharge or draw points (at the bottom). Though the main filling process generally takes place from the central filling point, in a number of situations, filling does take place from ports located on the outer side of the conical lid (The same holds true for the draw points).

Climbing along the wall of a tall silo for checking the level of stored grain as well as observing the contour shapes from above is dangerous because of the potential falls by the personnel. In addition the observation method of inventory level detection method is inaccurate and time-consuming. The safety issue itself mandates installing different kinds of level-sensing devices on top of the silos so that, management can track the accurate volume of the grains in the silos need to be kept at a buffer stock level.

1.2 Scope of the Thesis

The scope of this study is limited to investigating the practicality of distinct (discrete) element method (DEM) simulation in calculating the volume of particulate matter in silos. Three different silo models were numerically designed and simulated in order to visually study the surface contours of grains inside the silos.

Validations were also performed by experimenting on a physical silo model in the laboratory and studying the differences between numerical by calculating measured silo volumes. The calculated volumes used data from electronic sensors.

The volume value discrepancies between these models were performed pair-wisely as well as inclusively, so that insights as to the optimal locations, along with the minimum number of level sensor devices to be used for obtaining as accurate values as possible, be acquired.

1.3 Chapter Details

Chapter 2 describes important backgrounds behind the thesis, which consist of inventory screening in large silos and its problems, and description of level-sensing devices such as plumb-bob level indicators. The background follows with a description of the behavior of bulk solids within the silos and granular material characteristics as well as the micromechanics theory of particle measurement. The chapters later proceed with a brief description of the classic granular material mechanism of behavior and its resulting forces working upon lateral silo walls (Janssen Theory), continued with an explanation of the connection between the angle of repose and the friction coefficient of the granular material when piled on a flat surface (as of a large flat-bottom silo). The next section describes different innovative attempts in calculating the volume and estimating the geometry of the bulk solid stored in the silos. This chapter is concluded by a thorough explanation of the theory adopted for this thesis, the Discrete Element Method (DEM), as well as its application and importance towards granular flow behavior analysis. Several reasons are also given in support of adopting DEM over Finite Element Method Analysis (FEMA) for this research purpose. Chapter 3 states the drive behind this study which extensively explains the problems in volume calculation of grains in silo. Chapter 4 covers the methodology adopted for the thesis which explains the DEM and physical

simulation models. This is followed by chapter 5 which discusses the detailed results from simulation and the related implications. Chapter 6 includes further discussions of the significance and implications of the results.

Appendix of the thesis is comprised of 3 sections: part (A) includes a detailed literature review on DEM and granular materials working principles, part 2 (B) the codes written for the simulation models, the codes used for triaxial shear test, and part 3 (C) the codes written for numerical triaxial shear test.

Chapter-2

LITERATURE REVIEW

2.1 Level Sensors for Accumulated Material in Silos

In today's industry, establishing the volume of solid materials in a silo requires a system of measurement consisting of sensors installed at correct locations in the silo wall or lid, along with supporting software package that analyzes the data acquired by the sensors. Therefore, the measurement system always consists of a hardware component (any kind of level sensors, wiring, and transmitters), along with the software component (certain programs tailored for analyzing and interpreting the volume dimensions). The specific software can receive data through protocol converter. In Figures 2.1 and 2.2, schematics of typical silo volume measurement and the radar sensor systems are given. Moreover, in the Figure 2.3 and 2.4, user interface of a software package, which provides information about the level of material in silo and its volume, can be seen.

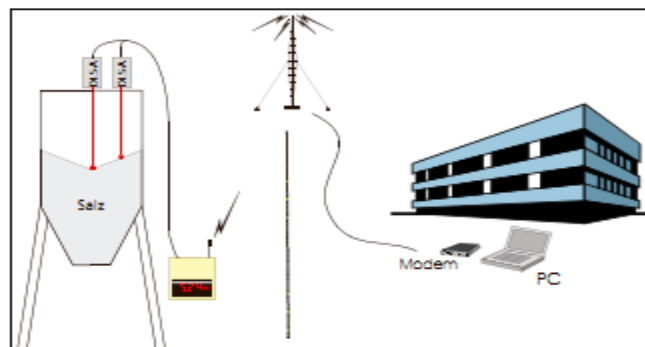


Figure 2.1 Overview of a measurement system. (Dimetex, 2004)

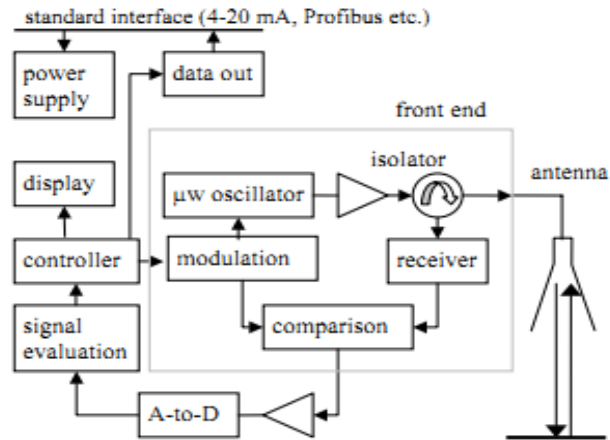


Figure 2.2 Block diagram of a radar system.
(Brumbi, 2006)

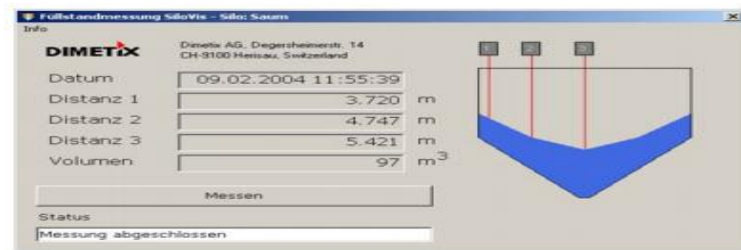


Figure 2.3 The SiloVis software triggers the filling level measurement and based on feedback calculates the silo volume in cubic meters. The filling level is being displayed graphically and the measured values are stored in a data file (Dimetex, 2004).



Figure 2.4 A display unit at the silo displays the empty space (in meters) or the filling level in percentage. (Dimetex, 2004)

The sensor mechanism thus would be able to analyze the volume change in real-time, continuous, or off-line if desired so.

Level sensors identify the altitude of any type of materials stored in the silo; these devices could be installed at multiple points above the bin storage so that, in case the material has bulk properties (neither fully solid, nor fluid), these devices can provide the system with more accurate level of grain inventory especially when the contour of the material is highly uneven and inconsistent. By doing so, the inventory control system can be easily automated. The benefit of multiple point measurement is that the resulting inventories would be more accurate at any time. It accounts for cone-up or cone-down geometries, multiple filling points, and materials prone to sidewall buildup and rat holing. It can detect uneven topography where there are points in the bin that are lower or higher than the majority of the bin contents. “If just one measurement is taken randomly that measurement might not truly be representing the volume of material remaining in the bin” (Christensen, 2010). In Figure 2.5, a representation of multiple-point 3D level sensor which is installed on a silo is given. Moreover, Table 2.1 summarizes the benefits of 3D measurement sensors.

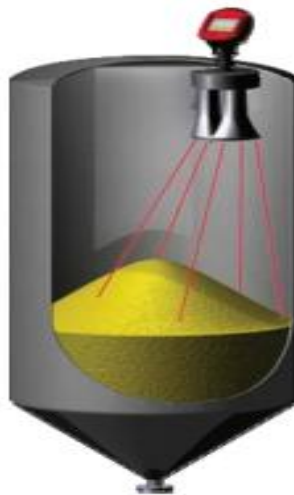


Figure 2.5. Multiple-Point 3D Bin Volume Measurement.

Table 2.1 3D level sensing device benefits (BinMaster, 2010)

3D MEASUREMENT BENEFITS	
Multiple Point Accuracy	Takes measurements from multiple points versus a single point, taking into account variations that can occur on material surfaces.
Non-Contact Measurement	Ideal for sanitary applications such as food, chemical or pharmaceutical processing. No risk of moving parts coming into contact or being buried by bin material.
Dust-Penetrating Technology	The acoustical-based, low frequency technology is unaffected by dust.
Virtually Any Material Type	Can be used in most any material with a bulk density greater than 12 pounds per cubic foot, including a variety of powders, granulates, pellets and other solids with no need for special calibration.
Self Cleaning Sensor	Stays clean, resisting build up of material on the sensors in even the dustiest environments, resulting in very low maintenance.
Long Measurement Range	Appropriate for tall bins (taller than they are wide) and is able to measure a range up to 200 feet.
Measures in Many Storage Vessels	Works in bunkers, hoppers, storage pits and open bins.

2.2 Level Sensor Types

There are various types of level-sensing devices for measuring the grain level inside the silos such as; plumb-bob, ultrasonic, laser devices and many more. These devices can provide either continuous or point value measurements for solid material levels.

A brief description of a few types is given as follows; Admittance, rotating paddle, vibrating, ultrasonic, and capacitance type level detectors.

2.2.1 Admittance-type Sensors

These sensors use a rod probe and radio frequency source to measure the change in admittance. (Admittance is the measure of impedance and is a measure of how easily current is allowed to flow). They operate in the low *MHZ* radio frequency range. The probe is driven through a protected cable. When the level changes around the rod, an analogous adjustment in the dielectric is experienced; this changes the admittance of the

capacitor and this variation is gauged to detect variation in height. An illustration is shown in Figure 2.6.

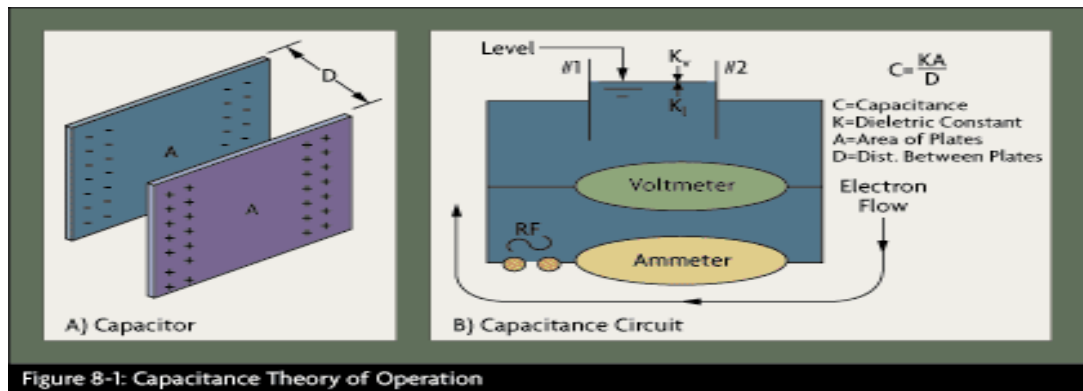


Figure 2.6 Admittance-type sensors. (OMEGA Press, 1995)

2.2.2 Rotating-paddle Sensors

These sensors have been in use for many years and they provide relatively valid measurement results; they make use of a geared motor, which rotates a paddle wheel and when the paddle is engaged in the granular material the motor starts to turn around its shaft until an extension mounted on the motor touches the mechanical switch which is the indication of the bulk level at that point.

2.2.3 Vibrating Point Sensors

By relevant selection of vibration frequency, these devices can read with high accuracy. Single-probe vibrating level sensors are best for bulk powder level. The vibration of the probe removes build-up of material on the probe element. Vibrating level sensors are not affected by dust and changes in temperature, pressure, or moisture content.

2.2.4 Ultrasonic Level Detectors

These devices could be utilized when there is difficulty making physical contact with the bulk or fluid for measurement; there is no need for a contact in these types of sensors to read a value for bulk solids and viscous liquids (remote sensing). Instead of a contact, these sensors release high frequency acoustic waves that are mirrored back and sensed via the transducer. By using this technique, one would be able to make height measurements without having to have physical contact with the subject material.

2.2.5 Capacitance Level Detectors

These devices show high efficiency sensing a wide variety of solids and liquids. This technique also utilizes probing rod and radio frequency signals applied to the capacitance circuit. These sensors are highly practical and they are easy to use and clean while showing high resistance to temperature extremes. The principle of this method is also based on point level sensing.

2.3 Granular Material Characteristics

2.3.1 Granular Material- General Description

A granular material is an assembly of distinct solid, macroscopic components distinguished by a loss of energy whenever the components interact with one another; these energy losses take place when the frictional forces between particles change to heat and, at the same time, kinetic energies of moving particles are also lost along the process. Examples of granular material are corn, bean, sand/rock, and powders. Granular materials

do not represent a single matter phase despite the fact that they may show characteristics similar to those of solids, liquids or gases, depending on the mean energy distribution between grains and the geometry of particles. Nevertheless, in every one of these conditions, bulk material show behaviors exclusive to their inherent physical characteristics.

When exhibiting liquid properties, bulk material flow in their unique pattern (like discharge flow of grains out of a silo under gravity). Granular materials' flow properties differ from those of solids. A few peculiarities of granular material:

1. Are likely to jam or form arches close to the exit sections.
2. Can support small shear stresses (average is usually considered for study)
3. Are mostly anisotropic (non-uniform), and
4. Have avalanche properties when piled on a surface under certain conditions (whenever the friction coefficient of the grains exceeds the angle of repose this event usually may happen).

2.3.2 Molecular Dynamics

One of the principal instruments in the hypothetical study of molecules is the method of molecular dynamics (MD) simulations. This computational method calculates the time-dependent behavior of a molecular system. Alder and Wainwright first introduced the molecular dynamics method in the late 1950's (Alder and Wainwright, 1959), to study the interactions of hard spheres (McCammon et al., 1977).

The importance of molecular dynamics in this research is based on the fact that discrete element simulation method employs some principle concepts of molecular dynamics,

since DEM treats each particle as a separate entity and then, analyzes the stress state developments between the finite pools of particles interacting with one another.

2.3.3 Description of Bulk Material flow in Silos and Silo Wall Pressure Patterns

“Because of the random variation of stockpile shape caused by mechanical operation, it is complicated to employ the real-time operation scheduling by offline calculating” (Chang & Lu, 2010). Laser level sensing devices are very accurate in representing the shape of the stockpile within the silos, however, dust can obscure the vision of such devices and as a result, geometrical details might not be fully captured.

The precise prediction of static and dynamic stresses in dry granular material could get burdensome even with the new technologies available. For instance, the stresses formed between granular materials in a confined space would not show linear behavior and for this reason, elastic displacements formed as a result of these stresses too, should be identified because these non-linear internal stresses between bulk particles would cause an uneven surface topography (in large silos, the inconsistency topography results in inaccurate volume measurement of granular material inside). “The stress within a silo packed with granular material has long been of an area of interest in the engineering and physics communities” (Landry et al., 2008). There are two main techniques in analysis of the silo problems; the conventional Janssen equation, which neglects a more detailed representation, could be applied on uniform granular substance and still in recent years many engineers use this theory for the design of silos. The exact movement of the particles and the stress distribution within the bulk material are yet unknown from the Janssen equation as the formula is based on the yield limit state without taking into

account the end effect from the drawing point. Besides the classical Janssen equation, distinct element method (DEM) is gaining popularity in analyses of silo volume and wall pressure behaviors. Two distinct techniques are employed when intending to perform a DEM analysis: One is force-displacement method introduced by Cundall and Strack in 1979 and the other is the energy-based method proposed by Shi et al. in 1993. Many other contributions have since been added to the method introduced by Shi throughout the following decade for enhancement of the energy-based EDEM or simply, to add additional modification on the original idea.

The distinct element method is in fact a contact problem and the main limitations of the method include the contact detection algorithm, contact mechanics, computation time, convergence, and instability of results. Nevertheless, the distinct element method can provide some useful results that are not possible with the finite element method (Cheng and Liu, 2009).

2.3.4 Behavior of Bulk Solid in Silos

Figure 2.7 shows a component of bulk solid in a bin filled with granular matter (wall friction coefficient is assumed to be zero in this case). The granular element is under vertical stress of S_v . As a consequence of this stress, the horizontal stress, namely S_h , works in the horizontal axis. The stress ratio of λ (Lambda) used commonly in soil mechanics is utilized to express the S_h to S_v ratio. This ratio is given in Equation 2.1.

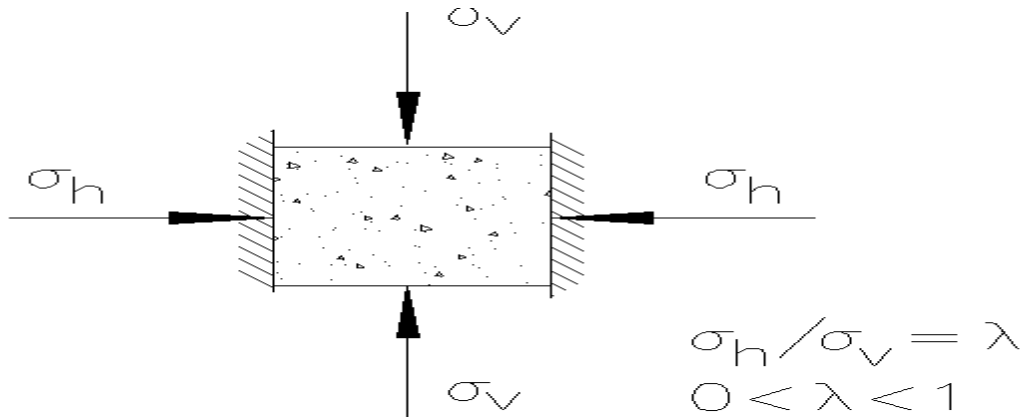


Figure 2.7 An element of bulk solid under stress (D. Schulze, 1996)

$$\lambda = s_h / s_v$$

Equation 2.1

Different granular matters have distinct stress ratio (λ); a completely solid material would have a stress ratio of zero, in contrast, in fluids this ratio is very close to 1. For bulk materials stored at rest, this ratio is typically in the range of 0.3 to 0.6 (Schulze, 2006).

For convenience, in stress calculation of bulk material, generally the material is considered a continuum rather than a series of distinct points. For this reason, the principles used in continuum problems could be utilized in analysis of bulk material in silos. If different planes cut all the way through a constituent of granular solid, it is seen that the shear and normal stresses work in dissimilar cutting planes, and as a result, the S_h and S_v stresses that work in dissimilar directions, have not same values. Major principle stress is the one that exerts maximum normal stress in granular material in one direction and is commonly represented by S_1 . In contrast, minor normal stress is the one that acts perpendicular to S_1 , creating minimum normal stress and is represented by S_2 . In

Figure 2.8, a comparison between liquid and granular solid pressure behavior and the resultant surface patterns within a cylindrical silo is shown.

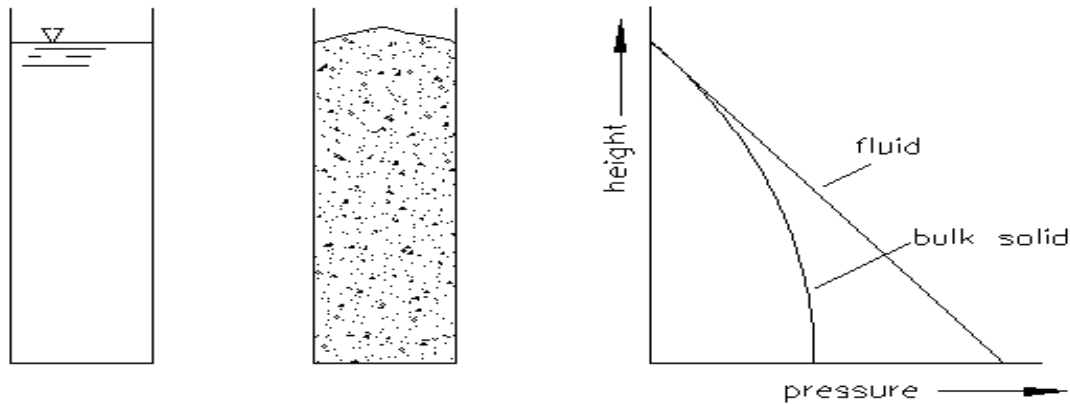


Figure 2.8 Pressure developments in fluids and bulk solids (Schulze, 1996)

2.4 Janssen Theory (Silos Vertical Walls Pressure Theory)

In 1895, Janssen constructed a model to illustrate vertical stresses in silos. Janssen was able to derive a straightforward function for the vertical stress by treating bulk material as a continuous matter while, a portion of vertical stress is converted to horizontal stress. Various assumptions should be considered while applying Janssen's theory; first and foremost, is the assumption that the friction between particles and walls obeys the Coulomb failure criterion of $F_t = \mu_w F_n$, where F_t is the amount of the tangential friction, F_n is the vertical force at the wall, and μ_w is the friction coefficient of particle-wall contacts. "This theory qualitatively describes the crossover to a depth-independent vertical stress, while quantitative inconsistencies concerning the Janssen theory and experimental data are commonly discernible" (Landry, et al., 2008). In the construction of silos, the distribution of stresses is one of the most important factors to be considered. In a liquid, hydrostatic pressure increases with depth. Granular materials tolerate vertical

stress, and for that reason, the lateral walls of a bin are able to support a portion of this vertical stress, only when $\mu_w > 0$. The problem of the resulting vertical stress in a silo after filling was investigated at various times, starting with Janssen (1895). Janssen's analysis is still widely practiced, even if it is based on a few hypotheses that are not completely examined yet.

2.5 Micro and Macro Behaviors of Bulk Materials

Bulk materials are special in that they neither demonstrate a complete solid behavior, nor do they behave as liquids. These materials are comprised of a set of distinct granular particles which interact at specific contact points only.

The entire shape of granular particles such as rocks, grains, and certain powders can be classified as materials with behavior not being either continuous or homogenous; they show discontinuity at certain points. In addition, these researches include dilation (bulk materials viscosity increases with the rate of its shear strain, also known as dilatants), liquefaction (the course of action when saturated, bulk material are transformed into a matter that shows flow properties), and many more. The relationship between micro and macro properties of granular material is not fully understood, even though it is believed that micro parameters significantly influence the general behavior of these types of material. One reason to the lack of understanding of such incident is that, "micro-characteristics of granular material are difficult to measure through experimental tests due to limitation of conventional techniques in obtaining micro-quantities such as micro-displacements, fabric quantities, and micro-strains" (Fu, 2005). One particular challenge for analysis of three-dimensional micro-structures is the fact that every single particle should be accounted for in the analysis as an independent rigid body. As Wang (2004)

stated, “the present means for particle identification requires human judgment”. Spatial arrangement of particles should be fully studied for this matter (Fu, 2005).

2.6 Granular Flow

When studying the behavior of granular flow within a silo, several factors influence the characteristics and behaviors of these particles. For example, if a wall of a hopper in a silo is not too steep, or the hopper wall is not smooth, particles may clog the hopper or stick on the inside.

2.7 Stress Analysis of Granular Material

For bulk material, stress refers to the average stress in a certain volume. Stress is defined in a continuum realm and in heterogeneous spaces such as granular medium, this stress is not definable at each discrete point (particles) and in micro-scale, the adopted theories from continuum mechanics are only applicable in ‘between particles’. The difficulty in modeling grain behaviors necessitates a modification of particles’ behavior to the continuum status presumed at the micro-level. The mathematical modeling is performed by certain averaging methods in DEM software.

2.8 Confined Granular Material Behavior

Interpreting a robust stress/pressure state for packed granular material (which are under discrete pressure zones), is problematical and the number of studies on this issue is limited. There have been a few models developed in order to accurately account for this ‘point-dependent stress’ condition in confined bulk material.

2.9 Bulk Material Volume Measurements

Determining the quantity of a three-dimensional object's volume based on estimating the values of these dimensions is a big challenge faced by many industries today. Volume-based inventory assessment's importance and its associated uncertainty are intensified further when there exist obstructions for proper access to the bin geometry which is needs to be measured. For instance, in coal or metal extraction sites, there is very limited access visually as well as physically, for a person or even for a fabricated robot arm to enter via a draw point located in a mine. Thus it is difficult to attain the measurements of dimensions and the real geometry of the whole interior. The obtained measurements later have to be passed to integrating algorithms in order to perform precise volume appraisals.

In cases where there is a limited capacity for capturing the geometric shape of material containment. Researchers have developed some models for calculating the 'unreachable' volume. The researches have strived to achieve an acceptable level of accuracy for their models, most of the studies lack in a practical solution for everyday volume measurements. Some studies have their bases in schemes on reverse engineering techniques. "Reverse engineering treats advanced equipment and imaging as research subjects, then measures a physical model or sample part with certain measurement means" (Feng et al, 2009). These methods essentially analyze a predesigned shape or device and then develop modifications and possibly improvements for the initial design. As the popularity of computer-aided design increases, more businesses are investing in this method which is also a subgroup of reverse engineering. The reverse engineering method in *CAD* case is taking measurements of an object and then rebuilding a *3D* model. The measured values can be obtained from physical model by using *3D* scanners. The *3D* scanning technology is one of the most important methods for the digitalization

of the objects and environment in the real world. The accurate quality of *3D* modeling has been carried out in a variety of fields including, quality control and reverse engineering. (Chang et al, 2010). The devices used in these domains analyze an actual object and collect information about their geometries. Later, the collected data are utilized to build a *3D* model from the digitized files. The *3D* scanners are intensively used in rapid-prototyping along with reverse engineering fields for data collection purposes. These devices are very similar to cameras and, they can get information about the topography and eventually dimensions that are not dark-colored. Many *3D* scanners function based on triangulation concept. These scanners are active type that utilize laser to explore the surroundings. In Figure 2.9, we can spot the ‘triangular’ trace formed by the laser projector with the *3D* point and the camera path along the *X* axis. A representation of point cloud generation triangulation-supported procedure is given in Figure 2.10.

Structured-light *3D* scanner is yet another type of triangulation measuring device that is capable of calculating three-dimensional shapes volume by using ‘projected light patterns’ and a camera. A basic work principle of such device, as well as an arrangement is given in Figures 2.12 and, 2.13 respectively; this apparatus projects a narrow band of light on a *3D* plane and creates a streak of light which looks contorted from any other standpoint except from the projector’s. These reflections can then be used in investigating the exact geometric shape of the object. Working principle of a structured light *3D* scanner is also given in Figure 2.12.

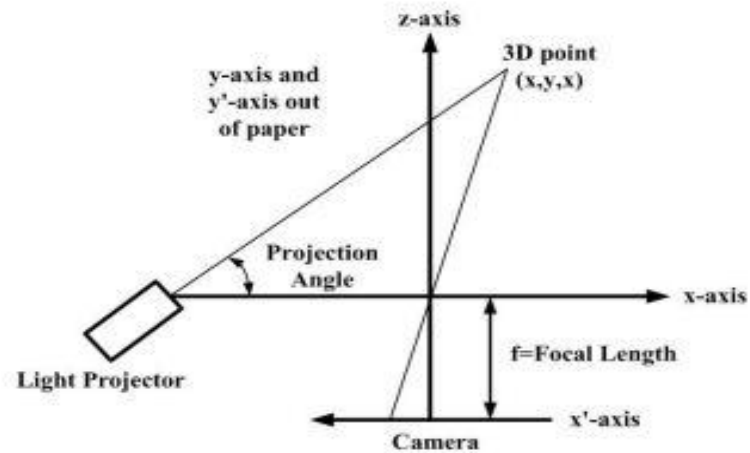


Figure 2.9 Camera-centered active triangulation geometry (Feng et al., 2009).

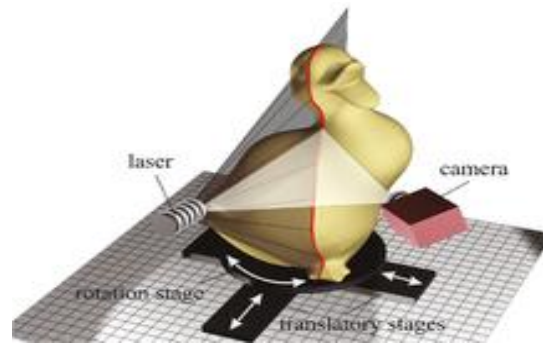


Figure 2.10 Point cloud generation using triangulation with a laser stripe (Cteutsch, 2007).

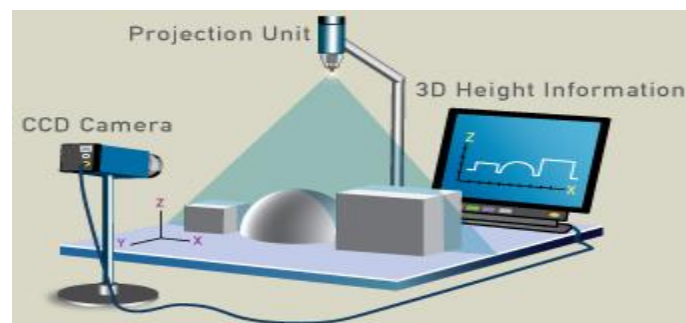


Figure 2.11 Structured-light 3D scanner (webexhibits.org, 2010).

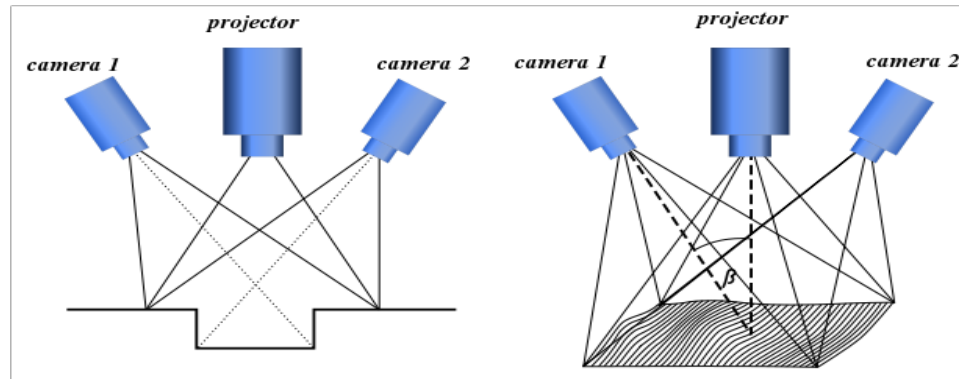


Figure 2.12 Working principle of a structured-light 3D scanner (Ezekowitz, 2008).

The 3D scanners are utilized in creating ‘point clouds’, which are a set of 3D vertices generally named by X , Y , and Z spatial points system. These vertices could be used in defining a representation of surface of objects with complex geometries. The 3D scanners measure numerous points on the surface of an item, and then give a point cloud yield. Point clouds, however, are not directly used in most of the 3D applications and as a result, they are generally converted to polygon or triangle mesh, or NURBS surface models via surface reconstruction technique. NURBS which is an acronym for Non-uniform rational basis spline, is a model used for producing surfaces. NURBS are most often used in CAD/CAM in many industries as well as in various 3D modeling packages. This application makes possible a presentation of complex geometries in compacted fashion. A representation of a NURB surface is given in the Figure 2.13 below.

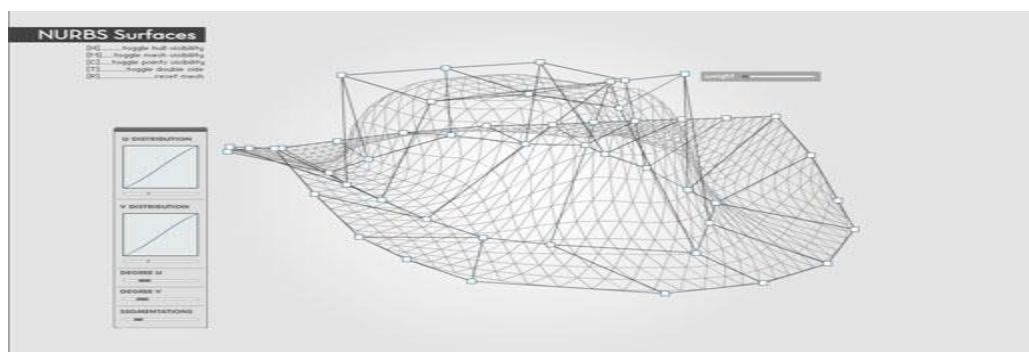


Figure 2.13 A NURBS Mesh (miaumiau interactive studio, 2011).

These techniques are only a few of the attempts made for measuring the volume of complex volumes (e.g., surfaces with distorted contour, geographical dimensional representation of terrains, and so on). There, however, exist a limited number of papers in the research literature covering the very concepts of volume measurement of complex shapes. In the next section, a review of some novel ideas proposed for volume measurements is covered.

Feng et al., (2009) have proposed a reverse engineering-based method for mass measurement of bulk materials with an irregular shape. This method obtains multi-point cloud data by frequent measurements of material pile surface. The research structure has already been given in Figure 2.12. Measurement is acquired via a structured light scanner to quantify a large-scale material stack and find the multi-view point cloud data, and the three-dimensional plane of the stockpile is recreated following point cloud data assignment. The coordinates of point (x, y, z) , as shown in the picture are obtained by known parameters such as, the horizontal distance of camera with the projector (b), the variable angle of projection (θ) and pixel sizes (x', y') , with simple geometric formula. The volume of the pile can then be estimated by this *3D* surface model. This study opts for a structured grating measuring system based on phase-shift and gray-code scheme. (A binary code with black conveying zero, and white conveying one logical and, n-bit gray-code in between). Following the image acquisition, every pixel of charge-coupled device acquires a gray value vector.

The automated registration method selected in Feng et al., study was based on 3-spheres-to-3-spheres algorithm; first, a list of sphere center candidates was created for automatic location of spheres and second, the registration process started for each pair of datasets.

In this noteworthy study, registration of *3D* data was based in Three Fiducial Points of sphere center (via deploying three fiducial sphere center points in order to establish a *3D* coordinate). For validation purposes, an experiment used a pile of rice located on a flat glass surface along with Table tennis balls glued with bamboo sticks which were placed on the surface of the rice mound. Measurement tabs were placed beside the rice pile over the flat glass as reference points. Later, the scanned single point cloud data was obtained before obtaining a polygon *3D* model, so that a complete *3D* surface model of rice was achieved. A coordinate plane was then created based on the measurement tabs placed next to the pile on the glass. Finally, a calculation of volume of small cylinder was performed (which was enclosed by each triangle of model surface based on its projection to base plane). The total volume therefore, was the integration of the small cylinder volumes. This procedure introduced a process of measurement of the stacked volume as well as quality of it by the means of reverse-engineering method. It has been proven reliable in calculation of the volume of complex shapes, however the validity of it remains theoretical and thus, for establishing the volume of real world industrial problems, the mentioned method encounters has shortcomings in establishing larger volume values.

Chang et al., (2010) made attempt in automating the bulk stockpile scanning using *3D* scanning technology. Since the shape of stockpile changes randomly induced by automatic processes, the researchers investigate a possible solution to implementing real-time operation scheduling using off-line information. The bulk stock automatic *3D* scanning-based modeling for real-time calculation of volume was suggested. In order to obtain *3D* point cloud data, the mechanism was supported with a laser radar system.

“Once the data are obtained, the 3D stockpile model was reconstructed and updated in real-time” (Chang et al., 2010). The authors also contended that the feasibility and effectiveness of this procedure have been validated in a real case study. The characteristic of the stockpile with the width of w is shown from top and side view along with the loading/unloading equipment which is presumed to be stacker-reclaimer are given in Figure 2.14 below.

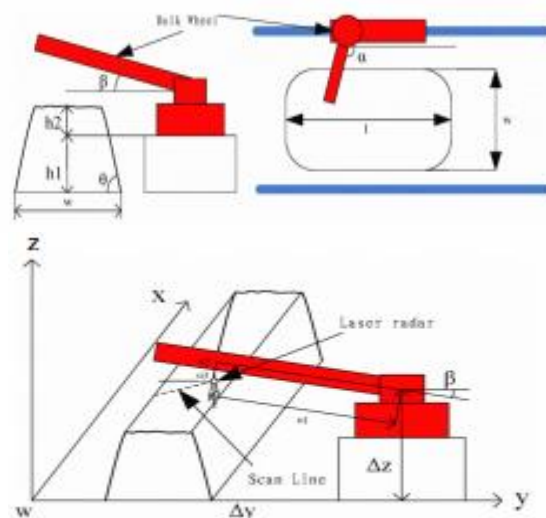


Figure 2.14 Stockpile shape characteristic and 3D scanning views (Chang et al., 2010).

X-ray tomography was implemented in a study by Grudzien et al., (2011) for quantity estimation of volume of granular materials in silos. The importance of this study was attributed to determining density distribution in bulk material in a confined silo. Finding density is very problematical due to the “existence of localization of deformation in the form of narrow zones of intense shearing” (Grudzien et al., 2011) and shear localizations occur mainly because of the walls roughness. The X-ray technique was implemented in

continuous exposure form and later, in the post-processing stage, the *1D* and *2D* plot images were analyzed in the main silo (excluding the conical hopper). The small scale experiment consists of rectangular silo with a hopper in below. The experiment schematic is given in Figure 2.15.

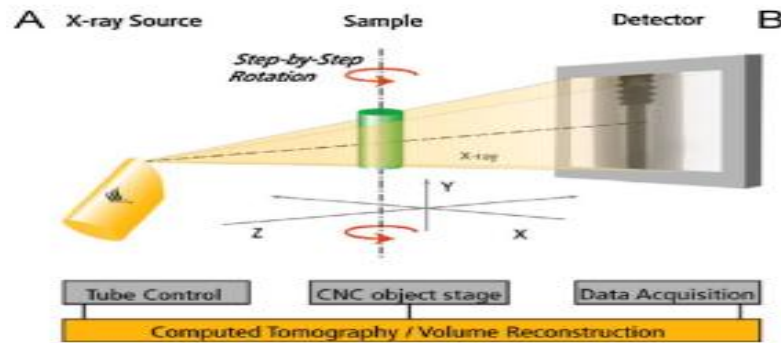


Figure 2.15 Experimental set-up: (A) schematically and (B) tomography (Grudzien et al., 2011).

rate. The X-ray was reflected through so that the detector which is fixed on the right side could get the tomography of the volume geometry. The main error sources in this study, according to the author, were the limitation in the size of X-ray source and detector resolution.

In one particular study, a measurement of capacitances consisting of parallel plate structures (designated as level sensors), was proposed as a solution for detecting the grain level in silo (Isiker and Canbolat, 2008). The error reported in their study was approximately 7 percent which, considering the ambiguity related to volume levels in silo, was a relatively sound approximation.

2.10 Review of a Number of Significant Parameters Influencing Flow Behavior of Granular Material in Silos

A plethora of research has been performed to deal with simulation modeling of granular flow in silos. In doing so, many studies have engaged with investigating the effects of the wall material, coefficient of friction of the walls, the size distribution of particles, material type, pressure profiles/ changes observed between the walls and the particles, and the velocity profiles of the granular flow depending on the level of grain particle with regards to the draw point or axis plane. Additionally, some papers have measured certain parameters such as the *MFI* (mass flow index) and discharge rate following the calibration and adjustment of a few parameters in their models.

The location-dependent behavior of stresses in silos has been studied in numerous research efforts. For example, in a full silo with conical hopper, the pattern of normal stress on the walls, S_w , is given in Figure 2.16 which represents possible static, discharge, filling scenarios for this silo (*a*, *b*, *c*, and *d* are the implicit paths of principal stress). It can be seen that the normal stress increases as we move toward the hopper along the bin part of the silo, but this increase in the stress value diminishes until the stress values reach a relative maximum value. The major principal stress of σ_1 direction is in the same direction of the silo's axis towards the hopper. Away from the central axis, σ_1 deviates increasingly from the vertical direction.

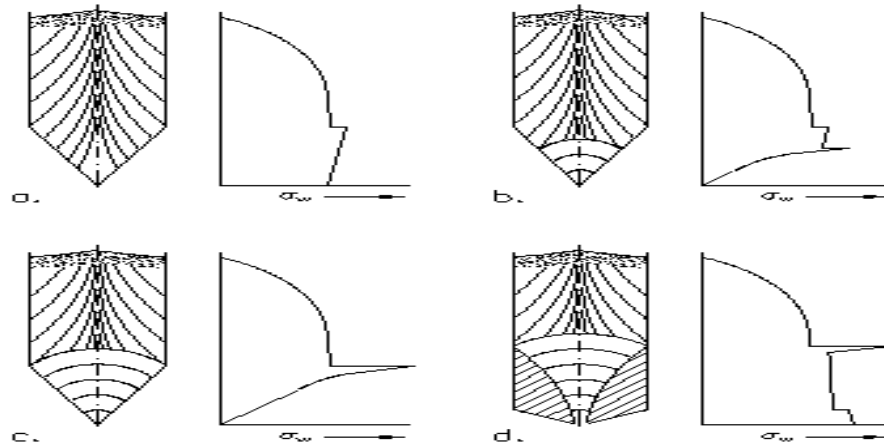


Figure 2.16 Possible paths of wall normal stress and implicit σ_I directions (Schulze, 1999).

The qualitative condition for the shear stress is given in Figure 2.17 for the filling state

(a) and, discharging state (b).

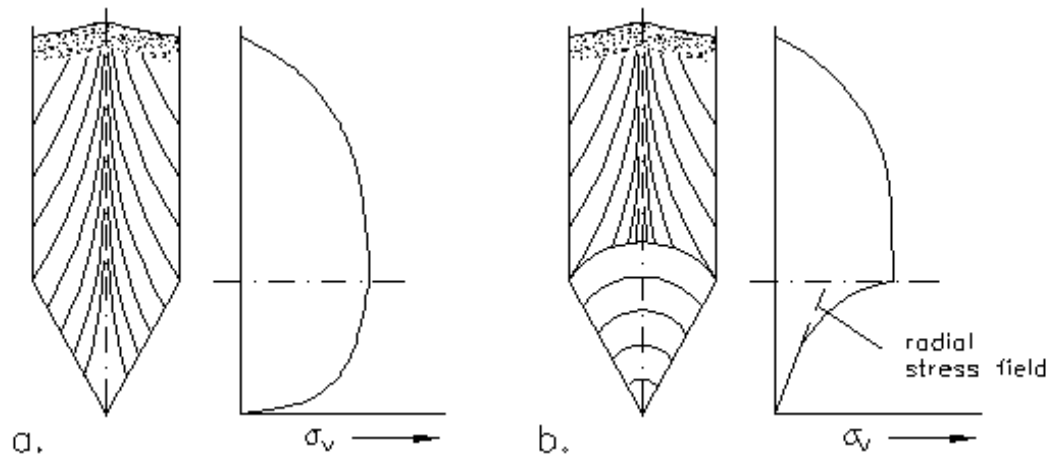


Figure 2.17 Possible paths of wall shear stress of σ_s during filling (a) and discharge (b) (Schulze, 1999).

stress at the exit (σ_s or σ_v) and, feeder force (F_h) against time. These graphs are given in

Figure 2.18.

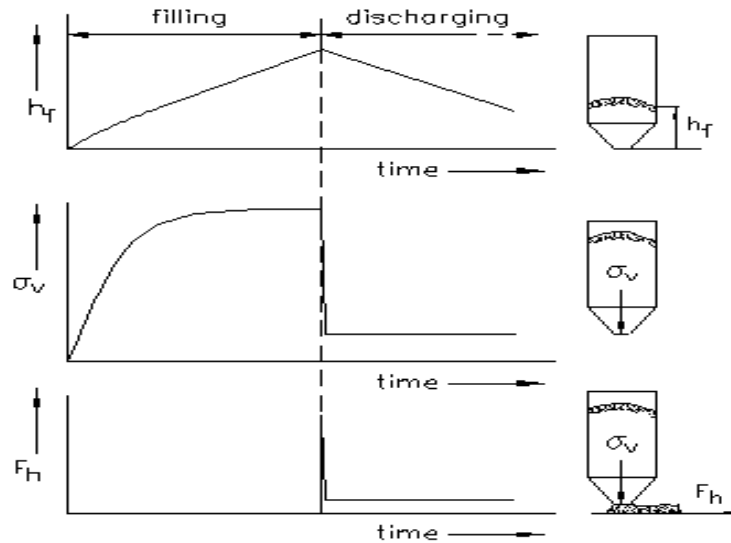


Figure 2.18 Filling height h_f , vertical stress at the outlet σ_v , and feeder force F_h with respect to time (Schulze, 1999).

By inspecting the Figure 2.18, during the filling phase, both shear stress and filling height increase. Once the discharge phase starts, the initial filling height starts to decrease as the material exits the system and at the same time, shear or vertical stress value decreases very quickly (because of the presence of passive stress fields).

Balevicius et al., (2005) affirmed that the problems of granular material filling and discharging in the hopper have always been accompanied by a number of important issues such as: pressure evolution on hopper walls, particle segregation, and vibration effects. Their study revolves on the application of DEM concept for simulating the filling and discharging of bulk material in a wedge-shaped hopper with an orifice draw point, in optimizing the discharge process parameters. The model has been validated by comparing pressure values of a physical model (employing classical Janssen theory which predicts pressure in macroscopic level), with those of resultant numerical values. The hopper

geometry and the discharge mass were taken as design parameters for the Balevicius et al., study.

A couple of graphs, illustrating the contrast between analytical values and DEM results, were presented in their work in terms of kinetic energy evolution of K , drawn in logarithmic scale. These graphs are presented in Figures 2.19 and 2.20.

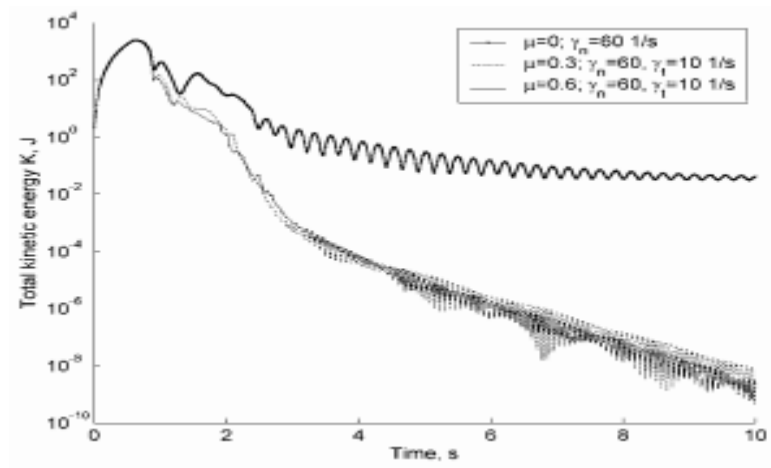


Figure 2.19 Evolution of total kinetic energy during the filling of particles with various friction coefficients (Balevicius et al, 2005).

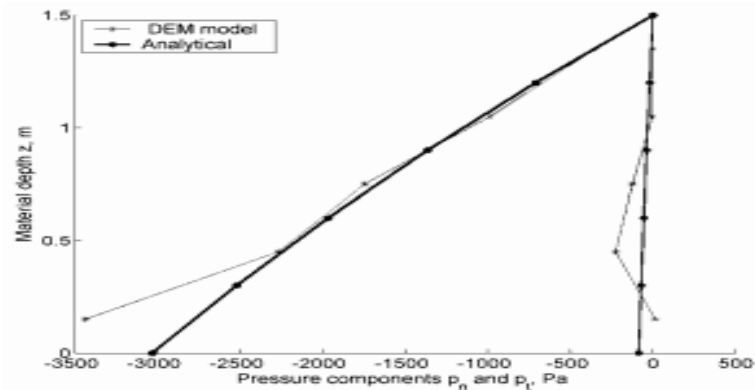


Figure 2.20 Comparison of numerical and analytical values obtained for tangential and normal pressures for the right wall of the hopper with $\mu=0.3$ (Balevicius, 2005).

Moreover, in order to compare the time variation of discharge mass for different angles of hopper walls, they have provided an informative graph shown in Figure 2.21.

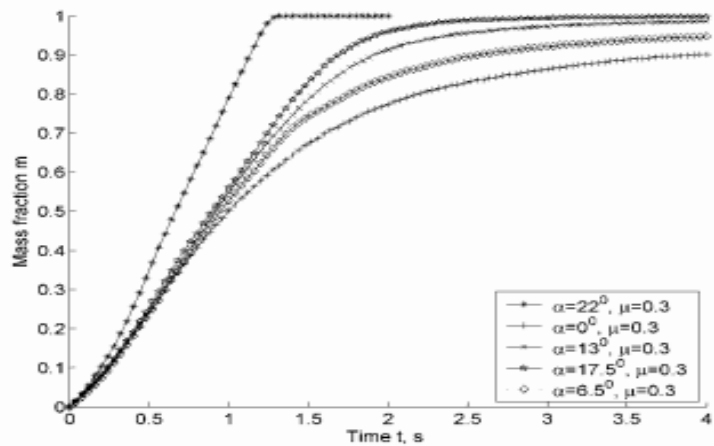


Figure 2.21 Time variation of relative discharge mass for various inclination angles of hopper wall (Balevicius, 2005).

The results presented in the above-mentioned study suggest that the flow behavior divides the set of the design parameters into several distinct regions, therefore, only by categorizing these regions (with constant parameter values) a valid analysis of flow discharge with the discharge mass fraction's could be carried out.

Another DEM simulation study was carried out by Montellano et al., (2011) for the purpose of modeling the flow of glass beads and corn grains during the discharge from a small silo model. In this study, three variables were tracked for validation: the mean bulk density at the end of the filling state, discharge rate and, the visual flow pattern. After performing a couple of calibration for the corn model (value modification of friction properties, among others) a better predictive model was achieved. Several designs were compared by changing the mass flow index ($MFI = \frac{v_{wall}}{v_{centerline}}$), where v represents

particle velocity at a given height, z) values and observing the resulting output. The main outcome from this discharge simulation was that friction coefficient, and the characteristics of discharge flow. MFI values less than 0.3 are considered as funnel flow and more than 0.3 as mass flow. The main goal of this study was to determine the patterns of flow during discharge along with wall pressure distribution at different phases of the filling and discharge processes (Montellano et al., 2011). As it is common in a simulation study, the numerical model was calibrated iteratively by observing the real model's discharge behavior, so that, by slight modification of some constants (i.e. stiffness, friction coefficient), the numerical model would offer a closer resemblance to the actual model. In Montellano et al., research, discharge rate, bulk density, visual patterns (qualitative), *MFI*, and vertical velocity profiles of certain groups of particles at different stages during discharge were considered for validation purposes. As for the wall pressure distributions, an average value (relative to simulation time) was computed using normal and tangential contact forces produced on the walls. The schematic model representing the vertical and tangential pressures can be seen in Figure 2.22 (Montellano et al., 2011).

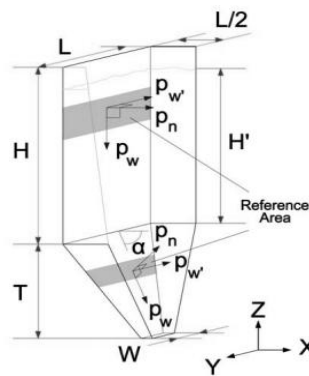


Figure 2.22 A simulation model geometry and the representative pressures (Montellano et al., 2010).

A graph illustrating velocity profiles at various heights (z) and MFIs from the draw point for the corn model can be seen in Figure 2.23.

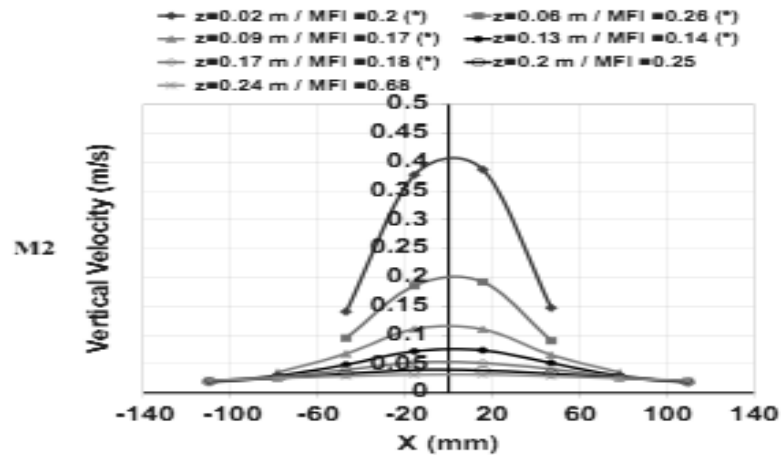


Figure 2.23 Vertical velocity profiles for corn model discharge from a hopper at different heights (z) and MFIs (Montellano et al, 2011).

It is clearly seen in the graph above that the closer the particles to the walls (larger x values in each direction), the lower the speed of exit of the particle from hopper. This is linked to the frictional forces affecting the particles with wall contacts.

It is also observed that, the higher the level in the hopper, the larger the difference between velocities of the particles closer to the center axis than those of farther away from center. However, as the height decreases (especially within the hopper region), this difference in velocity values become less and less.

Nazeri et al (2002) studied “the effects of ore shape on the static and dynamic loads on the ore pass gate assembly”. An ore pass system resembles the shape of a silo, with a hopper at its base therefore, a DEM simulation of ore flow which results in stresses on the ore pass walls could be indicative of those of a silo. The schematic of an ore pass system, used as the model in the study, is given in Figure 2.24. This research showed

proved that a rigid based DEM simulation method was predictive of loads as well as stresses on gate/ wall assemblies and on ore flow in ore passes.

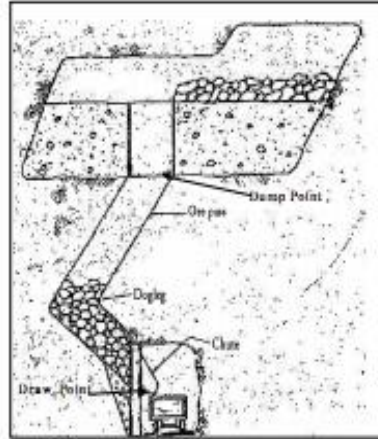


Figure 2.24 Schematic of an ore pass which resembles a bulk storage system. (Nazeri et al., 2002).

2.10.1 Particle Size and Distribution Influences on Silo Discharge Process

In order to create particles with discrete element method, owning information about the size and shape of the particles is imperative. The spherical particles are more efficient computational wise than are particles with irregular shapes.

Since DEM employs the contact algorithm in a ‘time-marching fashion’ in order to calculate the force-displacement values at each time-step, “this contact detection between irregular particles makes the calculation step computationally impractical to carry out due to the non-linearity of mathematical functions” (Mani et al., 2003).

There have been many attempts for reproducing the particle shapes as close to reality as possible in a more efficient way. O’Conner (1999) proposed a discrete function

representation in order to utilize producing “diverse shapes from super particles with quadratic structure”. Ting et al., (1993) considered “elliptical elements to simulate elements with the ratio of height-to-width greater than one in $2D$ ”. Many kinds of these studies have also been developed in $3D$ in the subsequent years.

2.10.2 Limitations in Simulating Large-Scale Models with DEM

The time and the computational power required for simulating a very large system of granular particles in a vessel (i.e., a very large silo with grains), are prohibitive since as the number of particles to be modeled increases, the time and computer power required for its modeling amplify in quadratic proportions. Parisi et al., (2004) developed a method in order to effectively model a very large silo discharge filled with bulk material; this model consists of partitioning a silo in layers to be analyzed sequentially by calculating stress and velocity profiles on the hypothetical interlayer boundaries.

A scheme of their theoretical model is given in Figure 2.25. The remainder of the details on DEM is presented in the appendix A of the thesis.

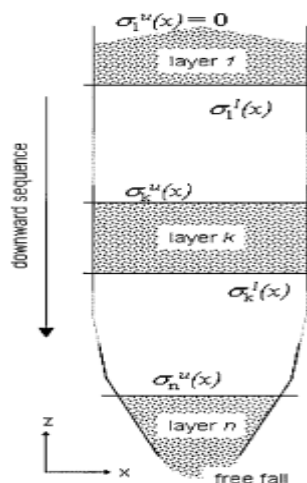


Figure 2.25 Downward- sequential model for stress field construction (Parisi et al., 2004).

Chapter-3

OBJECTIVE AND RATIONALE OF RESEARCH

3.1 Overview

Granular or bulk materials are a special type of materials which cannot be categorized either as being solid or fluid; the ‘discrete-point’ behavior of these materials are attributed to the peculiar shape and structure of the particles for which, the cause of this behavior can be traced to their microscopic makeup by studying the micromechanics of granular material. The resulting stresses formed between the discrete particles are not linear, hence the nonlinear behavior of the bulk material flow and random topographies found in them.

Volume measurement studies for bulk material are performed by using a number of novel technologies: *3D* scanners (mostly operate under the triangulation principle), structured-light *3D* scanners, remote sensing technologies (active and passive), Coordinate Measuring Machines (CMM) for depth mapping, and industrial CT scanners. The most common technologies available for volume measurement of bulk solids in research are, seldom used for industries involved in grain storage and /or production. In turn, the common practices in industries for volume measurement of granular material in storage bins involve installing and using different types of level sensors (i.e. vibrating, ultrasonic, capacitance), as these methods are more readily available, cost less, and are easier to operate, though, the resulting volume calculation values from these devices are less accurate than the more sophisticated research techniques.

The underlying principles of the majority of scanning-based technologies are on reverse engineering for reproducing the so-called ‘multi point-cloud data’ by which, a more detailed surface topography can be obtained. The data processing essence works as inverse problem; even though the dimensions to be measured may not be directly established, it can produce some valid observations with which, the ‘missing parts’ could be interpolated and thus estimated. Other studies discuss the complexity of working with, and creating a suitable environment for devices such as structured light scanner and coordinate measuring machines. The accuracy of such devices was high, as claimed in those studies. Other measurement techniques such as, industrial CT scanners and remote sensing devices, make use of X-ray or special radiation detector mechanisms in order to inversely reproduce a prototype of a bulk material surface.

3.1.1 Inadequacy of Preceding Silo DEM Simulations

Many *2D* and *3D* discrete element method simulation of silos have been done for the study of the silo wall pressure distributions, shear/ normal stress, discharge rates, and mass flow index analyses, in order to determine whether the discharge process was a funnel flow (where discharge velocities of particles closer to central discharge axis are significantly higher than those closer to the silo side walls within the silo) or mass flow (where discharge velocities of particles are similar at different region while discharging from the silo), however, not much has been carried out in order to analyze the surface contour of the granular material while the silo is discharging. The majority of the studies reviewed fell short of developing an algorithm by which volume of bulk material was to be established, or, the objectives of the authors did not involve volume measurements of bulk solids in storage bins.

Additionally, most of the studies have been performed using models with number of particles not exceeding 20000. This is a limitation imposed by DEM utilization as the time of the simulation increases sharply when the number of particles considered for the model augments and, as a result, numerous studies have embarked on modeling a 2D (which is less time-consuming as well as less intense computationally), rather than a more accurate 3D simulation. Consequently, these models did not precisely represent a real silo discharge process, thus not addressing the important details. Furthermore, most of the published research has been done for silos with a conical hopper at their base, as opposed to this study in which, a flat-bottom silo has been selected for the volume measurement studies.

3.2 Need for this Thesis Study

As explained earlier, a large industry, dedicated to manufacturing of level sensor for use in large silos has been formed in order to fulfill the conspicuous need for obtaining dependable volume measurement for bulk material inventories. In the existing market today, various kinds of level sensing devices are readily offered for purchase which are either very costly or, these devices do not determine accurate values of bulk material inventory levels in storage bins and as a result, storage companies studies expressed their dissatisfaction because of the low accuracy obtained when these devices were purchased and used in silos.

Limited studies (if any) were performed solely on determining the level of grain in silos; mainly, grain companies were not aware of the volume geometry and size of grains

within silos despite the fact that, for the management, having a good knowledge of inventory level approximation inside large bins may seem farfetched.

On the other hand, various studies have proposed some innovative techniques for investigating the flow pattern of bulk solids in discharging silos and the resulting stress/pressure patterns along the silo side walls. There were only a few number of studies emphasizing *3-D* modeling of a silo in order to identify the stage-by-stage pattern of topography in a discharging silo (dynamic study). The majority of the studies undertaken used distinct element method simulation were in *2D* or, in case of a *3D* model, the dimension of the models were so small that, smaller number of particles can be used to fill up the storage silo. Due to a limitation in existing DEM simulation packages where, an increase in number of particles to be used in model, would increase the simulation time quadratically and therefore, the necessary computational capacity for the computers has to be increased accordingly.

In the current thesis, a distinct (discrete) element method numerical model was developed in order to dynamically exhibit a discharging silo and the ensuing topography pattern changes on the bulk material surface in the silo model. In doing so, at any given time during the simulation, the discharge can be halted temporarily and the remaining bulk material volume in silo be calculated accurately.

This thesis simulation model, when operating in conjunction with DEM fundamental rules, imitates the approximate pattern of irregular surface contours given the correct constitutive as well as secondary material factors (such as normal /shear stiffness, friction coefficient) of the particles as input parameters. This piece of knowledge in turn, is

assumed to be indicative of the (scaled) locations of the points with lowest and/or highest descent during a certain simulation time. Of course, these point locations were determined and measured with respect to the cylinder's central axis and the side walls.

By capitalization on this piece of information (information as to the approximate locations of peaks and valleys on material surface) obtained from simulation at this stage, an idea as to the optimal location for the level-sensing devices (exactly above these distinct points) would be known. Thus, after some discharge process, the remaining volume of the bulk material could be determined easily by interpolating the points located between highest and lowest values. Figure 3.2 shows the proper mounting of level sensors just on top of the points with high and low surface levels (with respect to silo height, z). This will decrease the number of level sensing devices needed to be used while reducing the estimation error of the remaining volume of grains in the silo. The model is expected to increase both the efficiency and accuracy of inventory review (perpetual or periodic) processes in the grain companies.

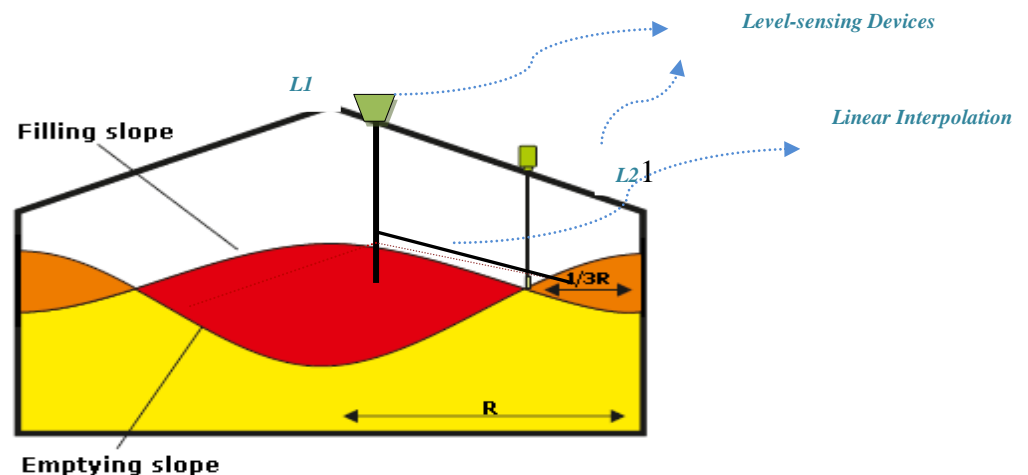


Figure 3.1 Possible representation of optimized locations for level-sensing devices $L1$ and $L2$, just above the peak and valley of bulk surface, respectively. This picture shows partially the top of a silo with radius R .

Once a better understanding of potential locations for level-sensing devices was revealed, companies can save on capital by more precise monitoring of inventory volume in the silos at all times. The points given below could perhaps be valuable inputs for management consideration in production.

1. Improved inventory accuracy; since a single-point imprecise measurement could cost thousands of dollars in inventory miscalculations.
2. Prevention of profit loss in situations when significantly different measurement values at different parts create considerable volume measurement discrepancies in silos with very large dimensions.
3. Measurements, when the material build-up within the silo resembles cone-up shape, are completely different than when the material build-up resembles cone-down shape. This inaccuracy could lead to unaccounted discrepancies when the inventory level is being monitored.
4. By detecting non-homogeneity in the bulk material surface, loads could be adjusted for the measurement of mass/ volume of the bulk material inside the silo.
5. Well-timed discovery of the disproportionate build-up explained in number four, can circumvent the businesses the possible damages which can affect the silo walls and its surroundings or worse yet, prevent the possible collapse of overloaded silo walls.

3.3 Objectives

The specific goals of this study are enumerated as below.

1. Develop a numerical model (distinct element method simulation) of a silo filled with bulk material, by assigning the real material properties to the model parameters and, visually studying the dynamic (discharge) behavior of bulk material and the surface topographies throughout the simulation.
2. Monitor various model output parameters such as porosity, location, velocity, stress, contact and, unbalanced forces throughout the simulation and establishing correlation among these parameters wherever possible.
3. Validate the numerical model by means of a laboratory experiment by monitoring the discharge of a physical silo model with different materials.
4. Determine the difference in volume measurements of both materials using single point measurement, as opposed to multiple point measurements.
5. Identify important parameters affecting the error values in point measurements of bulk material in storage silos.

The current thesis is being performed for the aim of introducing an algorithm by which the volume of the bulk material in large silos can be calculated dynamically throughout the discharge. Once the results are obtained, 'level point measurements' in the numerical model are established. This is performed in order to validate the efficiency, as well as the accuracy of single point measurement technique which is most commonly practiced in industry using simple level sensing devices such as plumb-bobs.

Chapter-4

METHODOLOGY

4.1 Overview

Three different numerical models of silos filled with bulk material were designed for this thesis. The discharge processes were initiated in order to study the flow patterns, as well as topography geometries of bulk material surface. Numerous graphs including, particle velocities, location, stresses on the silo walls and more, were analyzed to establish a correlation among these factors with regards to optimal placement of level sensors in real-world industrial silos.

Later, the numerical models were validated both visually and numerically by a laboratory experiment set up. In the laboratory, a physical silo model's discharges were analyzed in order to validate the numerical models.

The volume measurement analyses were also performed both in numerical and physical models, in order to calculate the percentage error incurred in real-world single-point level measurements of bulk material in silos.

Finally, after calibration of some input parameters for numerical model, secondary runs of simulation models were performed in order to obtain improved results.

4.2 Model Development

In this thesis, three distinct numerical models were developed as a case study as follows;

1. A flat-bottom cylindrical silo filled with spherical particles (50000+) with mechanical properties of the Polyethylene plastics; the discharge design in this model occurred from center, at the bottom of the silo. In order to validate the accurateness of mechanical properties (such as stiffness, friction coefficient values) for those of Polyethylene plastic pellets, a numerical triaxial test (shear box test) was performed in order to validate the correctness of the values assigned to these particles.
2. All the design parameters in this model were exactly the same as the first one except, the discharge point was at the side (bottom), as opposed to the center.
3. For this model, the silo design was exactly the same as the first model, except that, instead of Polyethylene plastic, corn kernel properties were assigned to the spherical particles. Also, the dimensions of the particles were larger than those in models 1 and 2 and as a result, the number of particles filling the silo was smaller (about 14000+). Triaxial tests were not performed for corn kernels, as a number of studies have already validated the mechanical property values for corn particles and for this reason, in the current thesis these values were used directly as inputs to the model.

For all three models, various types of graphs were monitored in order to establish a better conclusion.

Pair-wise comparison of numerical results and laboratory results (volume measurements during discharge at different stages) were used for the validation procedure for the models.

4.3 Description of Running the Simulation Package

Particle flow code in 3-D (*PFC3D*), a proprietary discrete element method simulation of Itasca Company, was utilized for this thesis. This software package requires writing specific codes in *PFC* and *FISH* languages for running. The codes can be read by *PFC3D* either as a text file or in a batch processing fashion by writing every command in the command line of the package.

The codes for this study were written for dynamic discharge of silo models along with numerical triaxial test for Polyethylene plastics. Inputs for the specific models were given such as viscous damping ratio of system, wall and particles stiffness and, particles bulk density, to name a few. Then the model was run in discrete fashion (time-steps) once appropriate gravitational acceleration (g) and other parameters necessary for the model were assigned.

The output of these DEM models included visual monitoring of bulk material flow, as well as many other useful graphs enabling the study of factor value changes (such as velocity of specific particles, mean unbalanced force between particles). Additionally, the volume of remaining material in the bin can be calculated at any point during simulation when using the software program.

4.4 Validating the Numerical Models by Laboratory Experiment Procedures

A prototype cylindrical bin (with specific height and diameter) model was considered for the purpose of the simulation model validation. Aspect ratio D/H was maintained in the physical model the same as in numerical one, in order for the scaling between two models would be applicable. After the initial filling stage (with Polyethylene plastic

pellets for the first two models and later corn kernels for the third one), the discharge processes were initiated from bottom center or side, depending on the specific design. A rectangular window facilitated observing the discharge process and taking multiple photographic snapshots were taken throughout the grain discharge.

4.5 Actual Procedure

By following an initial theoretical model, operating based on real values and obtaining relevant results, the model outputs were compared to values with the real-life system behaviors and then the numerical model parameters were readjusted followed by retesting such that the behavior of the numerical test complied with that of the real one.

This method was named as ‘progressive readjustment’ or, ‘micro-parameter calibration’. because the real micro-parameters properties can only be arrived at by applying a number of minor modifications in macro-parameters of the model. The approach taken in this thesis research was the predictive design analysis.

Following the completion of discharge processes both for numerical and laboratory models, the comparison was made between the results in order to check the accuracy of numerical model as being able to predict the real-life silo discharge processes. This was performed by visual comparison of surface pattern and, volume measurement of bulk material at different points in all the numerical and physical models.

After this stage, the values of some parameters were changed (when necessary) and then the calibrated numerical models were run for a second time as an interactive approach in order to obtain improved results.

4.5.1 Brief Overview of Elements to be Considered in Particle Flow Code 3D Model

4.5.1.1 Spherical Elements Resembling Granular Particles

Particle Flow Code *3D*, was a distinct (discrete) element method simulation software. This software, being similar to most DEM software solutions, represents particles as spherical objects with specified friction coefficients, densities and other micro/macro properties assigned by the users. The circular particles are stiff while the contacts have flexible properties. Therefore, the output of a system could be investigated by modifying the input parameters within the element and contact stages and, the granular system behavior was obtained by design from the contact model and its corresponding attributes.

Particles are each automatically given a distinct *ID* number so that these particles can be tracked throughout the simulation; for instance, the vertical velocities, locations in specified coordinates, stress states and interaction forces, could be graphed for the particles and later be analyzed by history commands.

4.5.1.2 Boundary Conditions of the Model (Walls or Sheets of Particles)

The *PFC3D* makes use of wall logic as boundary conditions applied to the model of interest. These walls could be generated at any dimension with any shape including the planar, finite, infinite, or general walls (cylindrical or disc).

Once a wall was created with desired dimensions, its mechanical properties such as stiffness as friction coefficient values can easily be ascribed in the command line of the software. The wall material was selected as corrugated metal for this study.

4.5.1.3 Initial Condition of the Models

The initial condition for the models was considered particles at rest, filled up to 75 percent of the vessel's height. This state of static was achieved by cycling the generated particles inside the vessel until their kinetic energy value (from the interaction forces and to some degree, the locked-in stresses between particles) converges to a value close to zero. When the unbalanced forces come close to a nonzero value, it was a sign that incessant movement of particles was taking place within the model. Since DEM software packages work in a time-marching fashion, *PFC3D* automatically calculates a stable time-step (discrete) for every model which stays constant (unless an external disturbance was added to the model) throughout the simulation.

4.5.1.4 Porosity Considerations

Desired porosity and required particle number trade-off must be carefully considered; “the standard objective in creating an irregular packing was to fill a given space with particles at a given porosity, and to ensure that the assembly was at equilibrium” (Itasca, 1999). As a solution for this issue, one can generate the specified number of particles within a vessel and then multiply the radius of these particles by a constant value (radius expansion method). Thus, in this case, the number of particles remains constant but the porosity increases or decreases according to the constant being larger or less than unity. All the cited issues have to be considered carefully and if necessary, a couple of models should be run in order to ensure that the model was able to reliably predict the actual system.

4.5.1.5 Contact Representation for the Models

Linear contact model was considered for all the designs. This model includes contact-bond behavior and provides sliding behavior with constant stiffness.

4.5.2 Laboratory Experiment for Validation and Calibration Purpose

A cylindrical bin was used for actual discharge process observation. Two kinds of grains were considered for this experiment namely, polyethylene plastics and corn. For measuring the surface level of the material in the silo, a laser level sensor device was utilized.

Chapter -5

RESULTS

5.1 Development of Numerical Models -Background

The exact replication of granular material behavior is not straightforward. Finite element method simulation attempts in modeling granular particles lacks accuracy because continuous simulation techniques boundary conditions are assumed fixed. The issue of inflexible boundary condition was solved with distinct element method (DEM), as it assumes a discontinuity in the state of stresses between granular particles.

Granular particles have a discontinuous structure within the space they occupy which was gauged by the porosity number (or average bulk density) that calculates the ratio of the free space between packed particles to the total space in which they reside. Thus, granular stress as well as pressure studies should be performed so that a relationship between stress values and uneven surface topographies to be determined.

Granular particles such as different types of grains, coal, and rocks were considered as neither fully solid, nor liquid and, as a result, the stress state calculations were adjusted as an average value across a given space occupied with bulk material. “Information on stresses, properties and discontinuities for granular material can only be known to some degrees at best and the concept of stress in a discontinuous medium is different from that in a continuum one” (Itasca, 2009).

In granular material flow studies, the random distribution of particles pattern, which almost always shows irregularities, was not fully quantifiable.

Since the real-life study of granular material behavior and its resultant stress analyses are difficult, the numerical model of this thesis used to determine the most significant factors influencing the pattern of the particles assembly. The issue of lack of knowledge in understanding the mechanisms shaping the grains behavior stems from data scarcity in ethanol plants and grain storage industries. It is generally difficult to have access to the far-reaching regions of a silo for measurements or even taking a 3D photographs within a large silo (because of dust and lack of light).

A numerical laboratory setup for study in order to observe the grains behavior, as well as changes arising from different mechanical properties of granular material was established.

The Iterative approach was opted for the models of this study. In Table 5.1 below, a range of modeling situations faced by researchers in geo-engineering depending on the degree of data availability, is given (Itasca, 1999).

Table 5.1 General spectrum of modeling situations (Itasca, 1999).

Typical situation	Complicated geology; inaccessible; no testing budget	← →	Simple geology; \$\$\$ spent on site investigation
Data	NONE	← →	COMPLETE
Approach	Investigation of mechanisms	← * Bracket field behavior by parameter studies * →	Predictive (direct use in design)

The *PFC3D* (*Itasca™*) can be utilized both in a fully predictive model and, as a numerical laboratory setup if so needed. The approach taken in this research was the predictive design analysis.

In order to verify a certain laboratory results of a bulk material, it was essential to perform some numerical tests that imitate these test results. Later, adjusting certain input model parameters up to the moment the numerical results conform to those of the physical model continued. Once these modified values were obtained through trial and error then these improved parameters were used as input for the DEM simulation system. Moreover, for the purpose of reducing simulation efforts, a couple of tests on the extreme values were performed and then proper values could be estimated via linear interpolation.

The detailed results of these experiments (experimental and numerical) are also given in this chapter.

5.1.1.1 Model I-Plastic pellets, center discharge

For this study, a cylindrical flat-bottom silo was designed (by writing specific codes in *PFC3D* language). A sketch of this numerical design is given in Figure 5.1 and this container model was used for all three models.

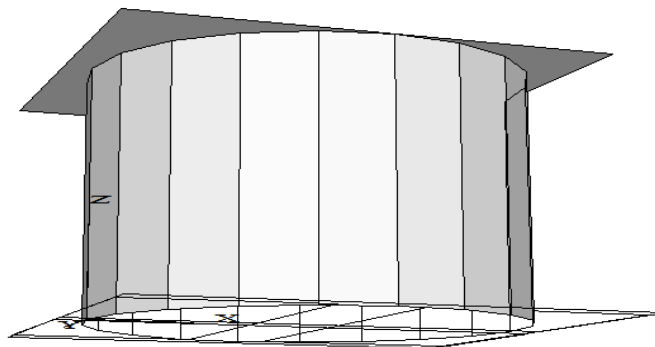


Figure 5.1 Cylindrical container model used in the study, with its top and bottom walls centered at $X=0.8$, $Y=0$ and, $Z=0$ meters. A specific wall at the center bottom or side bottom serves as discharge gate, depending on the design.

This model was created with 5000+ circular particles located in a cylindrical wall with a diameter, D , of 1.6 meters and height of 1 meter. At the bottom of the cylinder, 5 planar walls were added to contain the particles. One of these walls (at the bottom center) is removed later for the gravity-induced discharge to happen. The location of this single discharge point is at the center of the silo bottom; this discharge portal is a $0.04m \times 0.052m$ rectangle. Colored particles were used to represent layers for better interpretation of the flow pattern.

The normal and shear stiffness values were assigned to the particles and walls at the same stage. The values used for this model are summarized in Table 5.2.

These values were obtained by direct measurement or calibration methods by performing numerical triaxial test and validated for polyethylene plastic.

Once the boundaries (walls) and particles in it were generated, a viscous damping of 0.6 was considered in the model in order to dissipate the energy of the particles while cycling.

Table 5.2 Material Properties used in the numerical model 1.

Properties	Values
Particles Normal Stiffness , K_{np} [N/m]	0.5×10^6
Particles Shear Stiffness, K_{sp} [N/m]	0.5×10^6
Particles Friction Coefficient , μ_p	0.25
Particles Density, ρ_p [Kg/m ³]	1210
Particles Poisson's Ratio, ν_p	0.40
Viscous Damping Ratio, ζ	0.60
Walls Normal Stiffness, K_{nw}	1×10^8
Walls Shear Stiffness, K_{sw}	0.5×10^8
Walls Friction Coefficient, μ_w	0.2

In Figure 5.2, an image of cylindrical vessel filled with particles can be seen.

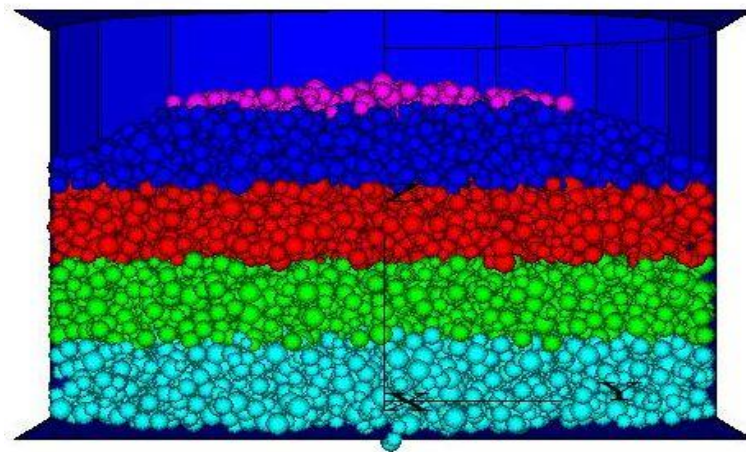


Figure 5.2 Model 1-plastic pellets, center discharge (; a cylindrical container filled with circular particles (resembling polyethylene plastic) of radii distributed uniformly

5.1.1.2 Model 2-Plastic pellets, side discharge

The side discharge model had the grains discharging from corner-bottom instead of center. A picture of discharge point location for this model is given in Figure 5.3 as seen from the bottom of the silo

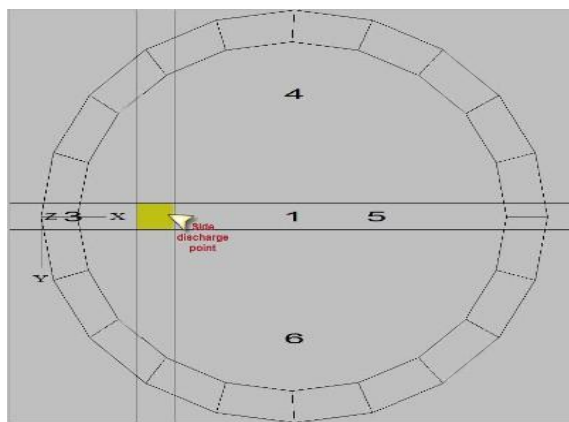


Figure 5.3 Side-discharge point, seen from the bottom of the silo.

5.1.1.3 Model 3-Corn kernel, center discharge

This model was created with 14500+ circular particles located in a cylindrical wall with a diameter, D , of 1.6 meters, and height of 1 meter. At the bottom of the cylinder, 5 planar walls were added to contain the particles. A rectangular flat wall (serving as discharge point) was removed later so that the gravity induced discharge occurred. The location of this single discharge point was at the center of the silo bottom; its dimensions were also $0.04m \times 0.052m$. Colored particles were used to represent layers for better interpretation of the flow pattern.

Particle size was chosen so that they equal the longitude value of the ‘tear-shape’ clumps proposed by Coetzee et al., (2006), however in this study the clump logic was not considered. The (initial) values chosen for the corn were particles with diameters uniformly distributed between 0.008 to 0.012 meters. As a reference, a depiction of real corn kernel is given in Figure 5.4.

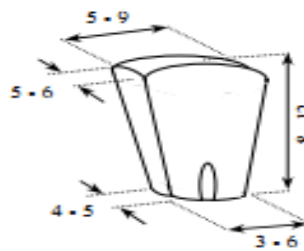


Figure 5.4 Physical corn grain dimensions in mm

(Coetzee et al, 2006).

The normal and shear stiffness values were assigned to the particles and walls at the same stage. The values used for this model are summarized in Table 5.3. These values have been obtained by direct measurement or calibration methods (triaxial test) before and

validated for corn. The irregular shape of some particles renders direct measurement techniques somewhat infeasible. “Direct measurement methods allow the value of a property to be obtained independent of the characteristics of the contact model” (Montellano et al, 2011).

By developing a code, particles were generated so that the initial target porosity of 0.50 was achieved. This code written in FISH programming language, automatically reiterated the generation of particles until the target porosity of the sample within vessel was achieved (by making use of radius expansion algorithm). The principle methodology is briefly described here:

Porosity is defined as; $n = 1 - V_p/V$, where V_p is the sum of all particles' volume and V is the volume of the vessel. Therefore, one can rewrite the following equalities;

$$nV = V - \sum \frac{4}{3}\pi R^3 \quad (\text{Itasca, 1999})$$

$$\sum R^3 = 3V(1 - n)/4\pi$$

Now, assuming that n_0 is the initial porosity and R_0 initial radii, one then can write;

$$\frac{\sum R^3}{\sum R_0^3} = \frac{1 - n}{1 - n_0} \quad \text{and} \quad m^3 = \frac{1 - n}{1 - n_0} \quad (\text{Itasca, 1999})$$

Finally the radius multiplier, m (the constant by which the initial radii of all spheres should be multiplied by so that a certain target porosity can be reached in the container) can be calculated by

$$m = \left(\frac{1-n}{1-n_0} \right)^{\frac{1}{3}} \quad (\text{Itasca, 1999})$$

The code that was written based on the equation, reiterates the calculation process in an algorithm until the target initial porosity of 50 percent was achieved. Of course, the size of the spherical particles were increased or decreased depending on the available space they fill and this caused a lack of control in assigning specific particle diameters. In the trade-off between porosity and radii, the particle size was compromised in this model. This method is called the automatic radius expansion method. In Figure 5.5, it can be seen that the particles appear larger than in the first two models, yet the porosity requirement was fulfilled by this densely packed model in the last one.

Table 5.3 Material mechanical properties used in the corn numerical model.

Properties	Values
Particles Normal Stiffness, K_{np} [N/m]	4.5×10^5
Particles Shear Stiffness, K_{sp} [N/m]	4.5×10^5
Particles Friction Coefficient, μ_p	0.30
Particles Density, ρ_p [Kg/m ³]	820
Particles Poisson's Ratio, ν_p	0.55
Viscous Damping Ratio, ζ	0.6
Walls Normal Stiffness, K_{nw}	1×10^8
Walls Shear Stiffness, K_{sw}	0.5×10^8
Walls Friction Coefficient, μ_w	0.2

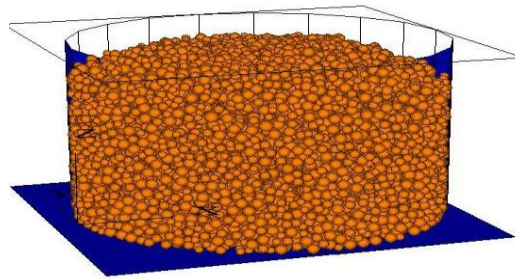


Figure 5.5 Model 3-Corn grains, center discharge: Cylindrical container filled with circular particles with an initial porosity of 0.50.

5.2 Running of the Simulation Models

5.2.1 Specific Procedures

After two hundred thousand complete simulation trials (time-steps) for each simulation model using the software, the models reached their initial resting stage where the dynamic as well as unbalanced locked-in forces between particles were considered very small. This can be inspected visually in the snapshot images taken from certain times during simulation as the particles settle down without considerable spaces among them. Subsequently, a number of cycling was performed in order for the particles to interact with each other (without including the gravitational or frictional forces of the walls or circular particles surfaces. This means that only contact forces were activated once stiffness values at this initial cycling stage were assigned.

Once more, after about a couple of hundreds more cycles (which are the number of events per time unit), friction coefficients, along with the gravity force were also included in the model.

At this stage, the system simulation was cycling within the enclosed cylinder until the ratio of maximum unbalanced forces between particles and maximum contact force values (mechanical ratio) converges to at least 0.001, or less.

The convergence of the mechanical ratio value to approximately zero was an indication of the particulate system being at the rest, meaning that the total resultant energy of the contact forces among particles had reached a negligible value.

5.2.2 Specific Results from Three Simulation Models

5.2.2.1 Model 1- Center Discharge of Polyethylene Plastic Pellets

The simulation started when the discharge gate in the bottom of the silo was removed. In Figure 5.6 this initial state can be seen.

Velocity intensity profiles, as well as the displacement vectors for the particles, are also given in Figures 5.8. As the plastic pellets move downward due to the gravitational force, their velocities also were affected. By examining the pictures of velocity and displacement vectors, one can see that only the upper portion and more specifically, the surface of the granular material had acceleration, since most of the assembly was stagnant just before the discharge.

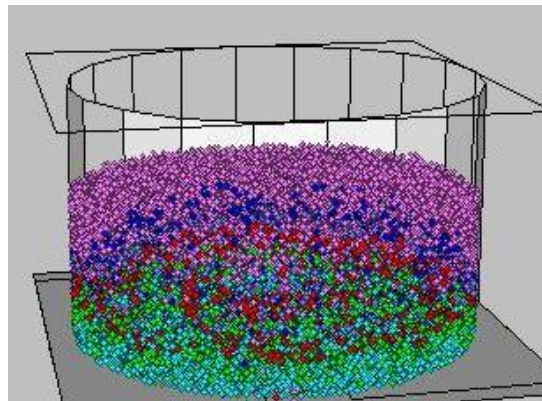


Figure 5.6 Initial contour state of center-discharge process.

The intensity of contact forces among particles and particle-wall can be accessed using *PFC3D* software. This is given in Figure 5.7.

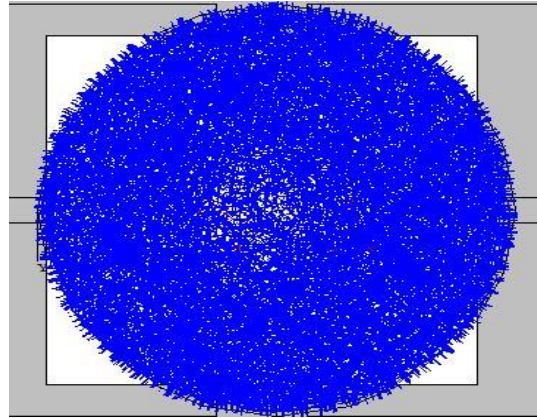


Figure 5.7 Contact forces as seen vertically from bottom.

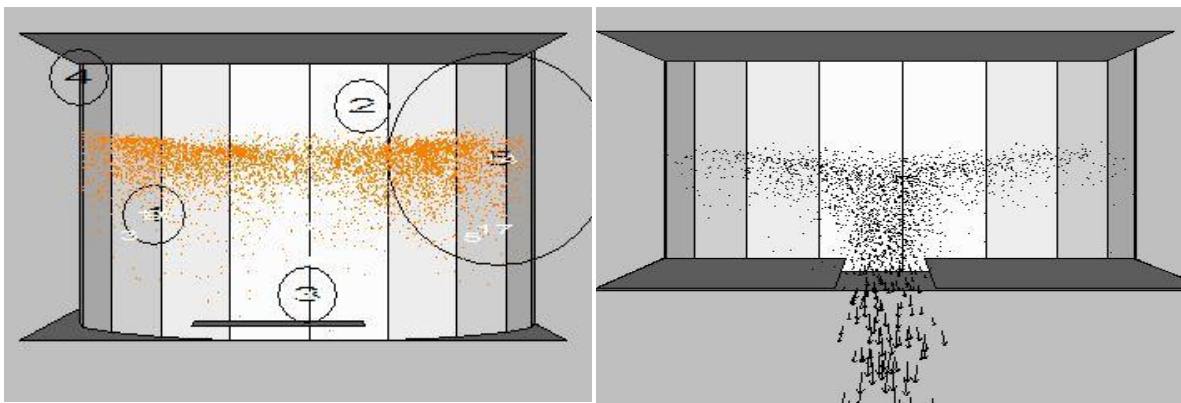


Figure 5.8 Initial velocity vectors (left) and, displacement vectors (right) – plastic pellets, center discharge

The strength of the chain forces was smaller in the center area of the bin shown in Figure 5.7 and due to the lack of friction between wall and particles caused by the center draw-point.

After about more than 2 million time steps trials of the simulation (discrete force-displacement calculation increment), some bulk exited the system, leaving the surface shape of the material more concave. This can be seen in Figure 5.8. The velocity as well as displacement vectors are given in Figure 5.9.

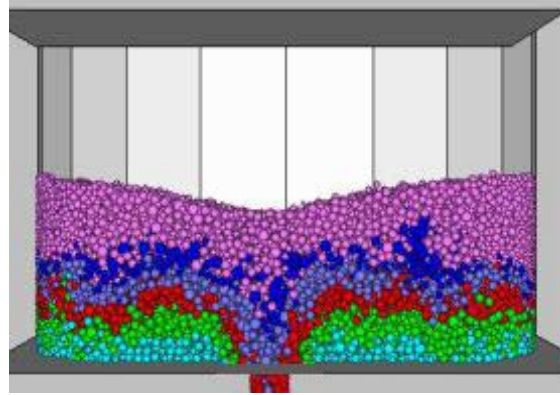


Figure 5.9 Contour state of center-discharge process well into discharge progression.

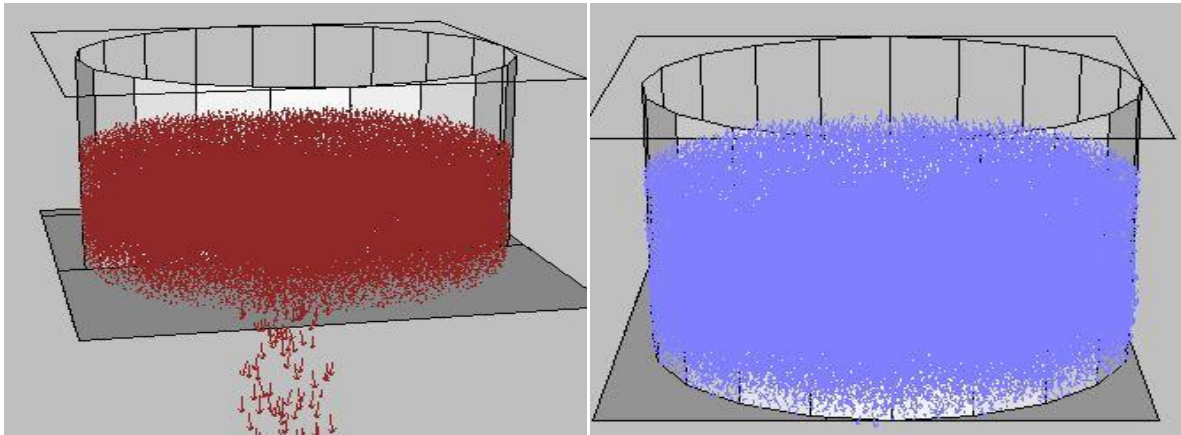


Figure 5.10 Velocity vectors (left) and, displacement vectors (right) well into discharge progression.

The contact forces at this point in the simulation are depicted in Figure 5.11.

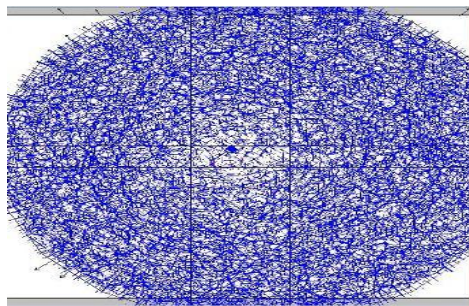


Figure 5.11 Contact forces as seen vertically from below at the middle of discharge process.

A closer look at above Figures indicates relatively higher velocities closer to the central axis, when compared to those closer to the walls. This is due to the proximity of discharge gate to the particles located closer to the central axle, as these particles can more freely flow out of the system because these spheres cannot bear wall friction forces. Finally, after about 2.6 million time steps, most of the grains exited the system with only a few remaining inside, and this part of simulation was therefore concluded. Figure 5.12 demonstrates this condition. Also, the velocity and displacement vector representations are provided in Figure 5.13.

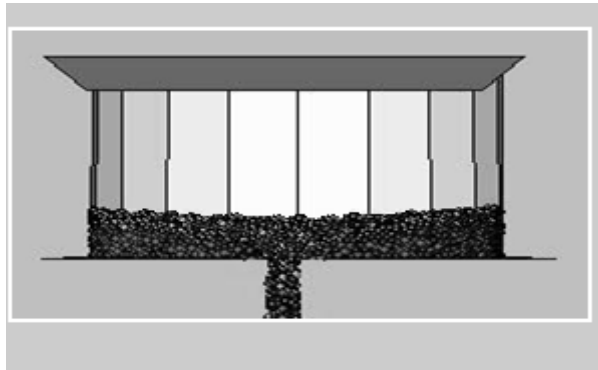


Figure 5.12 Contour state of center-discharge process in the end of discharge.

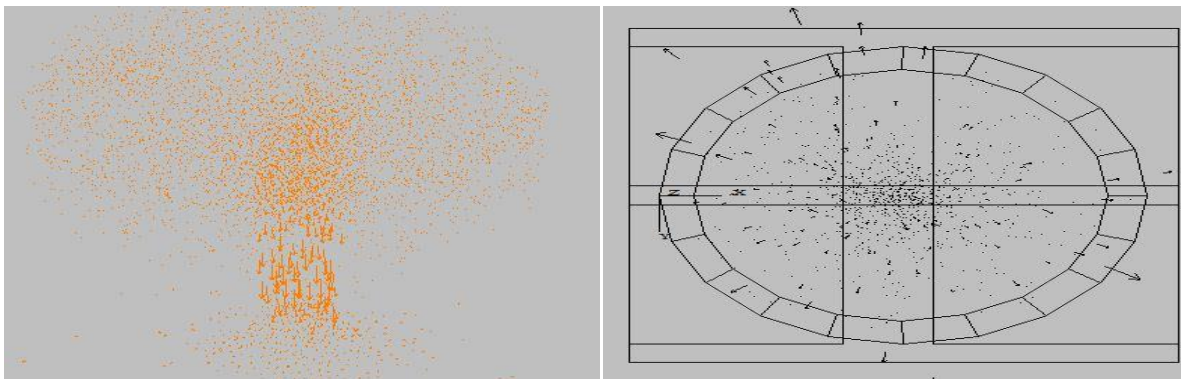


Figure 5.13 Velocity vectors (left, as seen from below) and, displacement vectors (right, as seen from bottom) in the end of discharge process.

Overall, the surface topography throughout the discharge simulation leaves the traces given in

Figure 5.14, as seen from side cross-section. It is discernible that surface region in the middle of the silo has a much sharper decline in level through the time than have the regions closer to the side walls since, this is a center discharge process.

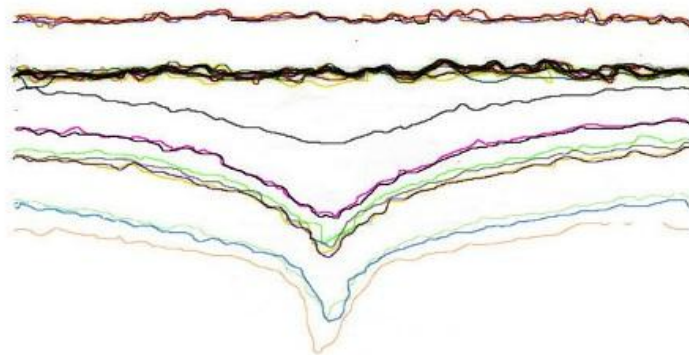


Figure 5.14 Surface topography decrease traces through center discharge process.

5.2.2.2 Model 2- Side Discharge of Polyethylene Plastic Pellets

All the graphical analyses performed for center discharge in the earlier part, were also performed on the silo discharge system. In Figure 5.15, an initial stage of flow for the side discharge simulation is given.

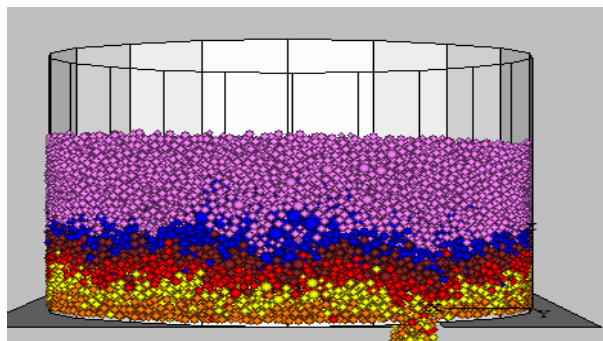


Figure 5.15 Initial stages of side-discharge of the silo.

The velocity and displacement vectors for this initial stage are also provided in Figure 5.16.

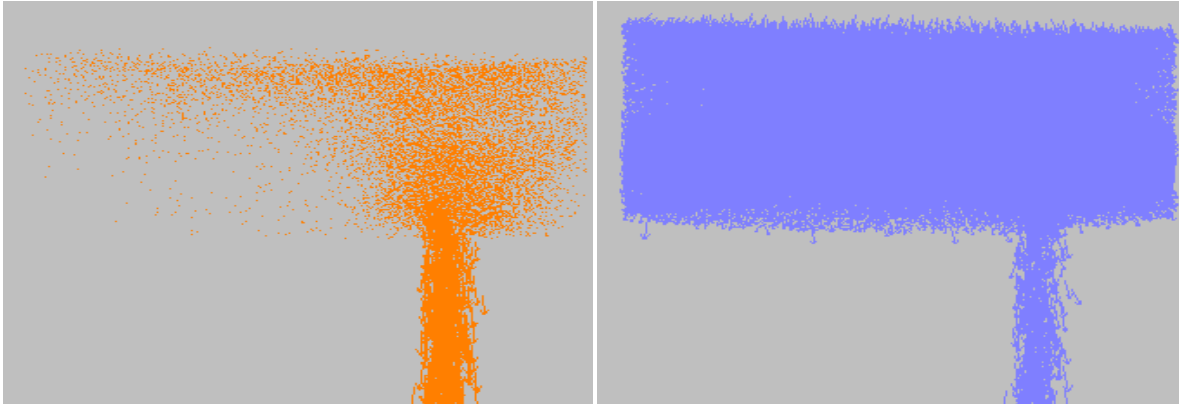


Figure 5.16 Velocity (left) and displacement vectors for initial stage of side discharge (right)

It is easily recognized from pictures that the particles in the side region have higher velocities, as the discharge was located in the side part (dense vectors in the right side). The particles in the other side virtually do not move in this early stage of discharge.

After more than 2 million simulation time steps, the discharging silo resembles the one in Figure 5.17 below.

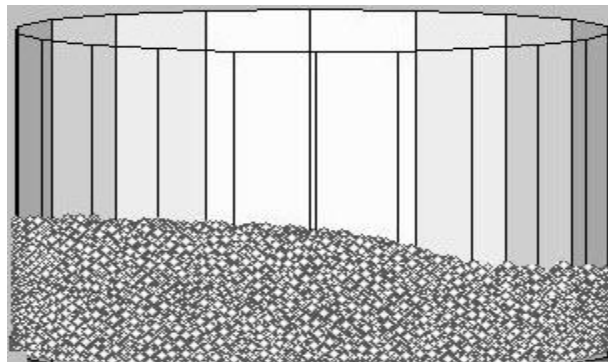


Figure 5.17 Midway through side discharge process of plastic pellets.

And the velocity as well as displacement vectors for particles are provided in Figure 5.18.

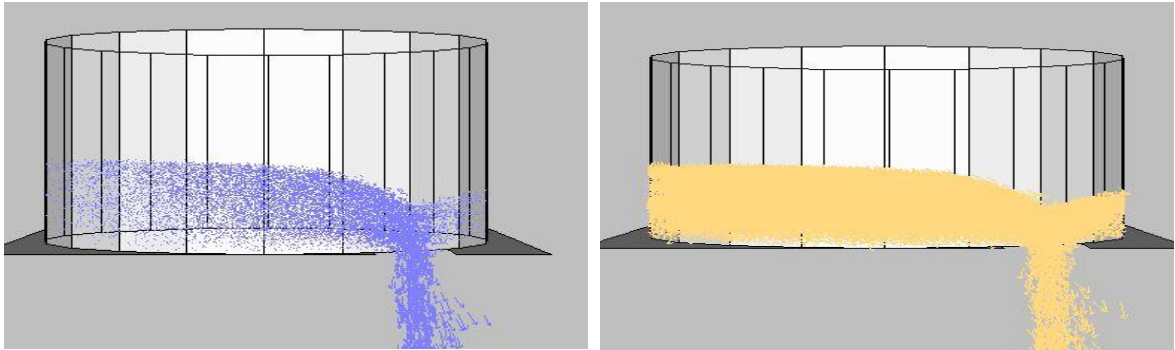


Figure 5.18 Velocity (left) and displacement vectors (right), for half way through side discharge of plastic pellets.

Again, one can spot larger vector density in the right side, indicating higher velocities and bigger displacements in the region closer to the discharge gate.

In the last section, the discharge process comes to an end, which is given in Figure 5.19 velocity and displacement vector schemes for the end part of discharge are provided in Figure 5.20 as well.

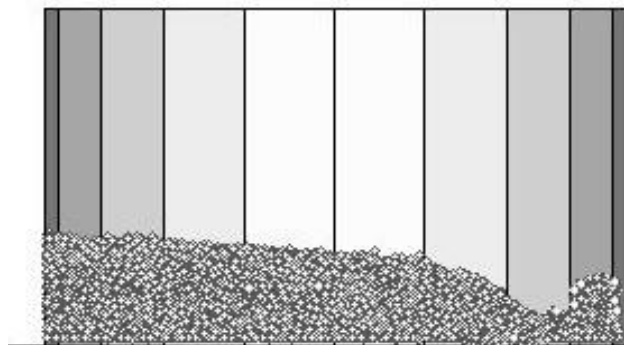


Figure 5.19 Final stages of side discharge of plastic pellets.

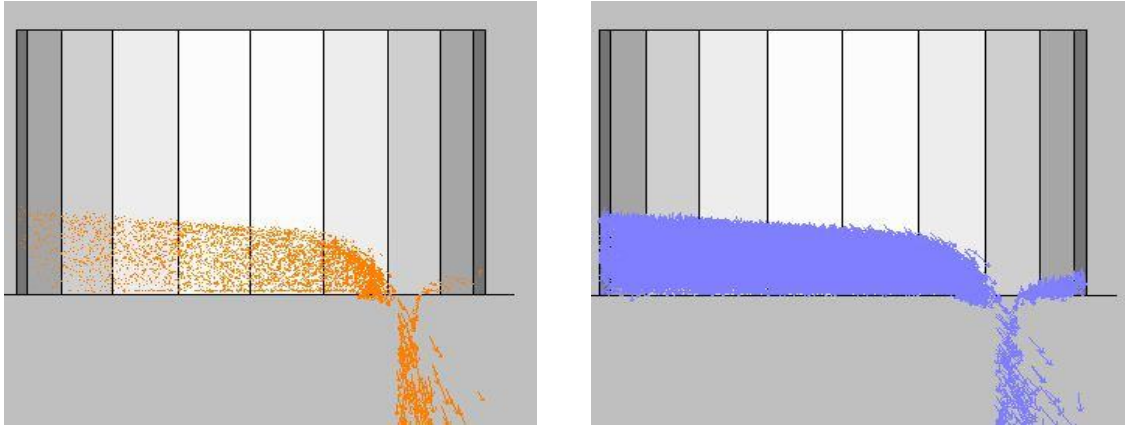


Figure 5.20 Velocity (left) and displacement vectors (right), for final part of side discharge of plastic pellets.

Overall, the surface topography during side discharge simulation leaves the shape given in Figure 5.21 as seen from side cross-section. One can detect that surface region in right side of the silo has a much sharper decline in level through the time than one has in left or center side.

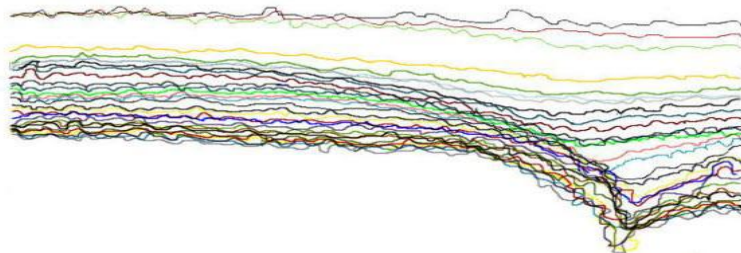


Figure 5.21 Surface topography decrease through side discharge process.

5.2.2.3 Model 3- Center Discharge of Corn with Initial Porosity of 0.50

Figure 5.22 shows the initial stage of the simulation in which the particles were resting inside the bin with a noticeable higher angle of repose at the peak. Additionally, the dark

region in the middle of the pack characterizes the contact forces among particles at rest, with ticker line being an indication of larger locked forces. Notice that the dark region was not present on the free surface of the pack.

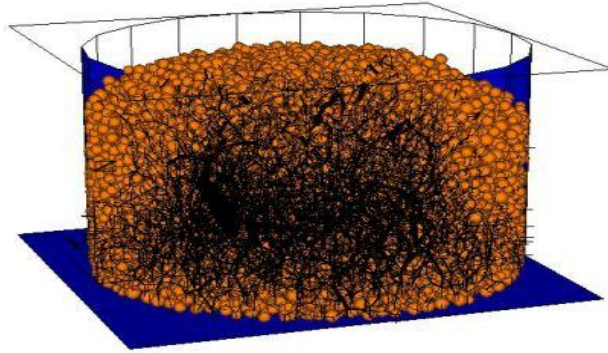


Figure 5.22 Initial stages of corn center discharge course.

Once the simulation started with removing the center gate at the bottom, the initial stages of velocity, as well as displacement vectors of particles could be monitored. This is presented in Figure 5.23.

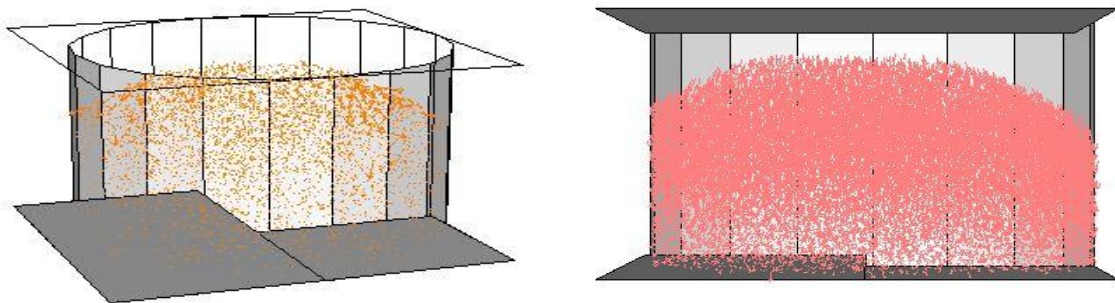


Figure 5.23 Velocity (left) and displacement (right) vectors for initial stage corn discharge.

By studying the patterns in Figure 5.24 above, again, one may notice that velocity of corn particles was higher in the upper levels, closer to surface. As for displacements, the

values seem to be of equal values in the center parts, while slightly stagnant closer to the side walls.

After approximately 1.75 million time steps towards discharge, the topography of the corn inside the bin looks like the picture given in Figure 5.24.

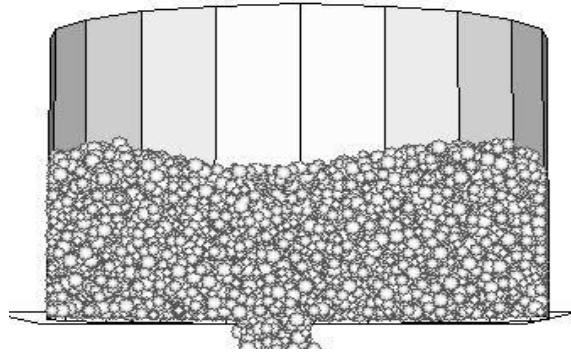


Figure 5.24 Remaining corn particles in the bin halfway through discharge.

The contact force graph at this stage is given in Figure 5.25 below; it is evident that wall-particle contacts at the base were larger than particle-particle contact forces.

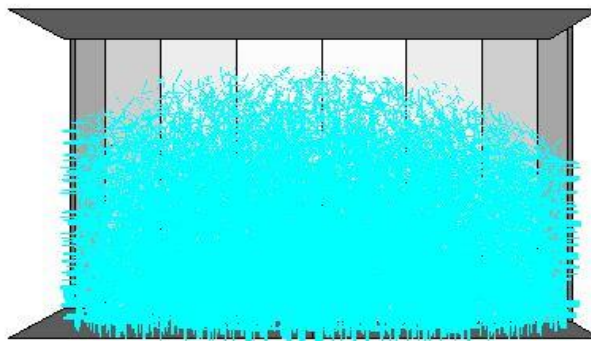


Figure 5.25 Contact forces halfway through discharge of corn particles.

Velocity and displacement state at this moment is provided in Figure 5.26. The contact forces at this stage can be seen in Figure 5.27.

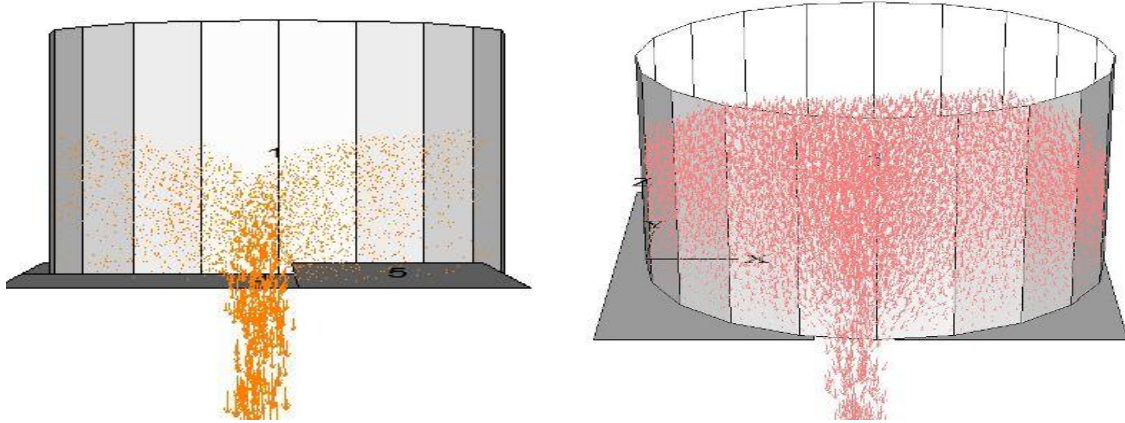


Figure 5.26 Velocity (left) and displacement (right) vectors of corn particles halfway through discharge.

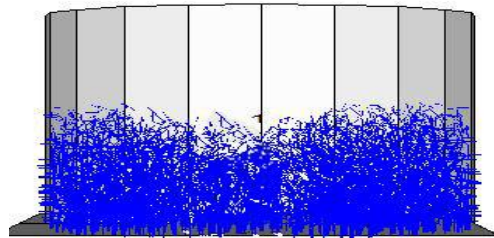


Figure 5.27 Contact forces for the final stage of corn discharge.

Lastly, the discharge process practically finishes when the particles no longer exit the bin (particles located at the side bottom region), the scheme of this stage is displayed in Figure 5.28.

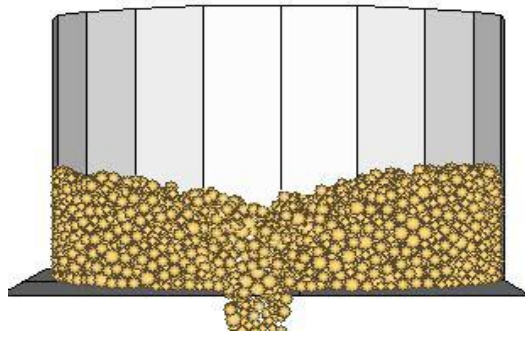


Figure 5.28 Final stage of corn discharge simulation.

Velocity and displacement of particles at this stage is displayed in Figure 5.29 below.

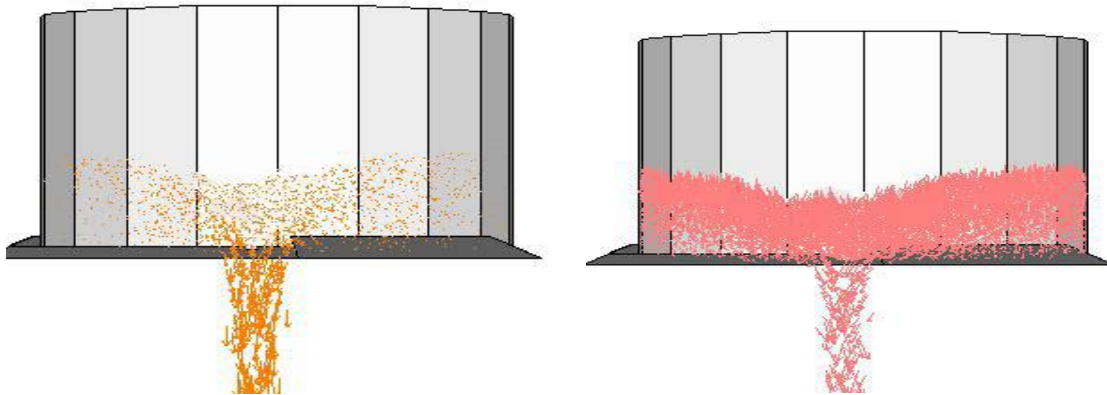


Figure 5.29 Velocity (left) and displacement (right) vectors at the final stage of corn discharge.

5.3 Laboratory Study Procedure

5.3.1 General Description

A physical silo model was used for the purpose of the model validation. This cylindrical silo has a diameter of 19 inches at the base and height of 23 inches. The silo was filled approximately half of the height with material. Aspect ratio D/H of 1.6 was preserved in the physical model as in the numerical one, so that the scaling between two models would be acceptable. Both the numerical and physical models were cylindrical with a symmetric

axle in center (imaginary). The model has a rectangular shaped window in its side so that, observing the material discharge and movements associated with it and taking photographs at certain points throughout the discharge process was possible. A picture of the model could be seen below in Figure 5.30.



Figure 5.30 Model silo used for validation.

It is clearly seen in the above picture that, at various locations along the window, the maximum height for the corresponding initial filling levels for the three models were marked in red stickers. Also, in order to facilitate level measurement process from the top of the model silo, the top cap, a circular transparent sheet of plastic, was marked at several locations so that, the matching coordinates between the numerical design and the physical model could be achieved. In Figure 5.31 the picture of the top cap, as seen from above, is given.

Once the coordinates (X , Y , and Z) were designated for the physical silo, the bottom part of the silo which was a flat circular part containing different sliding mechanisms was installed. These sliding mechanisms would serve as discharge points. For this study, the

center gates, as well as the outermost rectangular discharge points were used for experiment. A photograph of the discharge mechanism is given in Figure 5.32 as well.

The location of the discharge gates in the model can be seen in Figure 5.33.

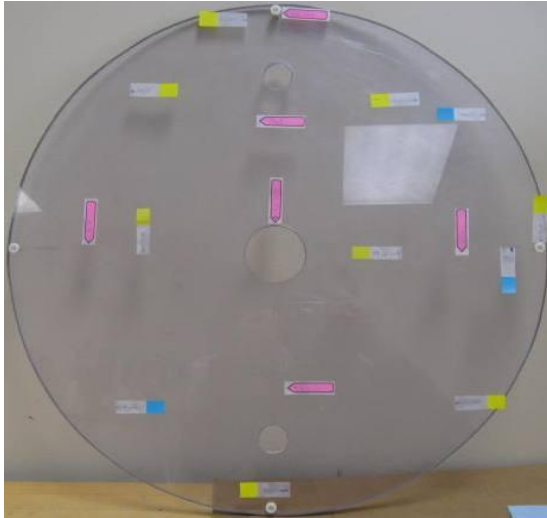


Figure 5.31 A picture of the silo model lid with coordinates marked at different locations.

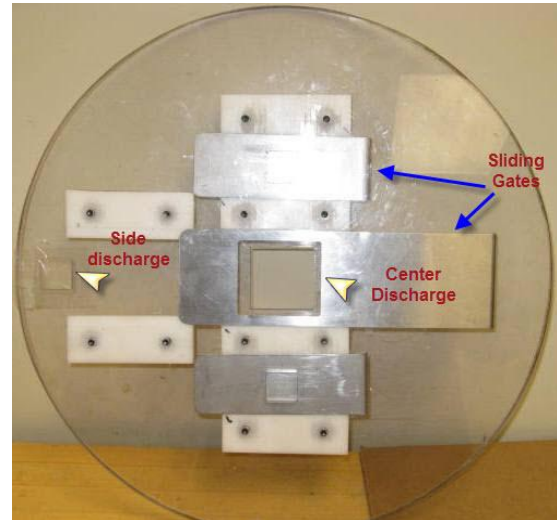


Figure 5.32 Discharge gates at the bottom.



Figure 5.33 Discharge mechanisms at the bottom of the model.

For measuring the surface level of the material in the silo, a laser level sensor device was utilized. The level sensor was positioned vertically over the pre-marked coordinates on the top cap and then by moving it to different points, the distance between the device and the maximum surface level was measured and recorded. The picture of the device is given in Figure 5.34. The silo was filled with polyethylene plastic particles, thereafter with corn kernels and their ensuing discharges were studied.



Figure 5.34 Laser level sensor device.



Figure 5.35 Polyethylene particles discharging out of the system.

5.3.2 Discharging Process

Starting from an initially full tank (according to the maximum heights for the center, side and corn discharge which are 8.1, 6.75 and 10.2 inches respectively), the discharge gate was slide open to allow material to flow out of the silo. The grain flows were suspended at various times according to the discharge rate (weight of exiting material per second), in order that this time matched up with the exact time, when the weight of the exiting material in the numerical model equaled that of the physical model. The material weight also was scaled in physical model according to the 'squared diameters ratio times heights

ratios between numerical and physical models' proportion' for comparison in validation. This expression is given in Equation 5.1 (The scale obeys the cylindrical volume formula of $\pi r^2 h$, which means the radii ratio squared times the heights ratio in the discharge rate expression; $\rho \cdot v/t$).

$$\left[\frac{D_{nm}}{D_{pm}} \right]^2 \times \frac{H_{nm}}{H_{pm}}$$

Equation 5.1

At every stoppage throughout discharge process, the surface levels of remaining material in silo were gauged with the laser sensors at the designated points on the lid. These data were also obtained with two distinct techniques for the numerical counterpart for the comparison; one method follows the experimental process, the other one takes into account the remaining number of particles in silo at the distinct interval and, the average porosity value associated with it. The volume of the remaining material at every stage was calculated with the inclusion of the height as being the average values of the records obtained by the sensor device. These processes were repeated for the three models (center discharge, side discharge for plastic and, center discharge for corn). The ρ value was the average bulk density of grains, which can be obtained from literature for the prototype, and was substitute in numerical model for its associated porosity value.

A sketch of fundamental volume measurements at specific time periods during laboratory discharge can be seen in Figure 5.36.

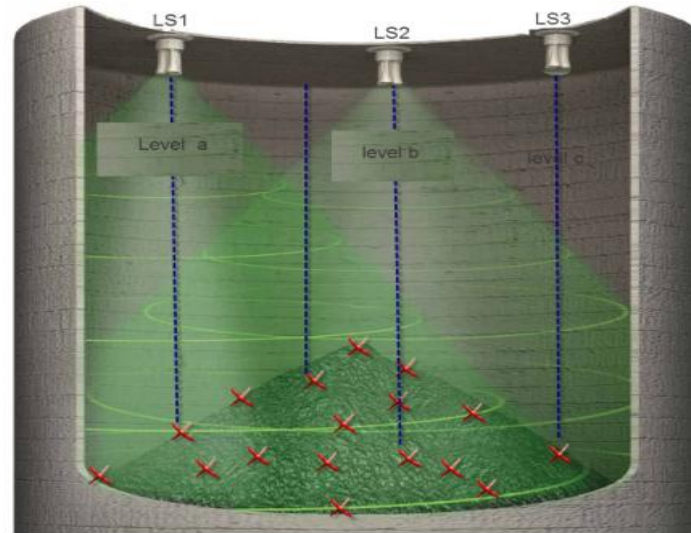


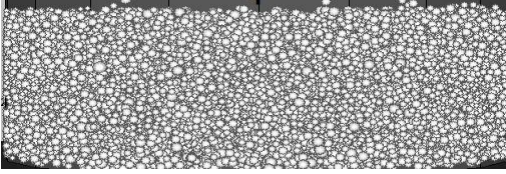

Figure 5.36 Random measurements of point levels for granular pack.

5.4 Comparing Simulation and Laboratory Results

5.4.1 Model 1- Center Discharge of Polyethylene Plastic Grains

Visual Comparison

For model 1, the contrast was made at intervals of 9, 15, 20, 24 and 27 seconds into discharging. At these specified intervals, the numerical simulations, as well as laboratory test discharge processes were halted temporarily in order to assist in detecting similarities. A couple of pair-wise comparisons are given in Figure 5.37. By studying the pictures, one can detect strong resemblance between the numerical and laboratory results, however, since a scale factor had been included, there were visible differences dimension-wise (height and width of the granular pack).

Time	Numerical Simulation	Laboratory Discharge Model
9 sec.		

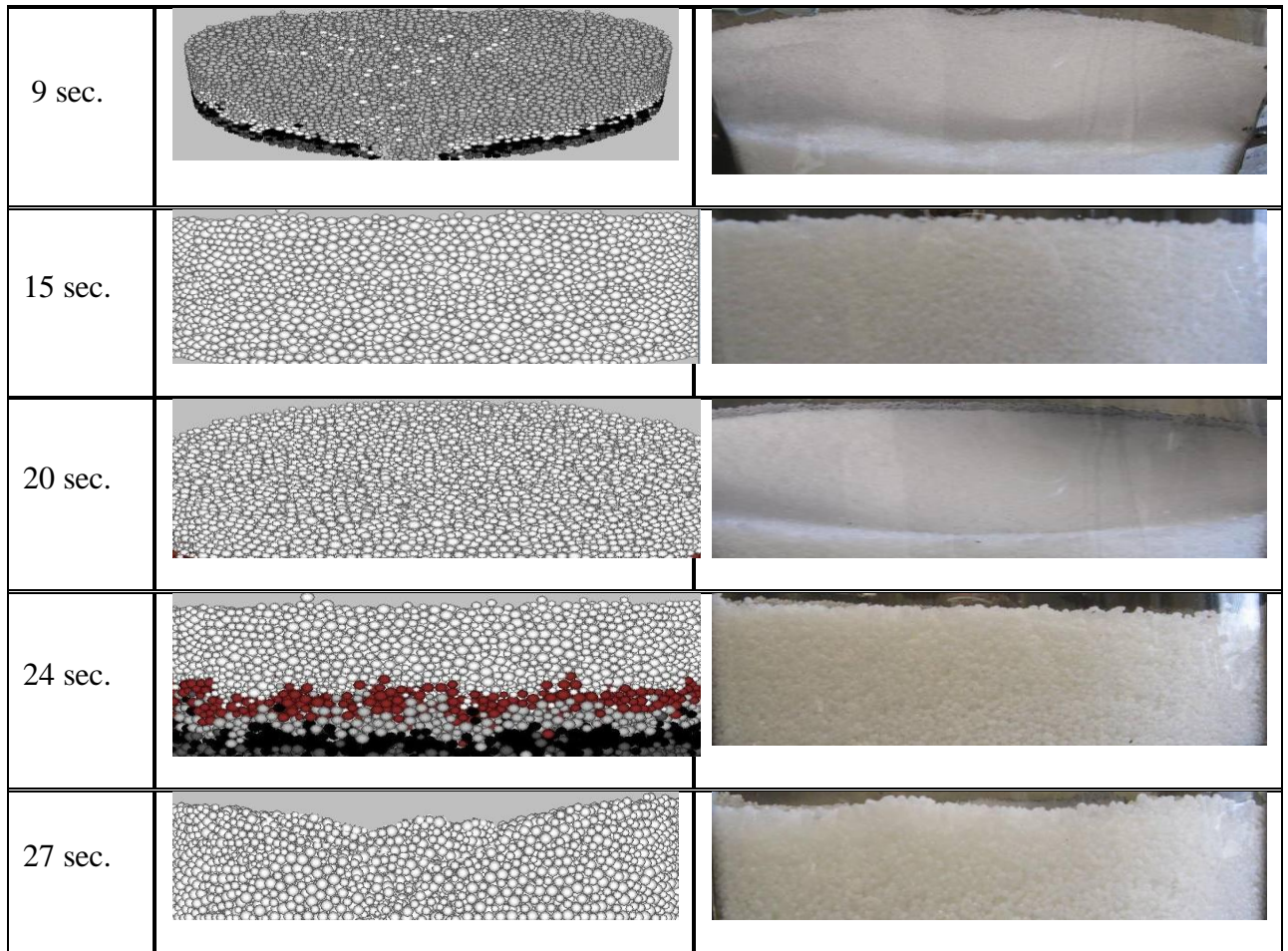


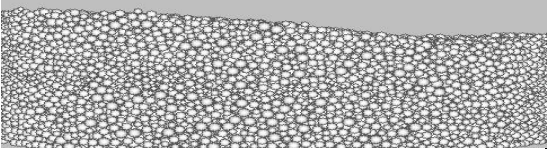

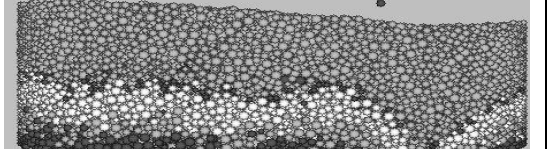

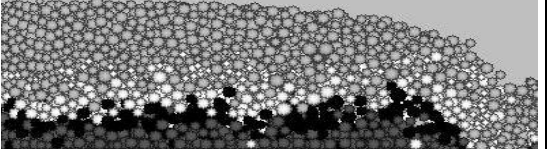

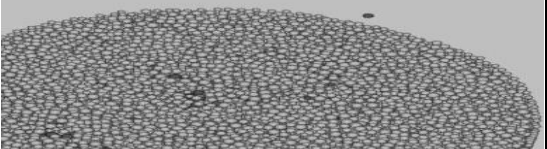

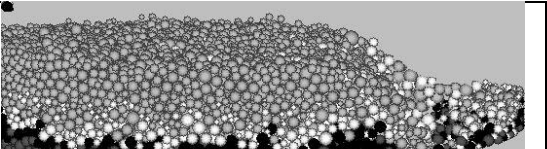

Figure 5.37 Visually comparing numerical simulation with laboratory results in center discharge of Polyethylene plastic pellets.

5.4.2 Model 2 -Side Discharge of Polyethylene Plastic Grains

Visual Comparison

The comparison was carried out at intervals of 14, 17, 22, and 34 seconds after the beginning of the discharge for the middle discharge test. At these specified intervals, the numerical simulations, as well as laboratory test discharge processes were halted temporarily in order to facilitate the exposure of similarities. The pair-wise comparison is given in Figure 5.38. By studying the pictures, one can also identify reasonable

resemblance between numerical and laboratory results, however, since a scale factor had been included, as had been in middle discharge, there were evident differences dimensionally (height and width of the granular pack). There were some discrepancies, which could be attributed to the errors in scaling of the physical model dimensions up to those of the numerical model. Also, the static forces between plastic pellets in the laboratory were large, causing the particles to be repellent because of the negatively polarized forces among them.

Time	Numerical Simulation	Laboratory Model Discharge
14 sec.		
17 sec.		
22 sec.		
22 sec.		
34 sec.		

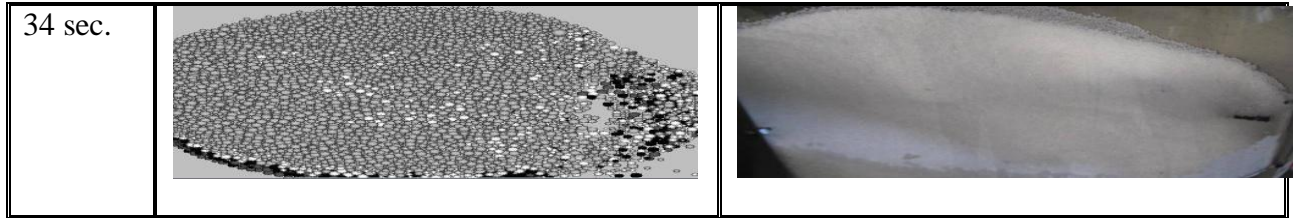


Figure 5.38 Comparing numerical results with laboratory side discharge results.

5.4.3 Model 3- Center Discharge of Corn grains

Visual Comparison

The comparison again was performed at intervals of 8, 14, 20, and 27 seconds after discharging began.

At these specified intervals, the numerical simulations, as well as laboratory test discharge processes were halted temporarily for contrasting. The photographs for pairwise comparison were given in Figure 5.39.

By studying the pictures, one can observe reasonable resemblance between numerical and laboratory results, however, since a scale factor had been included, there were visible differences dimensionally (height and width of the granular pack).

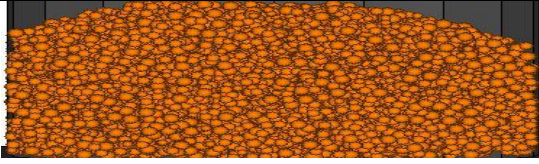

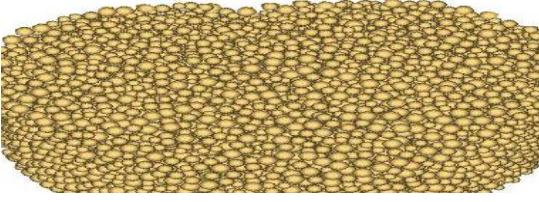

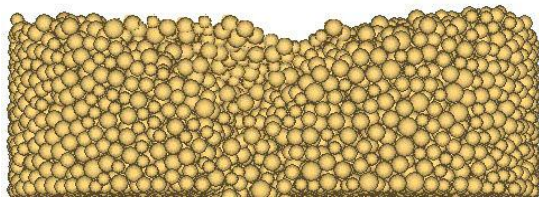

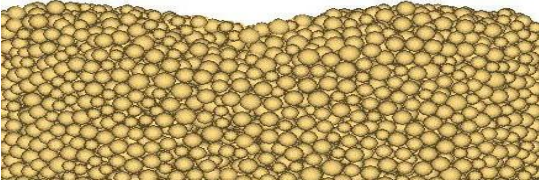

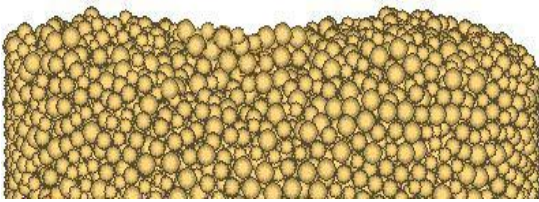

Time	Numerical Simulation	Laboratory Model Discharge
8 sec.		
14 sec.		
14 sec.		
20 sec.		
27 sec.		

Figure 5.39 Comparing numerical results with laboratory side discharge results.

Chapter-6

DETAILED RESULTS

6.1 Chapter Summary

In this section thorough validation processes, based on point volume measurements and granular discharge rates, are explained. A number of graphs, representing patterns of particles velocities at different locations, mean contact and unbalanced forces, particles displacements in terms of their velocities, and more were investigated in order to establish the optimal installation point for level sensing devices.

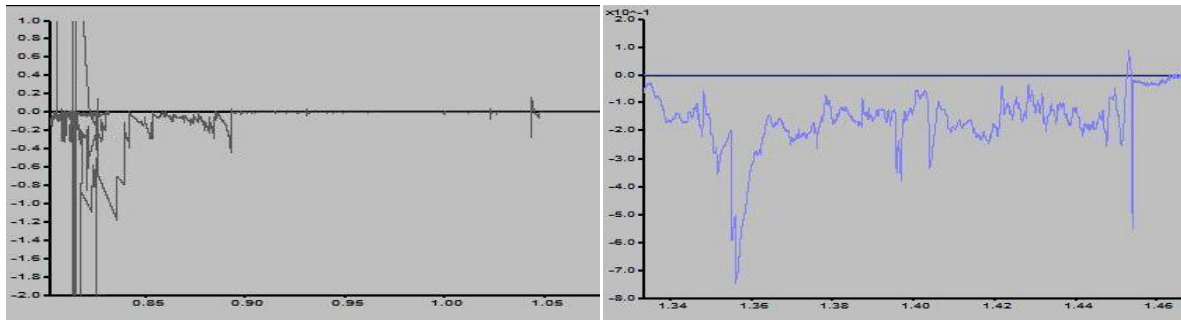
Point-based volume measurements were calculated both for numerical model and for laboratory model and then, these values were compared to determine error values, taking the laboratory test as being the correct one. Furthermore, re-runs of simulation models based on adjusted input values (mechanical properties of grains and frictional coefficients) were presented at the end of the chapter.

Finally, the triaxial shear test performed for polyethylene plastic is explained in this chapter.

6.2 Investigation of Various Parameters in Models

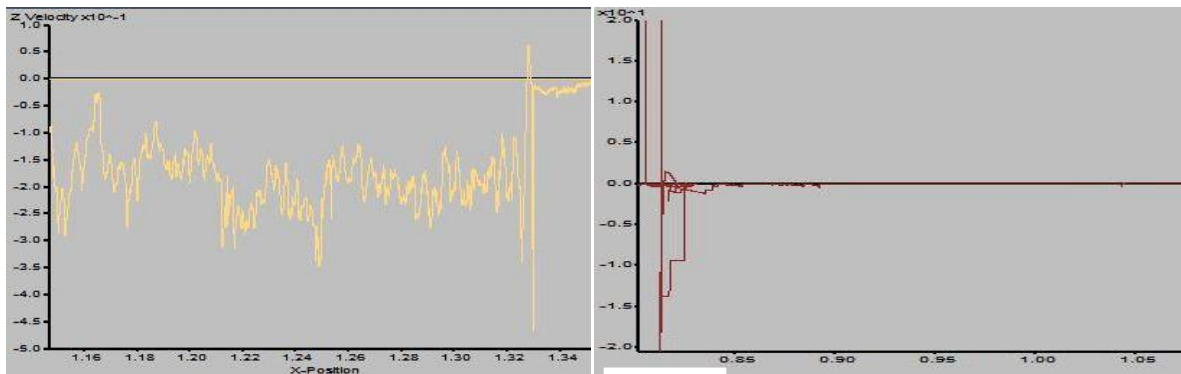
6.2.1 Model 1- Center Discharge of Polyethylene Plastic Pellets-Velocity change analyses of particles in Z-direction against their corresponding position in X, Y and, Z coordinates

In a series of graphs (Figure 6.1), obtained as simulation history data, the discharge velocity of designated particles with regards to their X coordinates in our system was observed.



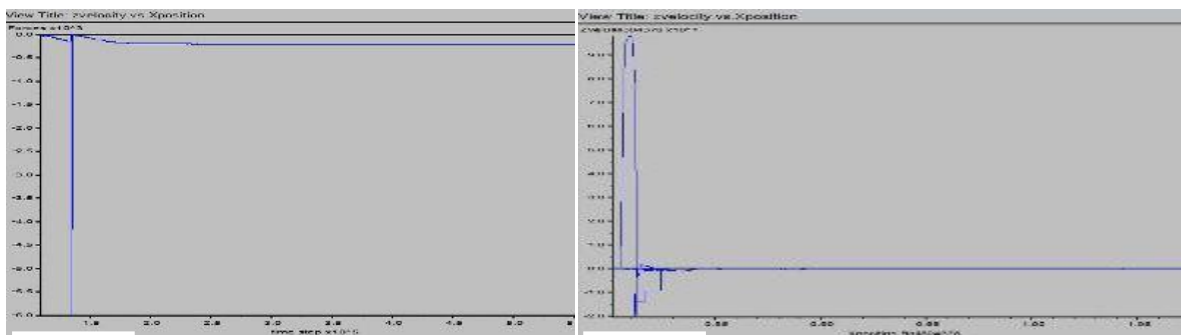
a.

b.



c.

d.



e.

f.

Figure 6.1 Vertical velocities [m/s^2] charts of certain particles vs. their respective X -positions [m] in the silo.

Graphs *a*, *d*, *e*, and *f* in 6.1 suggest that the designated particles velocities sharply increase in the negative direction when approaching above the discharge gate (which corresponds to about 0.8 meters in *X* direction). Other than within the mentioned range, the *Z* velocity of particles tended to oscillate slightly over a constant negative value outside the bin.

Graphs *b* and *c* in the same Figure depict the *Z*-velocity in the 0.8 to 1.6 m range of *X* direction, which does not encompass the discharge area. However, one may observe several large oscillations within 1.3-1.5 meters into *X* direction. These large fluctuations might have happened due to the energy of the locked particles being release when advancing towards the side walls.

Figure 6.2 depicts velocities in *Z* direction versus particles respective *Y* directions.

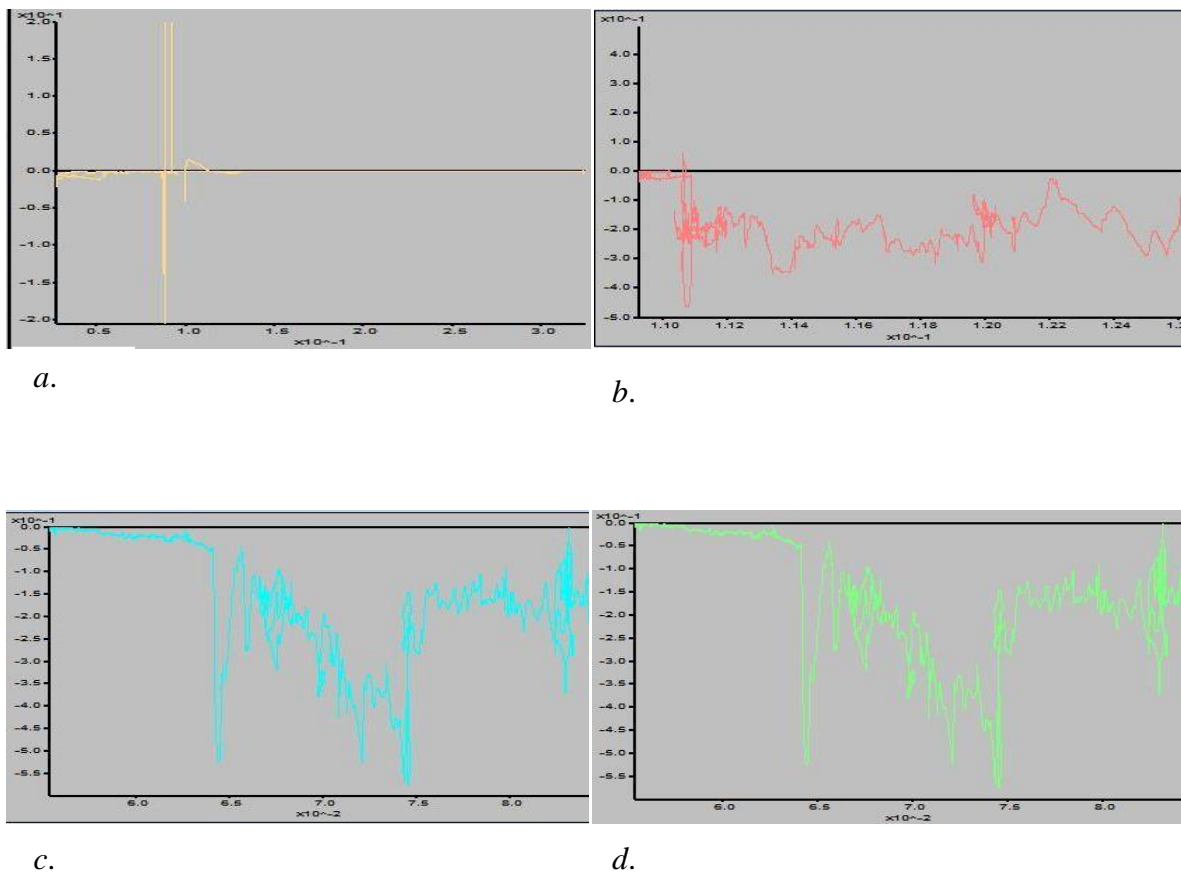
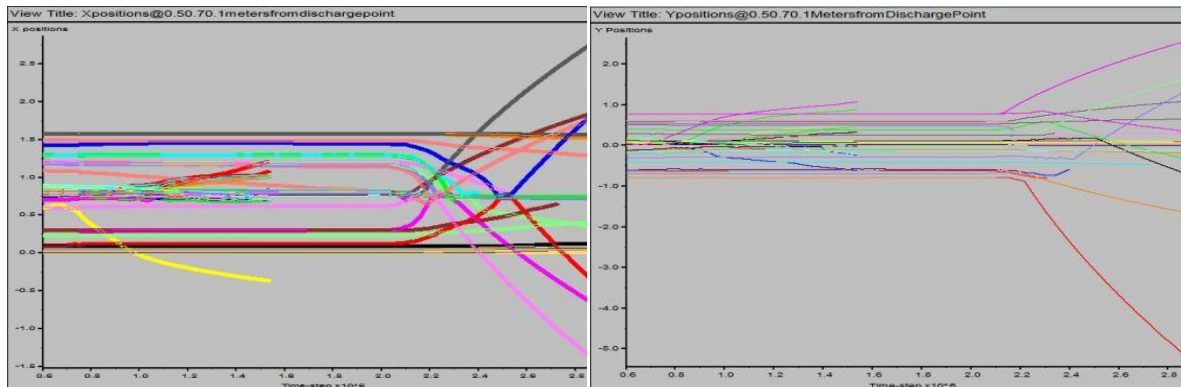


Figure 6.2 Velocity [m/s^2] charts of certain spheres vs. their respective *Y*-positions [m] in the silo.

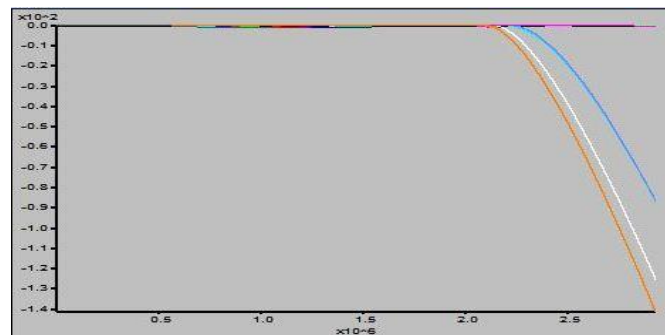
By studying the change of vertical velocity when Y changed for the same particle in the Figure above, one can determine that the velocity vacillates in the negative region around a constant value except for case a in which the particle passed the discharge gate region hence its sharp velocity increase in negative Z direction at about 0.8 m into Y direction. The particles speed graphed above were located very close to the side walls and that is why no excess velocity value is present.

In the following graphs (Figure 6.3), several particles were selected for study of their respective X , Y , and Z positions throughout the simulation. The patterns these particles leave are represented in the same graph for every X , Y , and Z position values for facilitating a better view of the whole system.



a.

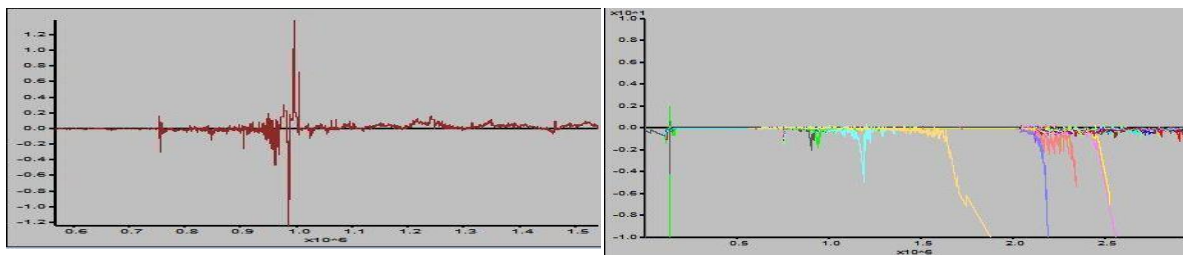
b.



c.

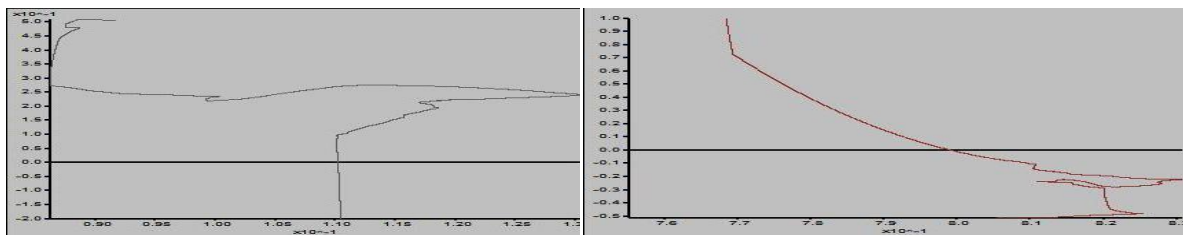
Figure 6.3 X , Y , and Z positions [m] of a collection of particles (a , b , and c graphs respectively) at different regions vs. time [s].

The divergence of positions beyond the model silo's dimension in graphs (a) and (b), which represent X and Y coordinates respectively, indicate their exit from the system, hence the larger values. As for graph c, which represents vertical coordinates of particles, one may observe that after approximately about 2 million time-steps, the particles exit the system thus their subjective altitudes plummet sharply beyond that time step to negative values. Initial location history of these particles were out of range for this graph, therefore, one may not see locations above level zero. In the following graphs (6.4) several other parameters were studied which deemed necessary in determining level sensing device's optimal locations.



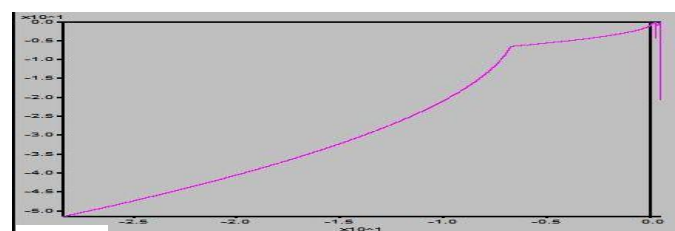
a.

b.



c.

d.



e.

Figure 6.4 a) X-velocity [m/s²] of a ball vs. time [s] b) Z-velocities [m/s²] of a couple of particles vs. time[s] c) Z position[m] of a ball vs. its Y position[m] d) Z position[m] of a ball vs. its X position[m] and, e) Z velocity [m/s²] of a ball vs. its vertical position [m].

In addition to graphs previously given, forces produced in Z and X axes directions to the cylindrical wall are depicted in Figure 6.5 below.

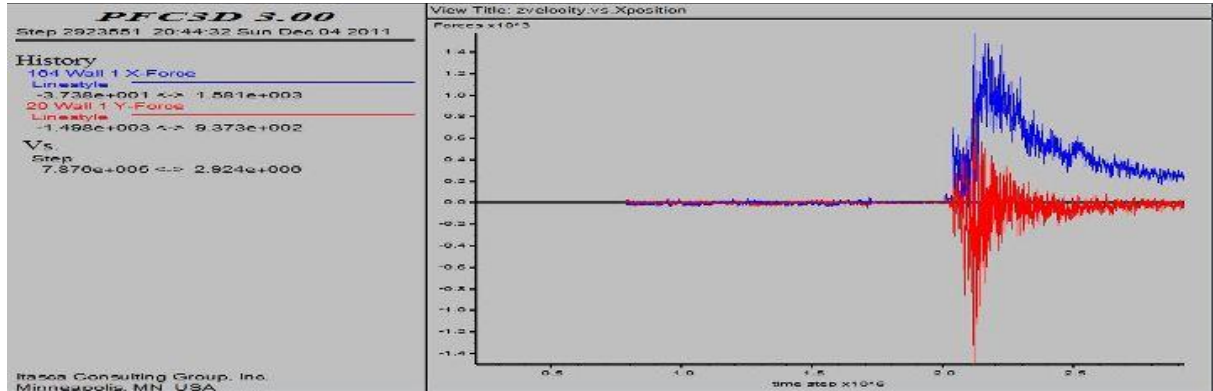


Figure 6.5 X and Y forces[N] generated from particle movements on the cylindrical wall in time [s].

There were spikes in force values roughly corresponding to 2.2 million time step (into final stages of discharge), which could have resulted from the locked-in forces between particles being released abruptly, as the possible bonds between particles were breaking.

6.2.2 Model 2- Side Discharge of Polyethylene Plastic Pellets-Velocity Change Analyses of Particles in Z-Direction against Particles' Resultant Position in X, Y and, Z Coordinates

In a series of graphs (Figure 6.6), obtained as simulation history data, one might monitor the discharge velocity of a couple of designated particles with regards to their X coordinates in the system.

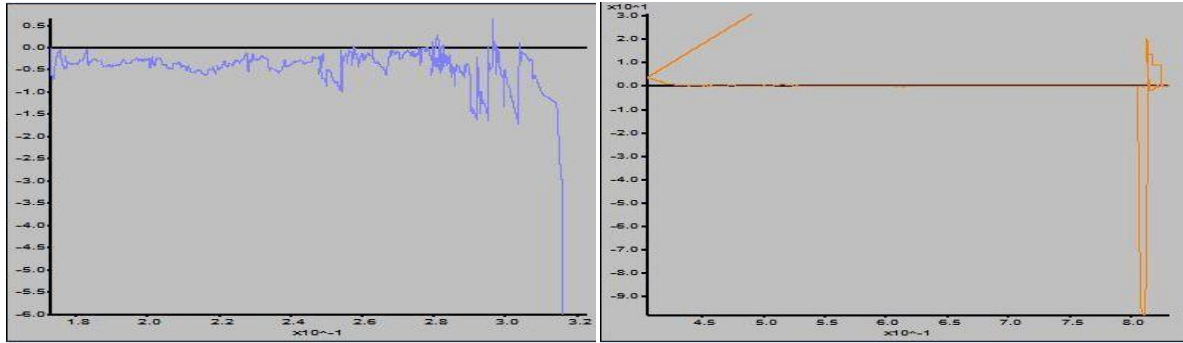


Figure 6.6 Vertical velocity [m/s^2] charts of certain particles vs. their respective X-positions [m] in the silo.

In the charts above, the sharp increase in velocities happens just above the discharge gate (close to right side wall) for both cases above, when the particles pass through discharge area. It is furthermore noticeable in Figures above that in other regions of the silo, the velocity fluctuates more or less around a constant value.

Figure 6.7 exhibits velocities in Z direction versus particles respective Y coordinates for two distinct particles (selected systematically based on their location's importance in the granular pack).

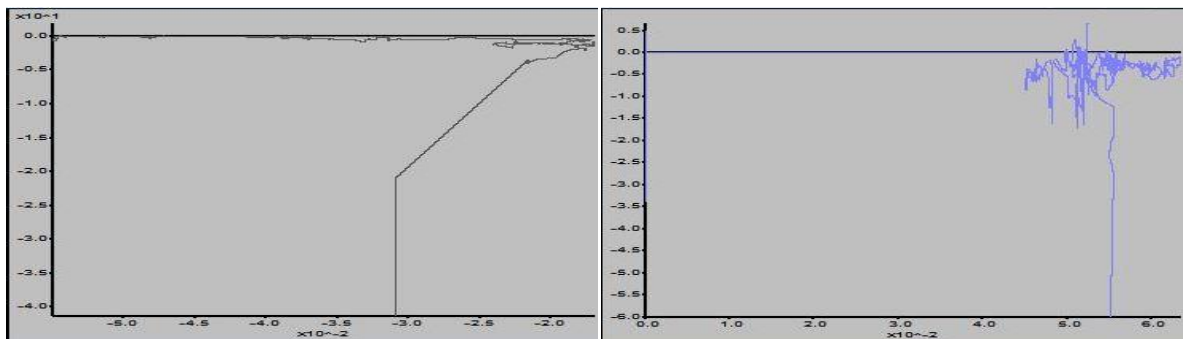
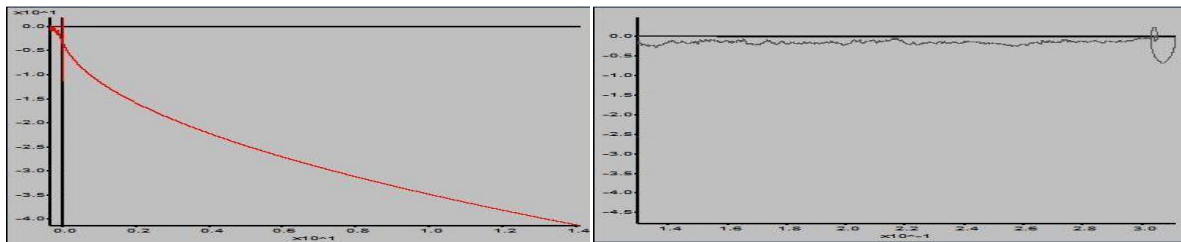


Figure 6.7 Vertical velocity [m/s^2] charts of certain particles vs. their respective Y-positions [m] in the silo.

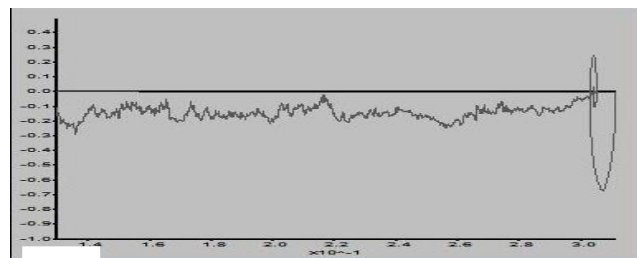
In Figure 6.7 above, one might spot a constant velocity as the particles move down by gravity. However there also is some pointed increase in velocities close to the central axis (roughly on 0.05 and 0.02 m in Y axis respectively) of the silo, which seems anomalous since in this case, the discharge happens in the right gate at the bottom. This sharp increase in velocity as particles advance in Y direction was not explicable at this stage.

In another set of charts, vertical velocities of some grains (located at different part of silo), are monitored against their vertical positions. This is given in Figure 6.8.



a.

b.



c.

Figure 6.8 Vertical velocity [m/s^2] charts of certain particles vs. their respective vertical positions [m] in the silo.

In Figure 6.8 graph (a), a decreasing trend in vertical velocity, as the particle approaches the bottom, is recognizable. This could be due to the fact that this individual particle did not make its way out of the system and as a result, it just subsided in the bottom and

stopped to move completely. In contrast, graphs (b) and (c) in the same Figure, demonstrate oscillating velocities with a constant mean, as the discharge process approaches to an end. This might verify the fact that, these two particles might have not exited the system but would have eventually, in case the simulation continued until much bigger time steps.

Figure 6.9 exhibits selected particles' vertical positions with respect to their axial position during discharge.

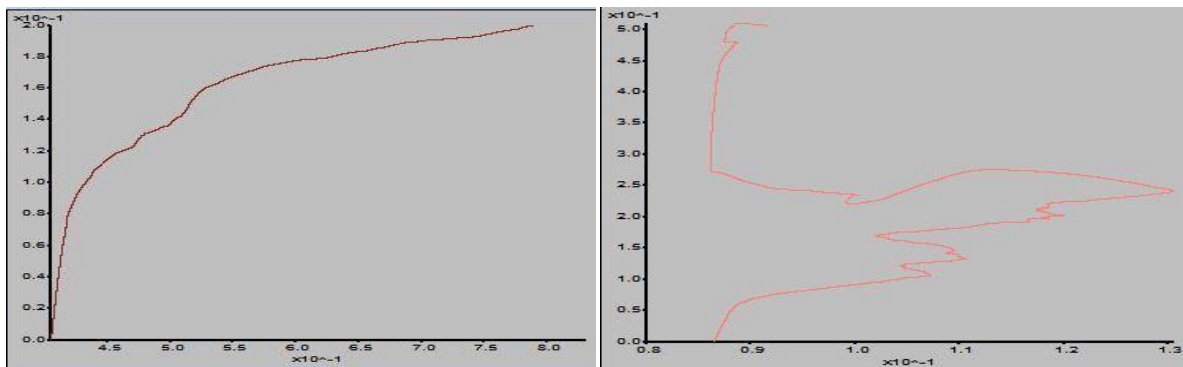


Figure 6.9 X path [m] vs. vertical path [m] (left) and, Y path [m] vs. vertical path [m] (right) of two pre-selected grain particles.

Figure 6.10 is given to demonstrate vertical (Z) velocities and vertical paths of a collection of particles during discharge process.

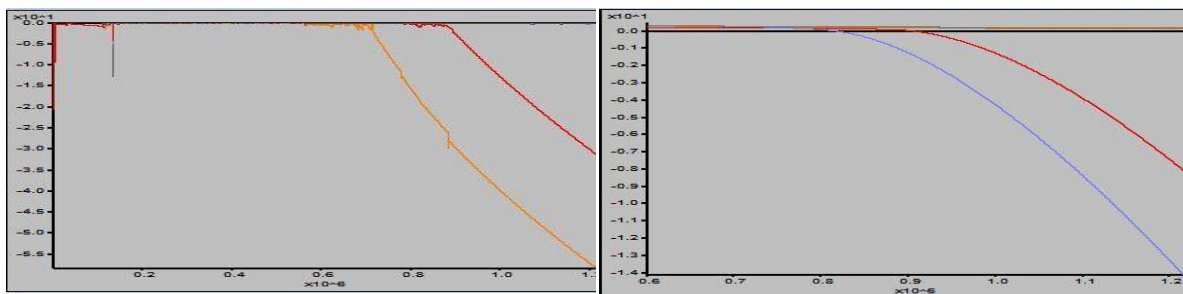


Figure 6.10 Vertical velocities [m] (left) and vertical positions [m] (right) of a collection of particles during simulation [s].

The quick decline of particles' velocity and their respective levels after approximately 1.2 million time steps, imply their exit of the system in the chart above.

Mean contact and, mean unbalanced forces within particle system during the whole discharge process were also recorded as a history file. In Figure 6.11 below, as the simulation approached a relatively steady-state discharge, these forces also decreased, and later stayed at a constant value. This indicates that the unbalanced and contact forces among particles had reached to a balanced state.

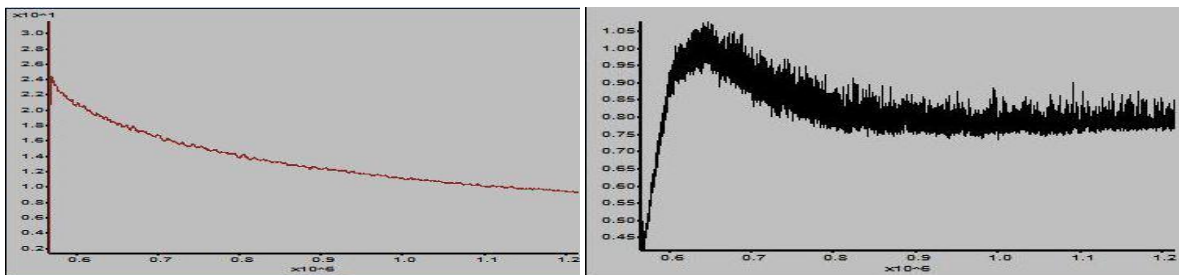
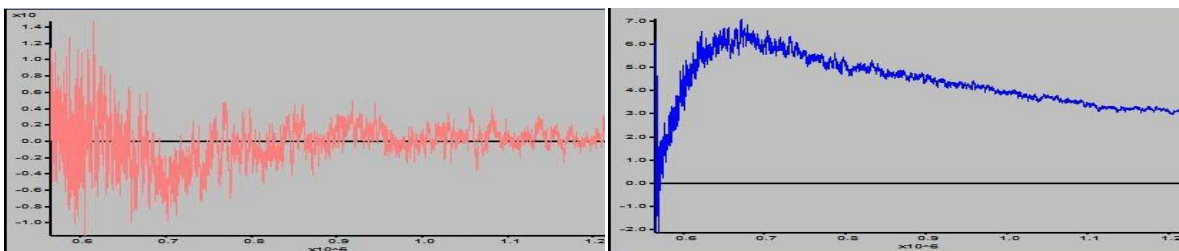


Figure 6.11 Mean contact forces [N] (left), and mean unbalanced forces [N] (right) of the system through discharge process.

Axial, as well as vertical forces tolerated by encompassing cylindrical wall and bottom walls, were analyzed through discharge, which is provided in Figure 6.12.



a.

b.

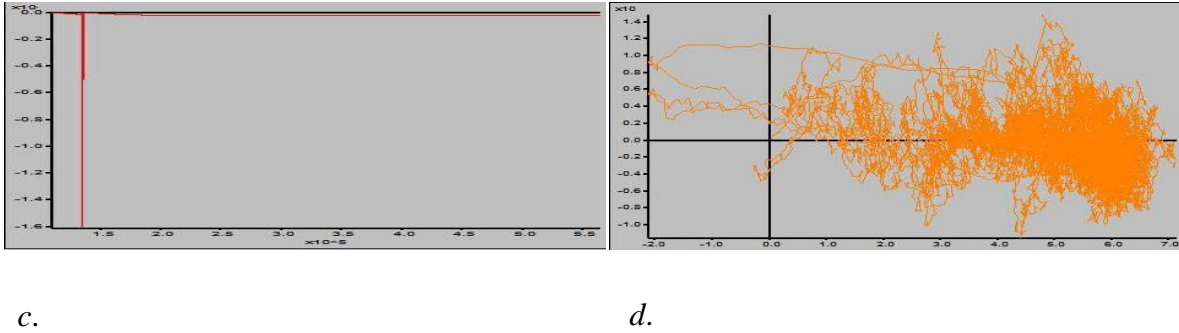


Figure 6.12 (a): Y force [N] of cylindrical wall vs. time [s], (b): X force [s] of cylindrical wall vs. time [s] (c): Z force [N] of flat-bottom wall vs. time [s] and, (d): Y force [N] of the cylindrical wall vs. its X force [N].

Finally, the porosity of granular pack (which corresponds to its bulk density), was monitored through discharge process which is provided in Figure 6.13.

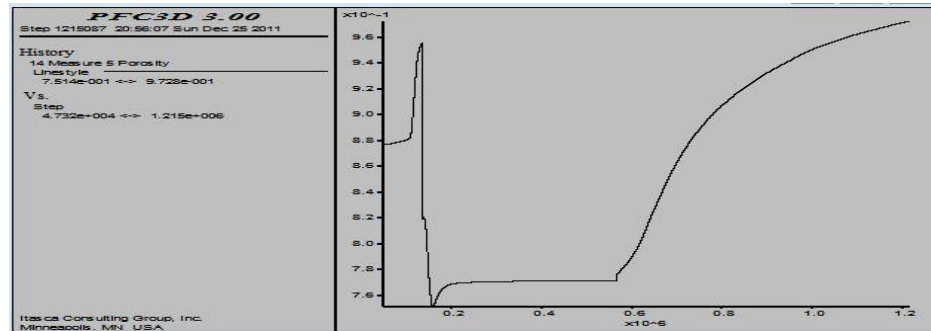


Figure 6.13 Porosity of grains for side discharge of plastic pellets vs. time [s].

From picture above that porosity initially fluctuated around 90 percent values and later on dropped to about 75 percent and then while the simulations approached an end, the porosity increased sharply. This increase indicate a rather emptiness where the measurement sphere had initially been located, since naturally the content of grain in silo decreases by time.

6.2.3 Model 3- Center Discharge of Corn with Initial Porosity of 0.50- Vertical Velocity Changes of Corn Particles with Respect to Their Axial X, Y, and Z Coordinates in the System

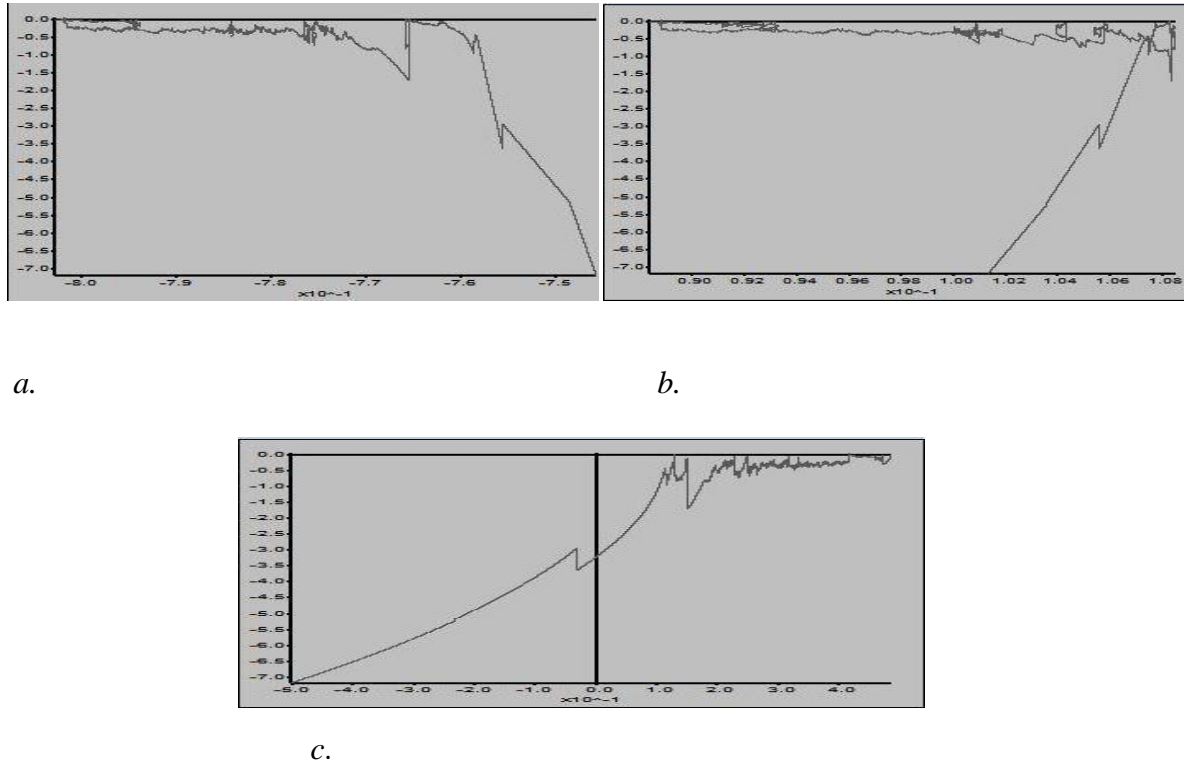


Figure 6.14 Vertical (Z) velocities [m/s^2] vs. X coordinate [m] (a), vs. Y coordinate [m] (b), and vs. height [m] for corn center discharge simulation.

It is visible from charts in Figure 6.14 that the velocity of discharging particles increases as they approached the exit (c). The sharp increase in velocity of particles in graphs (a) and (b) at the same Figure implies the exit of the designated particle from system, causing an unrestricted (frictionless) free falling.

In the remaining part of this section, vertical and axial force changes upon cylindrical as well as bottom walls are studied. The figures in graph 6.15 display the force patterns.

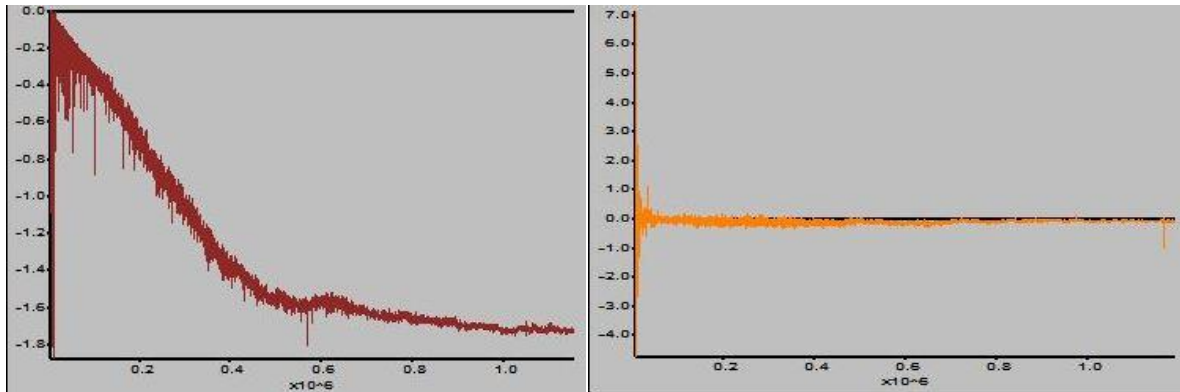


Figure 6.15 X force [N] (left) and Z force [N] (right) endured by cylindrical and bottom flat walls with time [s].

As the time proceeds, the applied vertical and axial forces decreased to a negligible constant value and continued in this way until the end. As the system has reached the steady-state discharge course, with contact forces between particles were in equilibrium.

Average stress value within particles as well as mean unbalanced force analyses were provided in Figure 6.16. The same rule applies to these when moving forward some considerable amount of time into the discharge.

Lastly, the porosity of system, from the beginning until the end of discharge, is tracked by the history file in Figure 6.17. It is understood that the porosity had remained constant from the onset until the advanced stages at the 40 percent values.

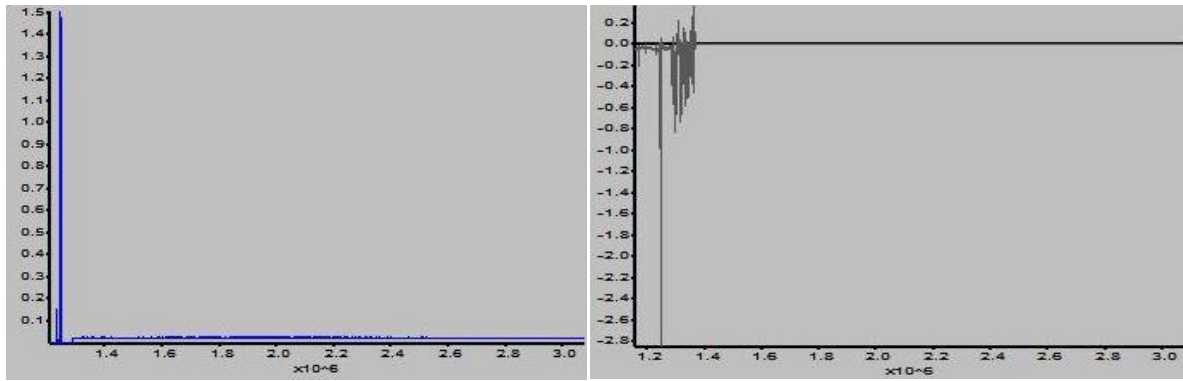


Figure 6.16 Mean unbalance force [N] (left) and average stress [KPa] tolerated by the particles (right) in corn discharge simulation [seconds].

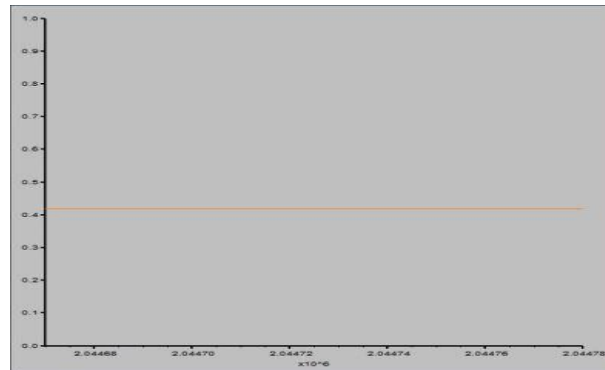


Figure 6.17 Porosity value of discharging corn in the silo vs. time [s].

6.3 Volume Measurement Validation

The height of the remaining granular pack and the resulting volume was also calculated and compared for both the numerical and laboratory model, in order to compute the percentage error that might arise in silo volume measurements.

6.3.1 Model 1- Center Discharge of Polyethylene Plastic Pellets

Below the comparison among values of numerical model and of physical model for center discharge of Polyethylene plastics is given in Table 6.1.

Table 6.1 Volume calculations for center discharged plastic pellets-18 point measurements.

Numerical/ physical discharge	Model 1-Center Discharge - Simulation					Model 1-Center Discharge- Lab Discharge				
Time [second]	9.92E+00	1.51E+01	2.00E+01	2.40E+01	2.73E+01	9.92E+00	1.51E+01	2.00E+01	2.40E+01	2.73E+01
Time-step [seconds/step]	1.76E-05	3.40E-06	2.30E-06	1.77E-06	1.31E-06	1.76E-05	3.40E-06	2.30E-06	1.77E-06	1.31E-06
Steps	564124	1517868	2129020	2261476	2519909	564124	1517868	2129020	2261476	2519909
Level of Material @ Different Surface Points [meter]	0.598	0.557	0.514	0.399	0.275	0.461	0.456	0.417	0.343	
	0.63	0.58	0.52	0.39	0.257	0.478	0.451	0.451	0.368	
	0.67	0.55	0.481	0.334	0.229	0.500	0.475	0.431	0.280	0.193
	0.622	0.561	0.521	0.372	0.258	0.480	0.475	0.446	0.402	0.243
	0.582	0.56	0.4	0.262	0.23	0.450	0.383	0.350	0.353	0.280
	0.624	0.574	0.48	0.357	0.233	0.500	0.465	0.402	0.275	
	0.62	0.557	0.523	0.399	0.275	0.461	0.446	0.314	0.310	
	0.611	0.566	0.5	0.364	0.233	0.465	0.470	0.387	0.319	0.256
	0.59	0.561	0.42	0.24	0.137	0.465	0.465	0.412	0.373	0.210
	0.59	0.575	0.478	0.32	0.2	0.490	0.363	0.363	0.339	
	0.6	0.46	0.413	0.297	0.187	0.485	0.378	0.241	0.231	0.187
	0.65	0.528	0.476	0.354	0.215	0.510	0.441	0.358	0.295	0.265
	0.64	0.54	0.486	0.37	0.238	0.489	0.417	0.363	0.304	0.265
	0.652	0.536	0.42	0.282	0.145	0.500	0.441	0.358	0.309	0.190
	0.583	0.558	0.428	0.26	0.13	0.480	0.480	0.407	0.363	
	0.657	0.548	0.51	0.37	0.247	0.490	0.441	0.387	0.329	0.280
	0.607	0.545	0.485	0.361	0.227	0.480	0.470	0.397	0.343	0.304
	0.65	0.553	0.431	0.374	0.21	0.520	0.436	0.314	0.314	
Average Height	0.621	0.551	0.471	0.339	0.218	0.467	0.442	0.382	0.328	0.280
Estimate Volume of Material in Silo [m ³]	1.25	1.11	0.95	0.68	0.44	0.939	0.888	0.767	0.658	0.562
Height Standard Deviation [m]	0.03	0.03	0.04	0.05	0.04	0.025	0.035	0.053	0.041	0.040
Real Volume of Material in Silo [m ³]	1.308	1.230	0.978	0.608	0.347					
Number of grains in silo	50030	47076	37425	23260	13259					
porosity	0.78	0.78	0.78	0.78	0.78					
Discharge Time [sec]	9.92E+00	1.51E+01	2.00E+01	2.40E+01	2.73E+01					
Avg. Height Difference percent	22.07%	19.67%	19.71%	18.62%	20.00%					
Avg. Volume Difference [m ³]	0.276	0.218	0.188	0.118	0.149					
Height STD [m]	2.59%	6.03%	10.37%	13.15%	15.10%					
volume discrep. [m3]	24.779%	19.738%	19.037%	3.437%	28.216%					

Table 6.2 Volume calculations for center discharged plastic pellets 3 point measurements.

Discharge Time [sec]	9.92E+00	1.51E+01	2.00E+01	2.40E+01	2.73E+01
Avg. Height Difference percent	18.44%	14.30%	16.94%	11.91%	33.53%
Avg. Volume Difference [m ³]	0.223	0.108	0.147	0.098	0.204
Height STD [m]	3.52%	6.55%	10.78%	6.14%	0.86%
volume discrep. [m3]	21.197%	9.828%	2.463%	17.780%	2.688%

Table 6.3 Volume calculations for center discharged plastic pellets 2 points (located at about 1/6 diameter of silo's side walls) measurements.

Discharge Time [sec]	9.92E+00	1.51E+01	2.00E+01	2.40E+01	2.73E+01
Avg. Height Difference percent	20.46%	17.42%	22.60%	10.41%	34.13%
Avg. Volume Difference [m ³]	0.258	0.193	0.206	0.078	0.156
Height STD [m]	0.65%	5.25%	6.35%	7.87%	
volume discrep. [m3]	25.690%	19.519%	16.660%	10.882%	27.987%

Table 6.4 Volume calculations for center discharged plastic pellets 2 (randomly selected points) measurements.

Discharge Time [sec]	9.92E+00	1.51E+01	2.00E+01	2.40E+01	2.73E+01
Avg. Height Difference percent	22.83%	19.38%	19.04%	11.21%	23.47%
Avg. Volume Difference [m ³]	0.153	0.130	0.070	0.022	0.000
Height STD [m]	1.83%	4.11%	8.10%	7.83%	
volume discrep. [m3]	27.025%	20.245%	23.354%	11.960%	18.497%

Table 6.5 Volume calculations for center discharged plastic pellets (Only 1 random point) measurements.

Discharge Time [sec]	9.92E+00	1.51E+01	2.00E+01	2.40E+01	2.73E+01
Avg. Height Difference percent	20.92%	13.71%	18.12%	4.85%	34.13%
Avg. Volume Difference [m ³]	0.255	0.150	0.177	0.035	0.156
Height STD [m]					
volume discrep. [m3]	23.058%	18.928%	21.300%	9.277%	23.195%

When solely considering single point measurements, the calculation error also increased significantly as the results in Table shows above. On the other hand, when the point measurements were selected at the 1/6 of diameter from the side walls of the silo, error values decreased considerably which was evident from comparing the results from Table

6.3 to those of the Table 6.4 in which the measurement points were selected randomly at the silo's lid.

6.3.2 Model 2 -Side Discharge of polyethylene plastic Grains

Volume Measurement Validation

The same volume measurement validation between numerical and laboratory results for side discharge is given in the following section.

Table 6.6 Volume calculations for side discharged plastic pellets-18 point measurements.

Numerical/ physical discharge	Model 2-Side Discharge -Simulation				Model 2-Side Discharge- Lab Discharge			
Time [second]	1.75E+01	1.90E+01	2.19E+01	3.43E+01	1.75E+01	1.47E+01	2.19E+01	3.43E+01
Time-step [seconds/step]	3.21E-06	1.93E-06	1.10E-06	8.90E-07	3.21E-06	1.93E-06	1.10E-06	8.90E-07
Steps	784581	1158381	2007503	2624276	784581	1158381	2007503	2624276
Level of Material @ Different Surface Points [meter]	0.554	0.528	0.375	0.339	0.469	0.484	0.455	
	0.575	0.511	0.368	0.322	0.494	0.367	0.484	0.377
	0.448	0.388	0.295	0.222	0.479	0.377	0.338	
	0.46	0.38	0.2	0.19	0.391	0.255	0.177	0.574
	0.512	0.471	0.347	0.27	0.372	0.396		
	0.563	0.496	0.346	0.313	0.479	0.474		0.348
	0.554	0.528	0.375	0.339	0.474	0.474	0.460	
	0.556	0.51	0.356	0.3	0.474	0.479		0.416
	0.511	0.449	0.327	0.284	0.469	0.465	0.372	
	0.434	0.354	0.287	0.267	0.484	0.382	0.289	
	0.5	0.456	0.328	0.255	0.474	0.421	0.338	0.357
	0.452	0.382	0.286	0.212	0.435	0.323	0.235	0.231
	0.548	0.496	0.35	0.328	0.484	0.484	0.406	0.387
	0.515	0.474	0.323	0.265	0.484	0.466		0.348
	0.516	0.456	0.339	0.285	0.504	0.479	0.396	0.396
	0.571	0.5	0.376	0.328	0.489	0.484		0.357
	0.45	0.36	0.284	0.212	0.401	0.274	0.177	0.206
	0.461	0.391	0.355	0.35	0.465	0.455		
Average Height	0.510	0.452	0.329	0.282	0.462	0.419	0.344	0.363
Estimate Volume of Materail in Silo [m ³]	1.03	0.91	0.66	0.57	0.930	0.842	0.691	0.730
Height Standard Deviation [m]	0.05	0.06	0.04	0.05	0.037	0.075	0.106	0.096
Real Volume of Materail in Silo [m ³]	1.038	1.018	0.668	0.517				
Number of grains in silo	44233	37969	25543	19774				
porosity	0.7	0.8	0.78	0.78				
Discharge Time [sec]	1.75E+01	1.90E+01	2.19E+01	3.43E+01				
Avg. Height Difference percent	10.94%	10.43%	17.28%	21.65%				
Avg. Volume Difference [m ³]	0.115	0.090	0.113	0.119				
Height STD [m]	6.31%	9.01%	10.44%	10.96%				
volume discrep. [m ³]	9.322%	7.254%	4.617%	11.056%				

Table 6.7 Volume calculations for side discharged plastic pellets 3 point measurements.

Time	1.75E+01	1.47E+01	2.19E+01	3.43E+01
Average Height Difference percent	7.73%	19.16%	68.86%	14.19%
Average Volume Difference [m ³]	5.06%	12.23%	85.06%	8.44%
Height Standard Deviation [m]	6.03%	4.03%	44.04%	10.61%
percent volume diff [m3]	24.876%	33.55%	25.13%	3.57%

Table 6.8 Volume calculations for side discharged plastic pellets 2- point (1/6D) measurements.

Time	1.75E+01	1.47E+01	2.19E+01	3.43E+01
Average Height Difference percent	5.81%	20.05%	37.72%	21.70%
Average Volume Difference [m ³]	5.27%	15.02%	21.54%	9.25%
Height Standard Deviation [m]	7.12%	5.27%		
percent volume diff [m3]	1.53%	11.56%	7.64%	29.26%

Table 6.9 Volume calculations for side discharged plastic pellets 2 random point measurements.

Time	1.75E+01	1.47E+01	2.19E+01	3.43E+01
Average Height Difference percent	8.90%	10.73%	24.62%	12.88%
Average Volume Difference [m ³]	8.16%	3.12%	11.67%	0.055
Height Standard Deviation [m]	7.37%	6.60%	9.80%	5.86%
percent volume diff [m3]	9.94%	6.18%	5.17%	36.039%

Table 6.10 Volume calculations for side discharged plastic pellets single point measurements.

Time	1.75E+01	1.47E+01	2.19E+01	3.43E+01
Average Height Difference percent	10.84%	23.78%	37.72%	21.70%
Average Volume Difference [m ³]				
Height Standard Deviation [m]	9.81%	17.21%	21.54%	9.25%
percent volume diff [m3]	2.77%	16.36%	21.09%	71.33%

6.3.3 Model 3 (Center Discharge of Corn)

Volume Measurement Validation

Table 6.11 Volume calculations for center discharged corn-18 point measurements.

Numerical/ physical discharge	Model 3 -50% Porosity - Center Discharge Maize				Model 3 -50% Porosity - Center Discharge Maize			
Time [second]	7.97E+00	1.39E+01	2.05E+01	2.76E+01	7.97E+00	1.39E+01	2.05E+01	2.76E+01
Time-step [seconds/step]	3.50E-06	2.85E-06	2.57E-06	2.31E-06	3.50E-06	2.85E-06	2.57E-06	2.31E-06
Steps	849832	2044670	2515850	3074990	849832	2044670	2515850	3074990
Level of Material @ Different Surface Points [meter]	0.724	0.579	0.492	0.417	0.72	0.656	0.455	
	0.74	0.581	0.494	0.417	0.681	0.589	0.398	0.39
	0.79	0.587	0.474	0.365	0.59		0.46	0.32
	0.739	0.568	0.486	0.414		0.53		
	0.77	0.48	0.357	0.313	0.686	0.532		0.33
	0.756	0.583	0.494	0.4	0.656	0.552	0.443	0.42
	0.7	0.552	0.492	0.416	0.7		0.48	0.376
	0.759	0.581	0.497	0.414	0.633	0.61	0.57	
	0.743	0.485	0.412	0.326	0.643	0.56	0.412	0.31
	0.789	0.523	0.447	0.367		0.59	0.43	0.28
	0.864	0.523	0.423	0.371		0.693	0.442	0.36
	0.861	0.588	0.477	0.371		0.644		0.34
	0.833	0.6	0.492	0.412	0.633	0.6	0.5	0.29
	0.823	0.534	0.413	0.316	0.623	0.62		0.289
	0.73	0.45	0.357	0.313	0.69		0.557	0.3
	0.794	0.596	0.5	0.412	0.694	0.67	0.533	0.28
	0.821	0.588	0.49	0.39	0.721	0.67	0.477	0.31
	0.8	0.56	0.398	0.391	0.72	0.58	0.46	0.37
Average Height	0.780	0.553	0.455	0.379	0.671	0.606	0.473	0.331
Estimate Volume of Materail in Silo [m^3]	1.57	1.11	0.92	0.76	1.35	1.22	0.95	0.67
Height Standard Deviation [m]	0.05	0.04	0.05	0.04	0.04	0.05	0.05	0.04
Real Volume of Materail in Silo [m^3]	0.376	0.290	0.202	0.140				
Number of grains in silo	14765	10599	7116	5225				
porosity	0.39	0.418	0.435	0.41				
	Discharge Time [sec]				7.97E+00	1.39E+01	2.05E+01	2.76E+01
	Avg. Height Difference percent				12.48%	10.59%	10.58%	11.93%
	Avg. Volume Difference [m^3]				0.198	0.116	0.133	0.092
	Height STD [m]				8.00%	7.94%	14.34%	9.68%
	volume discrep. [m3]				13.986%	9.691%	3.814%	12.703%

Table 6.12 Volume calculations for center discharged corn- 3 point measurements.

Time	7.97E+00	1.39E+01	2.05E+01	2.76E+01
Average Height Difference percent	11.09%	8.76%	9.12%	12.94%
Average Volume Difference [m^3]	0.181	0.346	0.075	0.102
Height Standard Deviation [m]	1.54%	7.34%	9.14%	10.71%
percent volume diff [m3]	4.502%	21.038%	6.451%	15.237%

Table 6.13 Volume calculations for center discharged corn 2- point (1/6D) measurements.

Time	7.97E+00	1.39E+01	2.05E+01	2.76E+01
Average Height Difference percent	11.09%	8.76%	9.12%	12.82%
Average Volume Difference [m ³]	0.181	0.103	0.075	0.101
Height Standard Deviation [m]	1.54%	7.34%	9.14%	10.88%
percent volume diff [m ³]	17.247%	3.129%	6.451%	15.128%

Table 6.14 Volume calculations for center discharged corn 2 random point measurements.

Time	7.97E+00	1.39E+01	2.05E+01	2.76E+01
Average Height Difference percent	7.97%	5.45%	19.43%	6.47%
Average Volume Difference [m ³]	0.119	0.008	0.097	0.027
Height Standard Deviation [m]		5.76%		
percent volume diff [m ³]	16.213%	3.747%	2.648%	15.990%

Table 6.15 Volume calculations for center discharged corn single point measurements.

Time	7.97E+00	1.39E+01	2.05E+01	2.76E+01
Average Height Difference percent	12.18%	13.95%	2.65%	20.51%
Average Volume Difference [m ³]	20.11%	16.49%	2.61%	16.08%
Height Standard Deviation [m]				
percent volume diff [m ³]	18.305%	3.129%	3.542%	15.128%

6.4 General Comparison

At this section, the average values of all three models were considered as a whole for comparison purpose.

Table 6.16 Average values for 18-point discharges throughout the complete simulation.

Discharge	18 point center PP	18 point side PP	18 points corn
Average Height Difference percent	20.01%	15.08%	11.40%
Average Volume Difference [m ³]	19.00%	10.93%	13.48%
Height Standard Deviation [m]	9.45%	9.18%	9.99%
percent volume diff [m ³]	19.04%	8.06%	10.05%

Table 6.17 Average values for 3-point discharges throughout the complete simulation.

Discharge	3 point center PP	3 point side PP	3 point corn
Average Height Difference percent	19.03%	27.49%	10.48%
Average Volume Difference [m ³]	15.58%	27.70%	17.59%
Height Standard Deviation [m]	5.57%	16.18%	7.18%
percent volume diff [m ³]	10.79%	21.78%	11.81%

Table 6.18 Average values for 2-point ($1/6D$) discharges throughout the complete simulation.

Discharge	2 points (1/6D) center PP	2 points (1/6D) side PP	2 points (1/6D) corn
Average Height Difference percent	21.01%	21.32%	10.45%
Average Volume Difference [m ³]	17.80%	12.77%	11.49%
Height Standard Deviation [m]	5.03%	6.19%	7.22%
percent volume diff [m ³]	20.15%	12.50%	10.49%

Table 6.19 Average values for 2-point discharges throughout the complete simulation.

Discharge	2 random point center PP	2 random point side PP	2 random point corn
Average Height Difference percent	19.19%	14.28%	9.83%
Average Volume Difference [m ³]	7.49%	7.11%	6.26%
Height Standard Deviation [m]	5.47%	7.41%	5.76%
percent volume diff [m ³]	20.22%	14.33%	9.65%

Table 6.20 Average values for single-point discharges throughout the complete simulation.

Discharge	1 point center PP	1 point side PP	1 point corn
Average Height Difference percent	18.34%	23.51%	12.32%
Average Volume Difference [m ³]	19.64%	14.45%	13.82%
Height Standard Deviation [m]			
percent volume diff [m ³]	19.15%	27.89%	10.03%

Table 6.21 Average values for 18-point measurements for 3 models.

18-point measurements for 3 models	
Average Height Difference percent	15.84%
Average Volume Difference [m ³]	14.819%
Height Standard Deviation [m]	0.10
percent volume diff [m ³]	12.90%

Table 6.22 Average values for 3-point measurements for 3 models.

3-point measurements for 3 models	
Average Height Difference percent	19.00%
Average Volume Difference [m ³]	19.929%
Height Standard Deviation [m]	0.09
percent volume diff [m ³]	14.49%

Table 6.23 Average values for 2-point (1/6D) measurements for 3 models.

2-point (1/6D) measurements for 3 models	
Average Height Difference percent	17.85%
Average Volume Difference [m ³]	14.31%
Height Standard Deviation [m]	6.14%
percent volume diff [m ³]	14.82%

Table 6.24 Average values for 2-point (random) measurements for 3 models.

2-point (random) measurements for 3 models	
Average Height Difference percent	14.80%
Average Volume Difference [m ³]	6.996%
Height Standard Deviation [m]	0.06
percent volume diff [m ³]	15.15%

Table 6.25 Average values for single point (random) measurements for 3 models.

Single random point measurements for 3 models	
Average Height Difference percent	18.06%
Average Volume Difference [m ³]	17.51%
Height Standard Deviation [m]	
percent volume diff [m ³]	19.02%

Table 6.26 Comparing Discrepancies in volume (%) of center and side discharges.

measurements	discharge method	
	Center	Side
18-point	8.02%	6.49%
3-point	10.15%	21.78%
2-point (1/6D)	15.85%	12.50%
2-point	15.52%	14.33%
Single-point	15.10%	27.89%
Average % error in volume	12.93%	16.60%

6.5 Validation by Discharge Flow Rate Values

\dot{m} is the mass flow rate which can be calculated as it is given in formula 5.1 where, Δm is the discharged mass and Δt is the time during which discharge took place.

$$\dot{m} = \frac{\Delta m}{\Delta t}$$

Equation 6.1

For the numerical simulation discharge rate, one should consider porosity of the pack, number of discharged particles and their average radius. By using the expression; $\dot{m} =$

$(4/3)\rho.n.\pi.r^3.\phi/t$, for all three models (porosity being represented by ϕ , n the number of remaining particles, ρ bulk density and r the average radius of spheres), discharge rate of every stage could be estimated. As for the physical model discharge rate, simply weighing the discharged particles at specified intervals would give an estimate of discharge rate as well.

Table 6.27 summarizes the discharge rate values for the numerical model.

Table 6.27 Average and discrete discharge rate values for numerical models.

Center discharge pp time [sec]	center discharge pp [kg/sec]	side discharge pp time [sec]	side discharge pp [kg/sec]	maize discharge time [sec]	center discharge corn [kg/sec]
15.00	10.05	17.00	10.51	8.00	
20.00	4.61	15.00	24.78	14.00	3.37
24.00	12.89	22.00	26.59	20.00	7.83
27.00	14.03	34.00	17.78	27.50	5.37
Average rate [kg/sec]	0.48		0.91		0.24
Discharge gate area adjusting factor [m2]	0.092		0.092		0.092
Validation discharge rate [kg/sec]	0.044		0.083		0.022

Table 6.28 Average and discrete discharge rate values for physical model discharges.

Center discharge pp time [sec]	center discharge pp [kg/sec]	side discharge pp time [sec]	side discharge pp [kg/sec]	maize discharge time [sec]	center discharge corn [kg/sec]
15.00	1.05	17.00	1.17	8.00	
20.00	0.45	15.00	1.70	14.00	0.27
24.00	1.16	22.00	2.09	20.00	0.65
27.00	1.05	34.00	1.44	27.50	0.47
Average rate [kg/sec]	0.043		0.073		0.020

Table 6.29 Average and discrete percentage errors.

	center discharge pp [kg/sec]	side discharge pp [kg/sec]	center discharge corn [kg/sec]
Discrete percentage error	0.895	0.889	
	0.902	0.931	0.919
	0.910	0.921	0.917
	0.925	0.919	0.912
Average rate percentage error	0.023	0.122	0.080

6.6 General Volume Measurement Results

From the results above, it was computed that the average percentage error for all the 18 point measurements to be 12.38, for 3 point measurements 14.79, 2 specific point measurements 14.38, 2 random point measurements 14.85 and, for single point measurements 19, were computed. The average error in volume calculations for 3 points measurement was higher than 2 point (located at 1/6 of silo diameter from side walls) measurements, as the latter one is often deliberately selected to minimize error values and this result attests to this fact.

As for all 3 model results comparison, for plastic pellet center discharge, the average volume percentage error for all the point measurements was about 17.68, for plastic pellet side discharge this value was roughly 16.72, and finally for the corn (center discharge) this value is around 10.50.

As it is evident from the results, corn discharge process was the most confirming (to the laboratory results), followed by center discharge of plastic pellet.

Considering *MFIs*, the mass discharge rate error is highest in side discharge as well (about 12 percent) followed by corn mass discharge rate (about 8 percent).

In Table 6.30 below, the change in volume measurement errors with decreasing the measurement point numbers is summarized.

Table 6.30 Volume measurement error value change comparisons with respect to 18-point measurements.

point measurement	error increase with from 18 point measurement value		
	pp center discharge	pp side discharge	maize center discharge
Three	6.82%	54.23%	53.63%
Two special	50.09%	20.22%	47.80%
Two	50.26%	30.44%	43.26%
Single	47.50%	64.25%	45.39%

Table 6.31 Volume measurement error value comparison between three and single point measurement.

point measurement	error increase from three point to single point measurement		
	pp center discharge	pp side discharge	maize center discharge
Single	0.58%	21.90%	0.23%

6.7 Recommendations

6.7.1 Calibration of the Simulation Parameters

Since high static forces were present between polyethylene plastic particles in the laboratory, the simulation results did not match exactly to those of the real model. In order to compensate for this static energy, it was decided to increase the friction coefficient among spheres in model 1 and 2 up to 0.65. Likewise, the friction coefficient between particles and walls was raised to 0.60. Besides, the viscous damping values for all the models were decreased to 0.30.

As for decreasing the discrepancies in corn discharge results and its numerical model results, the friction coefficients among corn particles and wall-corn particles to 0.55 and 0.6 respectively were increased; this is decided because the corn kernels had heavy amount of dust with them which might have increased the friction forces at all directions

in particle-particle and wall-particle touch points. This increase in friction would address the discrepancies and cause the gap (error) between numerical results and laboratory results to be diminished.

The rest of the input parameters (mechanical properties and dimensions) were kept unchanged and the three simulation runs for plastic pellets and corn were repeated. The re-run results for the three models are given in Table 6.32 below. It is easily seen from Table 6.33 that the discrepancies in volume have decreased to about 11 percent down about 3.47 from 14.47 percent for 18 point measurements.

Table 6.32 Volume measurement results of calibrated simulation for three models.

Numerical Simulation Results	2nd round- Model 1-Center Discharge					2nd Round-Model 2-Side Discharge				2nd Round-Model 3 -50% Porosity - Center Discharge			
Time [second]	9.95E+00	1.45E+01	2.20E+01	2.54E+01	2.81E+01	2.15E+01	2.10E+01	2.39E+01	3.23E+01	8.22E+00	1.43E+01	2.23E+01	2.90E+01
Time-step [seconds/step]	1.72E-05	3.50E-06	2.30E-06	1.74E-06	1.29E-06	3.31E-06	1.91E-06	1.70E-06	9.00E-07	3.80E-06	2.83E-06	2.95E-06	2.52E-06
Steps	564149	1517888	2129090	2261495	2519994	784590	1158380	2007512	2624274	849833	2044648	2515839	3074998
Level of Material @ Different Surface Points [meter]	0.51	0.494	0.49	0.394	0.23	0.57	0.57	0.405	0.301	0.724	0.649	0.494	0.39
	0.491	0.432	0.414	0.377	0.291	0.572	0.54	0.5	0.42	0.711	0.64	0.5	0.401
	0.54	0.522	0.46	0.3	0.236	0.444	0.42	0.42	0.355	0.7	0.604	0.433	0.347
	0.442	0.41	0.41	0.38	0.256	0.5	0.487	0.346	0.222	0.727	0.58	0.48	0.4
	0.512	0.453	0.42	0.362	0.271	0.524	0.52	0.49	0.267	0.728	0.562	0.517	0.32
	0.524	0.505	0.428	0.38	0.24	0.549	0.513	0.505	0.49	0.704	0.52	0.482	0.368
	0.493	0.446	0.438	0.37	0.2	0.53	0.53	0.488	0.46	0.761	0.603	0.55	0.39
	0.411	0.4	0.39	0.352	0.248	0.555	0.47	0.39	0.39	0.74	0.6	0.557	0.502
	0.502	0.49	0.4	0.33	0.211	0.539	0.43	0.358	0.336	0.74	0.554	0.41	0.297
	0.467	0.324	0.367	0.325	0.193	0.503	0.5	0.353	0.316	0.731	0.57	0.469	0.308
	0.48	0.426	0.31	0.31	0.191	0.5	0.468	0.328	0.35	0.708	0.611	0.449	0.39
	0.526	0.5	0.395	0.333	0.25	0.434	0.42	0.37	0.27	0.752	0.66	0.403	0.345
	0.62	0.47	0.47	0.394	0.256	0.55	0.55	0.352	0.35	0.697	0.57	0.57	0.3
	0.542	0.506	0.445	0.346	0.15	0.56	0.504	0.3	0.269	0.74	0.575	0.54	0.298
	0.489	0.398	0.311	0.294	0.155	0.553	0.491	0.36	0.324	0.725	0.598	0.436	0.32
	0.59	0.526	0.46	0.348	0.277	0.53	0.407	0.366	0.33	0.741	0.614	0.562	0.375
	0.457	0.52	0.443	0.4	0.253	0.511	0.429	0.307	0.202	0.78	0.609	0.493	0.404
	0.518	0.502	0.49	0.4	0.24	0.49	0.444	0.33	0.33	0.739	0.56	0.44	0.37
Average Height	0.506	0.462	0.419	0.355	0.230	0.523	0.483	0.387	0.332	0.730	0.595	0.488	0.363
Volume of Material in Silo [m ³]	1.02	0.93	0.84	0.71	0.46	1.05	0.97	0.78	0.67	1.47	1.20	0.98	0.73
Height Standard Deviation [m]	0.05	0.06	0.05	0.03	0.04	0.04	0.05	0.07	0.08	0.02	0.04	0.05	0.05

Table 6.33 Calibrated simulation and laboratory results comparison.

Discharge	Calibrated Results and Lab Results Discrepancies			Total Average
	center Plastic pellet	side Plastic pellet	center maize	
Average Height Difference	10.88%	15.73%	7.55%	11.39%
Average Volume Difference [m ³]	10.10%	13.04%	9.54%	10.89%
Height Standard Deviation [m]	7.65%	11.24%	5.96%	
percent volume diff [m ³]	10.06%	10.42%	5.48%	8.65%

6.8 Triaxial Shear Test Simulation

6.8.1 General Description

In order to establish the relationships between input parameters, a numerical triaxial shear test was performed so that, the associated stress-strain curves could be attained. This test is useful especially when dealing with inverse modeling with unknown micro-properties. The bulk properties of any granular material could be established by developing a series of test upon the material of interest. These tests can be carried out numerically simulating analogous tests usually performed in laboratory environment. Triaxial test can be utilized in obtaining an estimation of the elastic-plastic response of any synthetic material. If it was required to match certain laboratory results of a specific granular material such as corn, it was necessary for us to perform numerical tests which simulate the laboratory results. Later, one can adjust the input values for the model until the time when the behavior of the numerical sample equals that of the real one. The resulting fine-tuned values then could be used as better inputs for the real simulation (with larger particles).

Once the Young's modulus and average strain values were obtained using the relevant stress-strain graphs, these value were compared to the values given in literature. If these

values match, the initial parameters used as input to simulation model were assumed to be correct.

To this end, a shear box consisting of packed particles in a cylindrical confining wall was used; this cylindrical wall simulates the confinement upon the sample and for creating the effects of external compressing forces, two walls, one in top and the other one in the bottom of the cylindrical sample were generated. These walls simulate the loading platens.

The sample was loaded in a strain-managed mode; a constant velocity in vertical direction to the walls was assigned so that the walls can move closer, compressing the sample. During the whole stages the lateral (radial) velocities of the confining cylindrical wall were managed mechanically by means of a numerical servo-system. The code for this servomechanism was written in FISH programming language. Once the confinement process starts from all directions, the stress-strain endured by the granular sample (polyethylene) were established in the macro level through adding up the forces acting on walls and mapping out the corresponding gap between the moving top and bottom walls. Finally, several material stress-strain response graphs can be obtained by selecting certain stress/ strain values and tracing them throughout the test. Throughout the simulated test, the porosity of the sample was also kept unchanged.

It was important to note that this numerical shear-box test was only performed for Polyethylene plastic since the mechanical properties for corn particles had been obtained in the earlier studies and were used directly as input parameter for the model 3 (corn, center discharge).

6.8.2 Sample Preparation for Triaxial Test for Polyethylene Plastic Pellets

An initial mass of particles was first created that contains 8615 circular particles; the dimension of the sample containing the particles was 4×2 meters with initial porosity of 40% for this test. A couple of mechanical properties ascribed to the model include; shear and normal stress for walls and particles density. The initial radii of the sample particles range between 0.035 to 0.07 meters.

In Figure 6.18, the resulting compact sample can be seen. The corresponding *PFC3D* codes are given in the appendix (C).

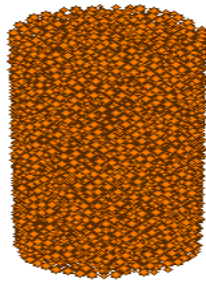


Figure 6.18 Initial sample of compact assembly prepared for the triaxial test.

6.8.3 Stress State Computation with Servo Control Process

At this stage, the stress state was established and controlled for the sample throughout the test. The confining stress was kept constant by modifying the cylindrical wall's velocity through a simulated servomechanism. The radial and axial strains were calculated by the formula given below in which, L was the resultant length of the sample and L_0 the initial length of it.

$$\epsilon = \frac{L - L_0}{\frac{1}{2}(L_0 + L)}$$

Sample strain calculation (Itasca, 1999).

6.8.4 Computation of Elastic Properties of the Sample

Since the sample was ready for the test, the elastic test could be performed at this stage to obtain the resulting graph for the axial deviatoric stress against strain for elastic load/unload test. The complete code for this test was also given in appendix (C). The resulting slope in this graph was the average Young's modulus value for the material under shear test.

The *Young's Modulus (E)* value can be derived from the slope of the stress-strain graph 5.1 and establishing the ratio below;

$$E = \frac{\Delta\sigma_a}{\Delta\epsilon_a} = \frac{\Delta\sigma_d}{\Delta\epsilon_a} \quad \text{Young's Modulus (Itasca, 1999).}$$

In the formula above, σ_a was the axial stress, ϵ_a the axial strain, σ_d the axial deviatoric stress, and since the confining stress was constant via the servo system, then $\Delta\sigma_a = \Delta\sigma_d$. $\epsilon_v = \epsilon_x + \epsilon_y + \epsilon_z$ was the volumetric strain, $\sigma_d = \sigma_a - \sigma_c$ was the axial deviatoric stress and finally, σ_c was the mean confining stress. The results from numerical experiment were given in Figures 6.19 and 6.20.

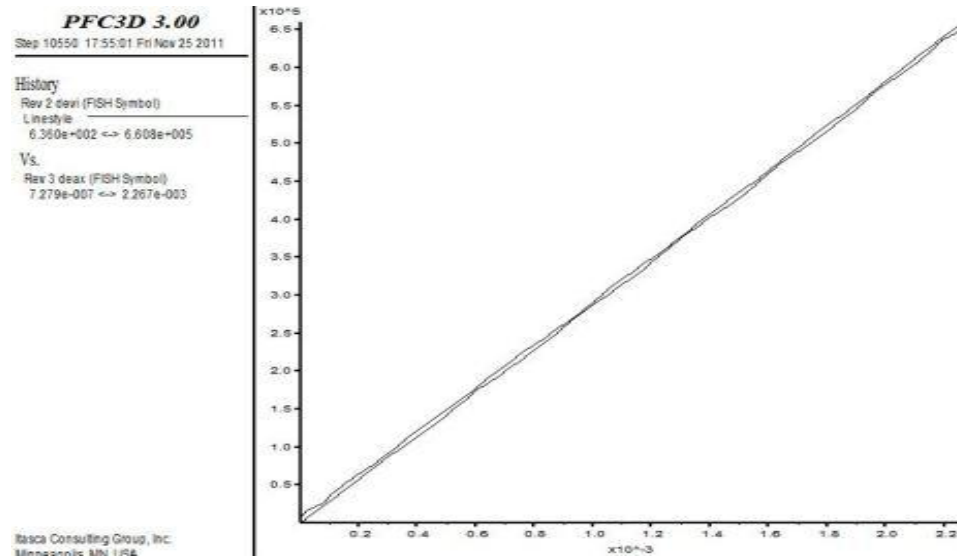


Figure 6.19 Axial deviatoric stress [KPa] vs. axial strain for elastic load/unload test.

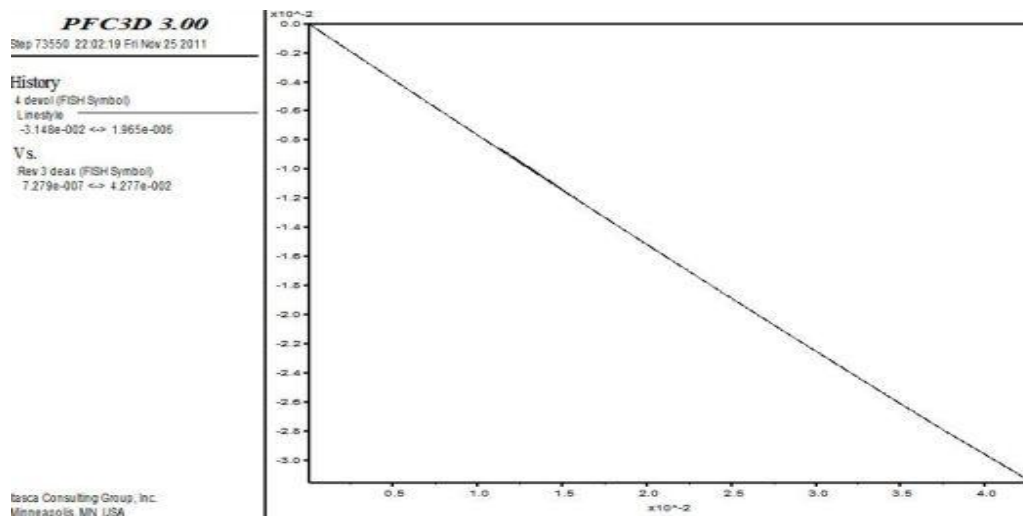


Figure 6.20 Volumetric strain vs. axial strain for elastic load/unload test.

From the graphs above, *Young's modulus* can be calculated as:

$$E = \frac{\Delta\sigma}{\Delta\varepsilon} = \frac{4.0 - 1.5}{1.6 - 0.6} \times 10^8 \approx 0.25 \text{ GPa}$$

Additionally, the Poisson's ratio ν , can be calculated by formula below:

$$\nu = -\frac{\Delta\epsilon_r}{\Delta\epsilon_a} = \frac{1}{2} \left(1 - \frac{\Delta\epsilon_v}{\Delta\epsilon_a} \right) \quad \text{Poisson's ratio (Itasca, 1999)}$$

Therefore in this case, $\nu \approx 0.5 \times \left(1 - \frac{0.2}{0.5} \right) \approx 0.30$; these values approximately correspond

to the Polyethylene plastic mechanical properties.

6.8.5 Test of Stress Failure for the Sample

Because bonding between particles for the actual simulation was not considered, at this stage this test was performed with no contact bonds among particles.

At this final step graphs, representing axial deviatoric stress versus the axial strain, were produced. The complete codes written for this stage can be seen in appendix (C).

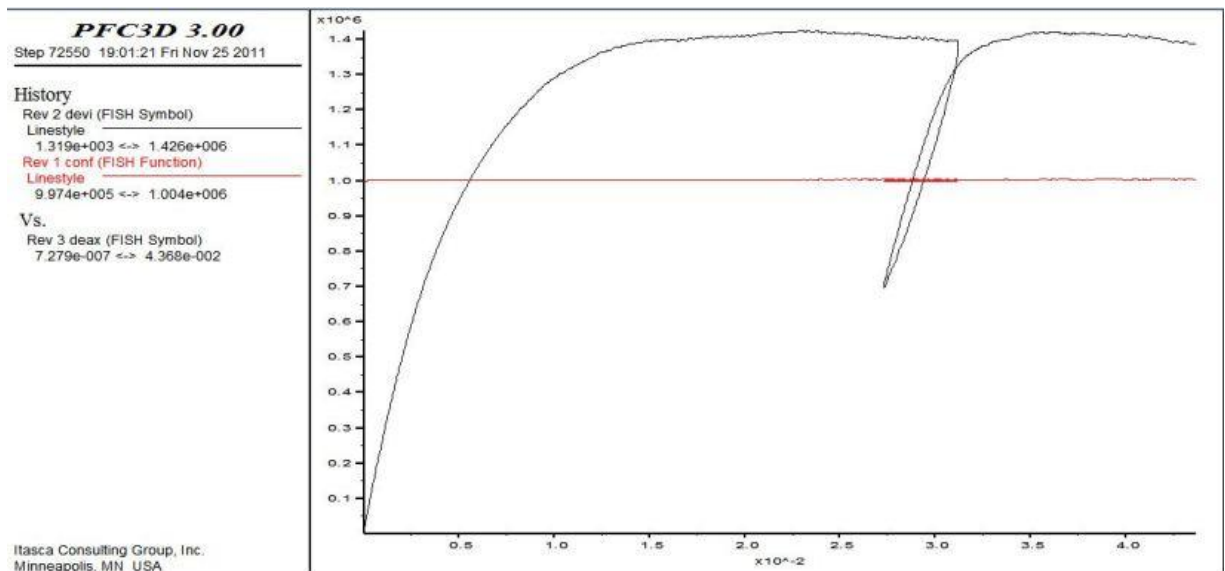


Figure 6.21 Axial deviatoric stress [KPa] and confining stress [KPa] vs. axial strain for grains without bond.

In the final stages, grains were considered to be bonded with strengths of 0.05 and 0.2 MN respectively and then observe the deviatoric stress and confining stress against axial strain for these granular matters. The resulting graphs were given in Figures 6.22 and 6.23.

It was discernible from the following two graphs that granular materials with larger contact bond strengths, fail at a much larger stress as it was the case in the latter one, the failure stress has not been reached yet.

The same applies to the graphs demonstrating volumetric strain against axial strain for the same materials with bond strengths of 0.05 and 0.1 MN respectively, as it was evident in the graphs 6.24 and 6.25. In the test with larger contact bond strength, the failure stress point has not been reached in the range of the graph.

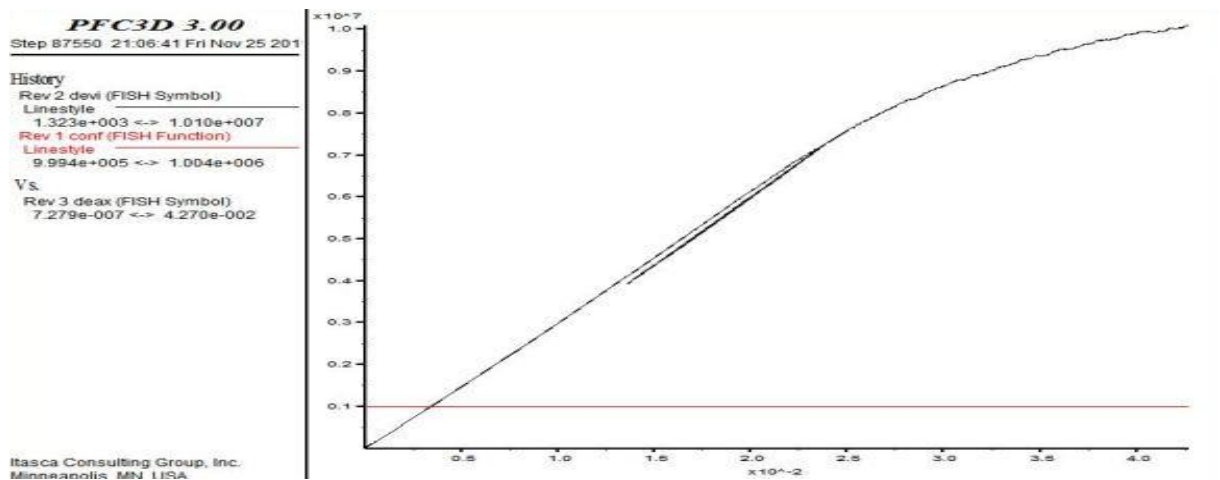


Figure 6.22 Axial deviatoric stress [KPa] and confining stress [KPa] vs. axial strain for bonded granular material with contact-bond strength of 0.05 MN.

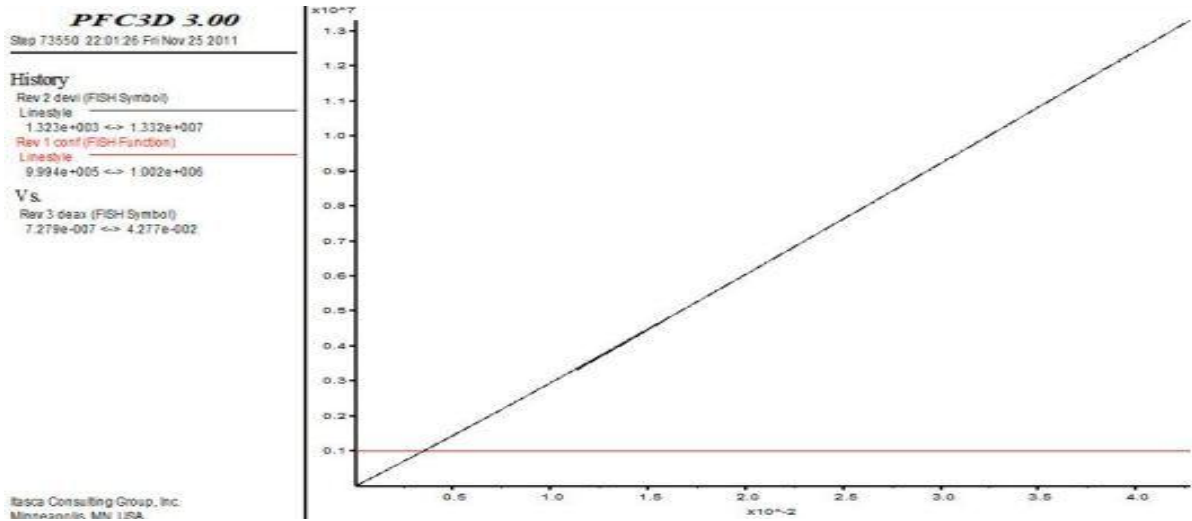


Figure 6.23 Axial deviatoric stress [KPa] and confining stress [KPa] vs. axial strain for bonded granular material with contact-bond strength of 0.1 MN.

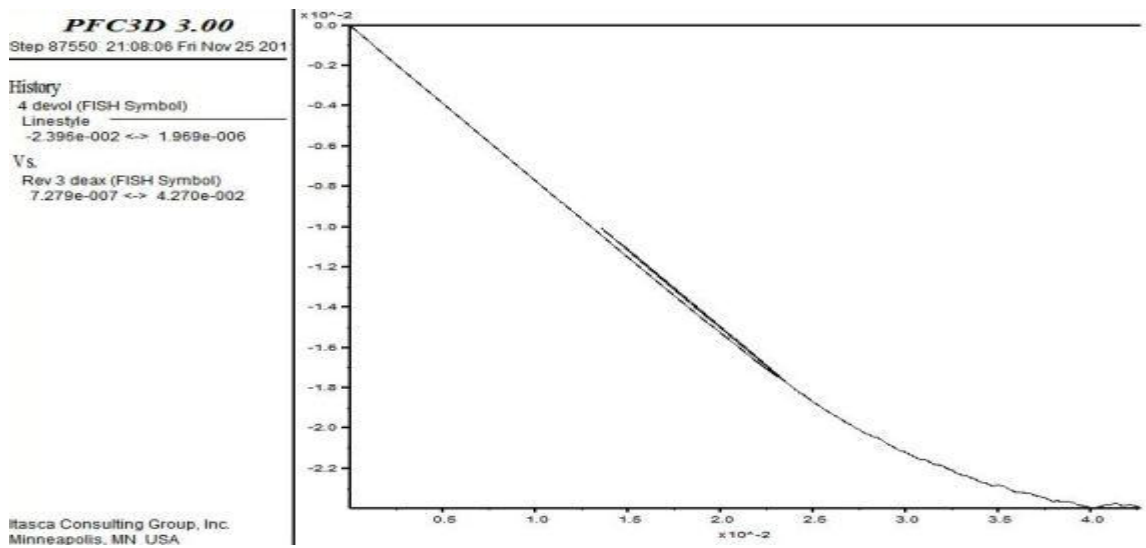


Figure 6.24 Volumetric strain vs. axial strain for bonded material with contact-bond strength of 0.05 MN

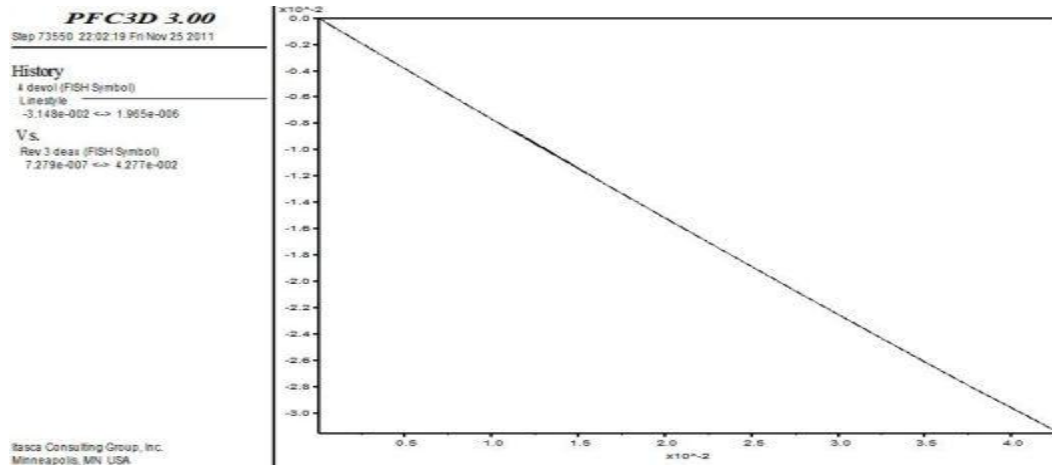


Figure 6.25 Volumetric strain vs. axial strain for bonded material with contact-bond strength of 0.1 MN

The Poisson's ratio and Young's modulus values were very close to those of polyethylene, hence, the ascribed stiffness values would be accurate to continue with.

Chapter-7

DISCUSSIONS

7.1 Specific Discussions

7.1.1 Modeling

A goal of this study was to determine the optimum location of level-sensing devices (in such a way that with minimum number of installed sensors, the most accurate volume measurement of the bulk material could be achieved), using DEM simulation models as case study.

Another objective for this study was to investigate the feasibility of finding out the error value of remaining granular material volume in silo after some discharge (so that a more accurate inventory Figure can be read at any point in time), again, using DEM simulation models. This thesis contrasts the volume accuracy incurred between when measured with only one or two level sensors with the accuracy when several level sensing devices were deployed .

Once several surface levels were determined during different stages of discharge, the results were then compared to values when only one or two point levels were used. The volume of the material within the silo was calculated according to the volume formula for cylinder ($V=\pi r^2 h$) and, the height at any point was substituted in the formula as arithmetic average of measured levels. The more measurement points that was utilized,

the more accurate the volume calculation was expected be because the surface contour of the material was inconsistent, hence unequal levels.

7.1.2 Simulation Models

7.1.2.1 Model 1 (polyethylene plastic pellets, side discharge)

For the center discharge of polyethylene plastic grains, as the graphs revealed, the velocity of particles near the free surface was larger at the initial stages. This trend changed after a considerable time passed so that all the particles more or less moved down with similar vertical velocities. This stage implies that a steady-state condition had been reached.

Moreover, once one studied the contour of the material throughout the simulation time, one noticed the bulk material takes the *V* shape and the valley part of it corresponds to the vicinity of the exit port located almost right in the middle of the system at the bottom.

Axial displacement of particles in *X* and *Y* directions tended to show different patterns depending on the location of the particles. As the particles advanced towards the middle axis in the axial direction, the displacement values also increased (since as they proceeded, most of the particles find their way towards the exit at different levels). Later, most of the particles showed very large displacement values, implying their exit in different axial direction (positive and negative coordinates). By inspecting the vertical velocities of some particles at different locations, one can easily deduce that by time, these values

increased sharply in the negative direction. As the particles descended, their vertical speeds increase logarithmically.

In the same way, by following X and Y axial velocities, one can observe a series of steadily fluctuating values all through the way, with only partial disturbances at the beginning of discharge.

The axial forces tolerated by cylindrical walls were also showing constant pattern, with values fluctuating around zero, however, at points along the downstream, some unexplainable sharp fluctuation in force values were experienced. This incident, happening well after discharge process had begun, could not be accounted for in this study. One might attribute the increase in force values to the release of locked-in stresses between packed particle groups and the resulting energy upon release, could increase the system's vibration that also triggers more disturbances. Visual comparison between laboratory discharge photographs with simulation screen captures, at specific time slots implied the accuracy of the numerical model to some degree.

As the particles approach to the central axis of the cylindrical bin, their vertical velocities increased, regardless of the level of the region the particle was located previously. The velocity shifts could undermine the technique of locating the level sensing devices farther from central axis, since such sensor placement may not be useful as previously was believed.

In the volume measurement section, the discrepancy between 18-point and 2-point measurements (points located at $1/6$ of the diameter from side walls) was about 1 percent (19 vs. 20 percent) through the whole discharge period. The reliability of 2-point

measurement (at $1/6D$) results were better than those of multiple point measurement method for center discharge, because the former was more or less the only viable option in industry. However the calibrated numerical model results indicate a 9 percent difference between these two methods (10 vs. 19 percent), so it was unclear from this study whether or not opting out multiple point measurement method would be a wise choice.

7.1.2.2 Model 2 (polyethylene plastic pellets, side discharge)

For the side discharge of the polyethylene plastic grains, initially the velocity of particles at the surface region of the bulk was higher than it was at the rest as it was the case for center discharge. However, after some time the steady-state discharge dominates the flow process, hence the similar vertical velocities for all particles.

Vertical velocity of particles sharply increased when X was 0.32 meters and Y was 0.8 meters. The former increase exactly corresponds to the location of the discharge point at the right, as opposed to the -0.03 and 0.05 meters which roughly were in the proximity of central axis. This sudden increase in velocity could be attributed to release of kinetic energy when aggregated particles collide with one another, and the amount of energy was proportional to the coefficient of restitution of the plastic particles.

The latter charts continued to study the effect of vertical level of specific particles on their velocities in the same perpendicular direction. The results were that, some particles maintained rather constant values while descending, whereas other particles velocities logarithmically increased while discharging, and later the values remained constant until the rest of simulation which also could be a sign of their departing the system.

Vertical velocity of particles generally sharply accelerated in gravity force direction after a couple of hundreds of timesteps, as the particles decreased altitude. These were also investigated comprehensively in graphical formats.

Observing the values for mean unbalanced and mean contact forces were of great importance prior to initiating a discharge process, since before any dynamic analysis, the particles system should arrive at a balanced state (with virtually zero locked-in stress values) so that no interference between these forces with dynamic analysis of the system could be guaranteed.

To this end, these forces were monitored carefully for the model and their pattern indicate decreasing values until the values approach zero and then maintain a negligible value until the end of simulation.

Likewise, axial forces in side discharge model first reached to a peak value in the beginning of discharge process, but later decreased to a constant non-zero value until the end of discharge process.

Concerning volume measurement validation of simulation results, the difference between 18-point and 2-point measurements (points located at $1/6$ of the diameter from side walls) was about 4.5 percent (8 vs. 12.49 percent) for the whole discharge time. The calibrated numerical model however, indicates an error of 2.42 percent (8 versus 10.42 percent).

7.1.2.3 Model 3 (corn discharge, center discharge)

For the central discharge of corn kernels with an initial porosity of 50 percent, a similar series of analyses was performed as for the plastic grain discharge simulations.

As it was presented in the former chapter, since the corn particles were considerably larger than plastic grains, the contact forces between them were larger. This fact was graphically apparent in the simulation screen shots provided in the former chapter.

Vertical velocities versus axial positions indicate a constantly fluctuating values with small amplitude and therefore, velocity values were independent of axial position of corn grains until they approached above (and around) central point. At the central axle region, the velocities sharply increase. With regards to the vertical velocity relationship with the altitude, it was observed that the velocity sharply increase as the particles descended, a very similar case to those of the polyethylene plastic grains.

Vertical forces initially start fluctuating by large amplitude but later on, as the system approached a steady-state discharge process, the oscillation in force values decreases to near zero value as the vertical unbalanced forces cancel out one another. The same behavioral pattern was observable in mean unbalanced and mean contact forces among particles.

With regards to volume measurement validation, the discrepancy between 18-point to 2-point measurements (points located at $1/6$ of the diameter from side walls) was about 0.50 percent (10 vs. 10.5 percent) through the whole discharge process. As for the calibrated model, the error actually increased about negative 4.52 percent (10 vs. 5.48 percent).

7.2 Laboratory Experiment for Validation

Laboratory discharge processes were performed for three models and then these results were compared to numerical models. The physical silo model in the laboratory results

were scaled up for the comparison purposes (cylindrical geometry with the same aspect ratio of the numerical models). One important measurement process was performed on the point levels located roughly afar the side walls about $1/6$ of the silo diameter. These locations typically are used in grain storage facilities such as ethanol plants.

In large industrial silos usually one or two measurement devices (i.e. plumb-bob, laser) were mounted at this special distance from bin side walls. This location was unique since when the initial compaction of the material in silo had a cone-up shape, the error quantity decreases because of cancelling out of void volume values with horizontal leftover volumes in the side (proof of this fact is very straightforward). A schematic of a level sensing device and its location above with the bin was given in Figure 7.1

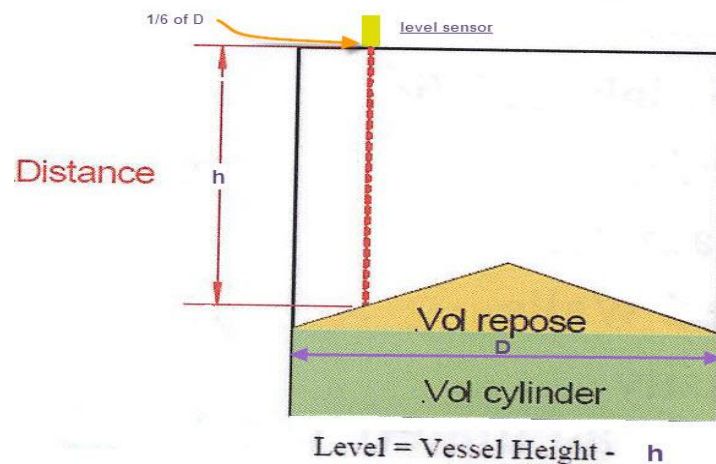


Figure 7.1 Level sensor installed at $1/6$ of the bin diameter.

For the abovementioned reasons, the tests were specifically performed at those special locations (left or right with respect to central axis), in order to find out whether this practice was accurate in estimating the volume of grains in silos. As the results indicated,

this procedure improved accuracy of reading slightly when compared to single point measurement method.

The chief rationale of this research were investigating the flow pattern of granular material in silo, and estimating the volume of bulk material inside at any point by, while taking into account the nonlinear force structure between them. The nonlinear and somewhat random distribution of particles on surface, and also the resulting amorphous contours formed on the free surface were the main factors preventing more accurate volume measurements from being calculated.

One general hypothesis that, particles closer to the discharge point accelerate towards exit more rapidly than do particles at side regions, was shown to be true in this study.

Large discrepancies were not incurred by industry operations who most commonly settle for the single or double point measurements in order to estimate the remaining granular bulk in very large silos (a percentage discrepancy around 5.0 to 6.5 if the simulation represents the condition as close to reality as possible). The issue arises most of the time in industry was that in silos with diameters as large as 100 feet, the error values amount to much larger discrepancies in volume, resulting in much heftier inventory valuation errors.

The symmetrical geometry of cylindrical bins provides valuable advantage when affording multiple point measurements in terms of time, personnel, or equipment in industry, is not feasible. With respect to the type of grains in a production facility, the error amount in auditing can change as well. In the present study as the discharge rate model for corn particle was more predictive than were those for polyethylene plastic

grains. Also, the average error value in single and 2 (both types), and 3 point measurements for corn discharge was less than those for plastic grains, while for multiple point measurements, the value of error was the least in plastic grain simulation. As a result, the method of volume measurements in silos should be customized to the type of grains to be or discharged.

As for different types of discharge, side or center, the results in this case showed that on average, center discharge was more predictable than side discharge (error % of *12.93* vs. *16.60*, respectively). Consequently, one might as well contend that side discharge process in industries should be practiced less frequently, if not avoided completely.

Finally, in the adjusted models, the results appeared to match more closely with those of the laboratory and while some improved results which was the result of progressive calibration were experienced. Rather than selecting particles' mechanical properties based on numerical Triaxial test (which was performed for the first runs), the second rounds' parameters were selected purely based on the response of physical discharge model, so that the new simulation more closely represent the actual process. The question of which model is the most predictive for the large industrial silo discharge processes, is hard to answer within the scope of this study, since the dimension factor must act a governing part in this case.

Regarding the optimum locations, and the number of level sensing devices, it was identified in this study that the commonly practiced method of placing two sensors at the distance from side walls of exactly $1/6$ of diameter is sufficient if the error values around *10* percent would be tolerated by the management. However, as explained earlier, a more

thorough experimental design, tackling the effects of every factor contributing to the measurement error increase, can be carried out for getting more conclusive results.

7.3 Limitations

Some of the constraints faced in this study might have been overcome by holding important assumptions while other factors still can be regarded as a foundation for inaccuracies or even impediments. A couple of possibly important factors which might have affected the process of obtaining more accurate results for this study are listed below.

1. One issue is the time, as well as computationally prohibitive nature of DEM; by using a personal computer with a fair processing speed / memory, to simulate particle flow in a silo model with a diameter of 1.6 meters and a height of 1 meter, one can expect to get results in two weeks for each model (complete discharge). Modeling a silo with real-life dimensions can take half a dozen months per model if an average computer is being used for it; thus, more accurate models require much more powerful computers with parallel processing capabilities.
2. In the physical models which were used for the validation/ verification purposes, the proportion of particles dimension to the silo dimension is much larger than it is in real-life industrial silos. Even in the numerical model for polyethylene plastic grains, since the dimensions were larger than those of the physical one, the exact

same ratio is not maintained albeit the scaling factor were used in order to decrease this difference.

3. Real industrial silos which are used for grain storage are difficult to see inside them because of several factors including dust, height, lack of light, and lack of accessible windows among other things. Most of the silos during the time this research was being developed, were only partially full (due to the harvest season), and also getting permission to climb on a very tall silo was a challenge, so it was not practical to include a full-size silo discharge process results in our study.
4. Nonlinear nature of bulk material behavior when stocked or in flow makes a more accurate study of it less practical. Particles form a random structure at any given time and a slightest disturbance makes them rearrange in a totally different random shape. One of the few non-random shapes that bulk material can take is the so-called hill with a specific angle of repose which is related to friction coefficient of particles. Other than that, bulk materials neither flow like liquid, nor have specific shapes like solids. Consequently, along with DEM, complicated molecular dynamics research application should be performed at the same time, so that a better understanding of relationships between arbitrary forces and the shape of bulk material either at flow, or stagnant, could be reached.

5. For the reason specified in part 4, one needs to investigate the effect of size in simulating the discharge of bulk matter from silos, and in that case the result of the models presented in this paper might show some dissimilarity with those of the larger, more complex models.
6. The shape of corn kernels is not a completely round sphere, as was represented in the numerical model earlier, rather, grains have a *V* (or tear-drop) shape. This issue could have been solved by using clumps or super-particles by bonding two or more particles. In this study, nonetheless, this design was not constructed as the version of software availability for this paper lacked this feature.

7.4 Future Work and Extension /Recommendations

Obviously a much larger numerical model could be constructed using computers with high computational capacity, or with ones' with parallel processing capabilities. In doing so, more predictive models could be produced. The ratio of granular particles' dimensions to silo dimensions could be maintained more closely in this model.

The experiments could be carried out using various types of material, so that an experimental design set could be constructed and different factors influence on discharge rate and pattern could be studies one at a time with this method.

The granular particles could be represented as clumps, as explained earlier, so that an enhanced contact force prediction and thus improved volume measurements might be achieved.

For more accurate volume estimation, various speed sensors could be installed at surface of bulk material at different locations on silo and, following the discharge, the log file of sensor signals can be studied to see if there is a connection between higher axial or vertical speeds of particles and, the rate with which these particles descent towards discharge point; If there is a strong correlation then the availability number of level-sensing devices could be installed exactly above those region with higher velocity.

Additionally, as explained earlier, after some discharge process, the remaining volume of the bulk material could be determined easily by linear interpolation of the points located between highest and lowest values for all the models. This procedure would require a computer program to construct an algorithm to systematically estimate the curved surface topographies linearly.

Lastly, for a more precise outcome, other external factors such as, temperature, moisture content of grains, dryness, and so on, should be taken into account, either directly in the model or, by performing subsequent experimental designs.

References

- Balevicius, R., Kapianauskas, R., Mroz, Z., & Sielamowicz, I. (2005). Modelling of filling and discharge of granular materials in hoppers by discrete element method: optimization of some flow parameters. *6th World Congresses of Structural and Multidisciplinary Optimization* (pp. 1-10). Rio de Janeiro: Laboratory of Numerical Modelling- Institute of Fundamental Technological Research.
- Brumbi, D. (2006). Industrial Level Sensing with Radar . *Frequenz* , 1-5.
- Chang, D., Lu, H., & Mi, W. (2010). Bulk Terminal Stockpile Automatic Modeling Based on 3D Scanning Technology. *International Conference on Future Information Technology and Management Engineering* (pp. 67-70). Shanghai: IEEE.
- Chen, F. (2009). *Coupled Flow Discrete Element Method Application in Granular Porous Media using Open Source Codes*. Knoxville: University of Tennessee-Knoxville.
- Cheng, Y., Liu, Z. N., Song, W. D., & Au, S. K. (2009). Laboratory Test and Particle Flow Simulation of Silos Problem with Nonhomogeneous Materials. *JOURNAL OF GEOTECHNICAL AND GEOENVIRONMENTAL ENGINEERING* , 1754-1761.
- Chuayjan, W., Pothiphan, S., Wiwatanapataphee, B., & Wu, Y. (2010). NUMERICAL SIMULATION OF GRANULAR FLOW DURING FILLING AND DISCHARGING OF A SILO. *International Journal of Pure and Applied Mathematics* , 347-364.
- Coetzee, C. J., Basson, A. H., & Vermeer, P. A. (2006). DISCRETE AND CONTINUUM MODELLING OF SILO DISCHARGE. *R&D Journal, A Publication of the South African Institution of Mechanical Engineering* , 26-38.
- DIMETIX Dimetix AG. (2004 йил 10-May). *Silo level measurement with Silolevell*. Retrieved 2011 йил 2-August from Dimetix: www.dimetix.com
- Feise, H., & Daiss, A. (2003). BUILDING A NUMERICAL MODEL FOR BULK MATERIALS FROM STANDARD SHEAR TEST DATA. *Task Quarterly* , 539-547.
- Feng, L., Yanbo, H., & Xiaoqing, W. (2009). Mass Measurement Method of Bulk Materials Based on Reverse Engineering. *International Conference on Intelligent Human-Machine Systems and Cybernetics* (pp. 81-84). Zhengzhou: IEEE.
- Fu, Y. (2005 йил December). EXPERIMENTAL QUANTIFICATION AND DEM SIMULATION OF MICRO-MACRO BEHAVIORS OF GRANULAR MATERIALS USING X-RAY TOMOGRAPHY IMAGING. *EXPERIMENTAL QUANTIFICATION AND DEM SIMULATION OF MICRO-MACRO BEHAVIORS OF GRANULAR*

MATERIALS USING X-RAY TOMOGRAPHY IMAGING . Tongji, Shanghai, China: Tongji University.

Garner Industries. (2011 йил 4-April). *3D level scanner*. Retrieved 2011 йил 1-August from Binmaster: <http://binmaster.com/3DLevelScanner/finc.html>

González-Montellano, C., Ayuga, F., & Ooi, J. Y. (2010). Discrete element modelling of grain flow in a planar silo: influence of simulation parameters. *Springer-Verlag* , 149-158.

Gonzalez-Montellano, C., Ramirez, A., Gallego, E., & Ayuga, F. (2011). Validation and experimental calibration of 3D discrete element models for the simulation of the discharge flow in silos. *Chemical Engineering Science* , 5116-5124.

Grudzien, K., Niedostatkiewicz, M., Adrien, J., Tejchman, J., & Maire, E. (2011). Quantitative estimation of volume changes of granular materials during silo flow using X-ray tomography. *Elsevier* , 59-67.

Isiker, H., & Canbolat, H. (2009). Concept for a novel grain level measurement method in silos. *Elsevier, Computers and Electronics in Agriculture* , 258-267.

Itasca: Engineering Consulting and Software. (2011 йил 20-July). PFC3D Particle Flow Code in 3 Dimensions Manual. Minneapolis, Minnesota, USA. From www.itascacg.com

Jonsen, P. (2001). *Methods for simulation of powder filling*. Luleå : Civilingenjorsprogrammet Teknisk fysik, Luleå tekniska universitet.

Landry, J. W., Grest, G. S., Silbert, L. E., & Plimpton, S. J. (2003). Confined granular packings: structure, stress, and forces. *Cond.Mat.Soft* , 1-11.

Lewis, R. W., Gethin, D. T., Yang, X. S., & Rowe, R. C. (2005). A combined finite-discrete element method for simulating pharmaceutical powder tableting. *INTERNATIONAL JOURNAL FOR NUMERICAL METHODS IN ENGINEERING* , 62:853-869.

Manchanda, R. (2011 йил May). Mechanical, Failure and Flow Properties of Sands: Micromechanical Models. Austin, Texas, USA: University of Texas at Austin.

Mani, S., Roberge, M., Tabil, L. G., & Sokhansanj, S. (2003 йил 6-9-July). Modeling of Densification of Biomass Grinds using Discrete Element Method by PFC3D. Montreal, Quebec, Canada.

Nazeri, H., Mustoe, G. W., Rozgonyi, T., & Wienecke, C. (2002). *IMPLEMENTATION OF A DISCRETE ELEMENT METHODOLOGY FOR THE MODELING OF GRAVITY FLOW OF ORE IN ORE PASSES*. Golden: Colorado School of Mines; Advanced Terra testing, Inc.

- Oñate, E., & Rojek, J. (2004). Combination of discrete element and finite element methods for dynamic analysis of geomechanics problems. *Elsevier, Computer methods in applied mechanics and engineering* , 3087-3128.
- Parisi, D. R., Masson, S., & Martinez, J. (2004). Partitioned Distinct Element Method Simulation of Granular Flow within Industrial Silos. *ASCE* , 771-779.
- Parker, B. M. (2009 йил 20-November). Simulation and Analysis of Particle Flow Through an Aggregate Stockpile. *Simulation and Analysis of Particle Flow Through an Aggregate Stockpile* . Blacksburg, VA, USA: Virginia Polytechnic Institute and State University.
- Ponce-Garcia, N., Figueroa, D., Lopez-Huape, G., Martinez, H., & Martinez-Peniche, R. (2008). Study of Viscoelastic Properties of Wheat Kernels Using Compression Load Method. *Cereal Chem, AACC International, Inc.* , 667-672.
- Preh, A., & Poisel, R. (2007). *PFC3D Applications*. Vienna: Institute for Engineering Geology, Vienna University of Technology.
- Rombach, G. A., & Neumann, F. (2004). 3-D FINITE ELEMENT MODELLING OF GRANULAR FLOW IN SILOS. *17th ASCE Engineering Mechanics Conference* (pp. 1-8). Newark: University of Delaware.
- Rotter, J. M., Holst, M. G., Ooi, J., & Sanad, A. (1998). Silo pressure predictions using discrete–element and finite–element analyses. *Philosophical Transactions of The Royal Society* , 2685-2712.
- Sliva, A., & Zegzulka, J. (2004). THE 3DIMENSIONAL (TRIAXIAL) INDICATOR FOR A BULK SOLID PRESSURE. *Acta Metallurgica Slovaca* , 225-229.
- Sr. Lewis, J. D. *Technology Review Level Measurement of Bulk Solids in Bins, Silos and Hoppers*.
- Time Little. (2007). *Trends in Level Measurement*. 2007 Siemens Milltronics Process Instruments Inc.
- Vanel, L., Claudin, J. P., Cates, M., Clement, E., & Wittmer, J. (1999). Stresses in silos: Comparison between theoretical models and new experiments. *Cond-mat* .
- Vidal, P., Guaita, M., & Ayuga, F. (2005). Analysis of Dynamic Discharge Pressures in Cylindrical Slender Silos with a Flat Bottom or with a Hopper: Comparison with Eurocode 1. *Elsevier* , 335-348.

Youfu, H., Xiaohui, C., Daoming, W., & Qiangqiang, H. (2011). Distinct Element Method Simulation of Discharging in Coal Silos. *Forth International Conference of Intelligent Computation Technology and Automation* (pp. 784-787). Xuzhou: IEEE.

Zhang, Q., & Britton, M. G. (2003). A micromechanics model for predicting dynamic loads during discharge in bulk solids storage structures. *CANADIAN BIOSYSTEMS ENGINEERING* , 5.21- 5.25.

Zhou, Y., Wright, B., Yang, R., Xu, B., & Yu, A. (1999). Rolling friction in the dynamic simulation of sandpile formation. *Elsevier Physica* , 536-553.

Zhu, H., & Yu, A. (2002). Averaging method of granular materials. *The American Physical Society* , 1-10.

Appendix-A

DISTINCT ELEMENT METHOD (DEM)

A.1 General Description

There are two major approaches for the analysis of behavior of granular particles in micro-structure level: continuum and discrete.

Continuum analysis of granular materials is very difficult because the calibration of a constitutive model includes lots of material constants without clear physical meaning. The discrete approach has an exceptional advantage in identifying micromechanics of particulate matter by modeling these grains as packed assemblies of discrete constituents since “the particle arrangement can be modeled explicitly and the material constants have clear physical meaning” (Fu, 2005).

Substantial attempts were done in order to define the material parameters for DEM and FEM models so that making logical evaluations between the two methods to be practical (Rotter et al., 1998).

Discrete element method first was applied for the purpose of addressing problems in mechanics of rock by Cundall and Stack in 1979. In DEM, the interaction amongst particles is considered as “a dynamic process that achieves a static equilibrium when the

internal forces are balanced” (Mani et al., 2003). This procedure is an explicit numerical method proposed to serve as a model of dynamic behavior of particle-particle or, particle-walls interactions, if these particles are confined in some kind of storage bin.

A complete nonlinear and dynamic behavior of distinct particles, interacting with one another, could be captured using numerical method of DEM.

DEM has provided a numerical means for analyzing the progressive movements and interactions of bodies in granular assemblies. Its algorithm applies Newton’s second law to each particle within the system. The continual movement of each body results from the non-equilibrium of different forces exerted on it. DEM explicitly models the dynamic motion and mechanical interaction of each body at discrete points in time, with each point being termed as a time step. For this purpose, integration of equations of motion and contact laws is necessary (Nazeri et al., 2002).

The force-displacement relationship principle applies for these particles if they are in a compressed state. DEM considers each and every particle as a rigid body with their movements and contacts being traced easily and the resulting forces caused by interaction of these elements with one another could be calculated.

A DEM simulation operates under a time-marching algorithm in which the dynamic movements and non-linear behavior of the confined or flowing particles’ stresses are identified during each time-step. Selecting a stable time-step (could be a fraction of a second), is a key factor for the simulation’s fast convergence to a stable condition. In DEM spherical elements if used, are very efficient in terms of computational intensity and this also reduces the time dedicated for these types of simulation problems. Unlike

finite element method, the boundary conditions are not considered fixed in DEM and so, highly flexible boundary conditions could be applied when using the latter method. An important point here is that, a real representation of element shapes in DEM as far as limitations allow, is a determining factor in getting acceptable results. Most of the software programs dedicated for DEM simulations are equipped with automatic contact detection capability among particles which is a valuable feature in addressing such problems as granular flow in silo and many other similar models. When the particle shapes are irregular, however, this contact detection algorithm might not operate as efficient since, DEM would require much more time-steps to arrive at a solution.

In the macroscopic level, we might observe friction, contact plasticity (recoil), and possible cohesion, adhesion or electrostatic attraction between colliding spheres and in addition to those forces mentioned, in a much larger scales, we might witness the gravity force attractions between particles because of the large mass they possess. (these forces usually are accounted for between large astronomical objects). Coulomb forces (electrostatic attraction or repulsion of particles having electric charge), Pauli repulsion (a quantum mechanical principle stating that no two identical particles with half-integer spin may occupy the same quantum state concurrently) and, Van Der Waals force (sum of the attracting or repulsive forces between molecules) could exist among the interacting particles.

Generally, the continuum approach works at macroscopic level and, the distinct method works at micro level. In continuum approach, the macroscopic behavior of granular flow is described by the balance equations facilitated with constitutive relations and boundary conditions and, the most pressing issue with continuum methods lies in the determination

of suitable constitutive relations. However, in DEM approach, it is not necessary to frame global hypotheses such as steady-state, uniform constituency, and constitutive relations (Zhu and Yu, 2002). In Table A.1, the parameters generally used for discrete and continuum systems are contrasted for the equation of balance.

Table A.1 Quantities included in the balance equations of discrete and continuum system (Zhu, and Yu, 2002).

Discrete system		Continuum system ^a	
m_i	Mass of particle i	ρ	Mass density
\mathbf{v}_i	Velocity of particle i	\mathbf{u}	Velocity
$\boldsymbol{\omega}_i$	Angular velocity of particle i	$\boldsymbol{\omega}$	Angular velocity
$m_i \mathbf{v}_i$	Linear momentum of particle i	$\mathbf{l} \cdot \boldsymbol{\omega}$	Internal spin density
$\mathbf{l}_i \cdot \boldsymbol{\omega}_i$	Angular momentum of particle i	\mathbf{T}	Stress tensor
$\mathbf{f}_{ij}^a, \mathbf{f}_i^b$	Interaction forces acting on particle i exerted by particle j and boundary	\mathbf{M}	Couple stress tensor
\mathbf{g}	Body force per unit mass acting on particle	\mathbf{M}^r	Rate of supply of internal spin to particles
$\mathbf{m}_{ij}^a, \mathbf{m}_i^b$	Torques acting on particle i exerted by particle j and boundary	E	Energy density
E_i	Energy of particle i	\mathbf{q}^E	Total flux of kinetic energy and intrinsic energy
W_{ij}, W_i^a, W_i^b	Rates of mechanical work done by particle j , the boundary, and the body force on particle i	\dot{h}	Heat source density
Q_{ij}, Q_i^a	Rates of heat transfer from particle j and boundary to particle i		
H_i	Heat source of particle i		

In distinct element method, the particles are considered rigid bodies but minor overlap between them is allowed through a stiffness model. All the deformations, however, take place in the contacts. An illustration of contact forces as well as resultant deformations in a packed assembly of grains is given in Figure A.1. The thicker black lines is an indication of contact forces (hence stresses) are more dominant in those areas, as seen in the right Figure below.

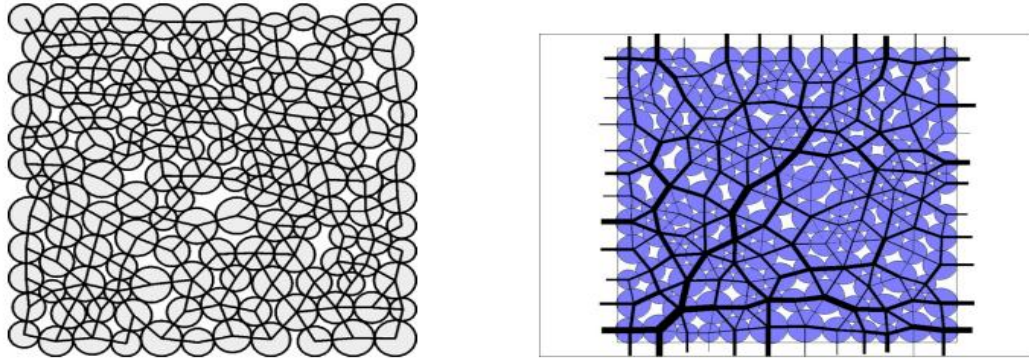


Figure A.1 Contact-only deformation and the contact forces between grains (Preh & Poisel, 2007).

A.2 Boundary conditions in DEM Simulation

True representation of particles' boundary conditions is very important in modeling when their dynamics are influenced by shape and mechanical performance of the boundary.

DEM can represent two forms of boundary condition namely, imaginary (periodic) and physical (real). Periodic boundaries allow a particle to pass across one side of the problem domain and automatically reappear on the opposite boundary in the same position and same initial velocity as the original particle; "they do not require any contact detection" (Mani, 2003). The use of periodic boundary conditions necessitates having information on initial conditions of particles (Kremmer and Favier, 2001). As mentioned earlier, the particles in DEM are considered as rigid bodies nevertheless, a small overlap between them is permitted at the contact points. For a granular material, since the stress changes with time (especially when the systems is slightly disturbed or vibrated), the system can be regarded as a semi-static one. Computations of contact forces and their related displacements in a packed or flowing assemblage are performed by tracing each and every particle movement and at the same time, solving associated Newtonian equation of motion. The governing formula is given by the equation 8.1 below.

$$M\ddot{x} + D\dot{x} + R(x) = F$$

Equation A.1

\ddot{x} , \dot{x} and x are acceleration, velocity, and displacement vectors, respectively in the equation above. M is the displaced mass, D is the damping coefficient, R is the internal restoring force, and F is the external force. The damping coefficient helps dissipate kinetic energy. In most of the packages the time-step is adjusted automatically according to local conditions. It is important to mention that the velocities and accelerations within each time-step are presumed to be constant in DEM simulations.

This time-step could be so small that during a single time-step, the disturbance in one particle cannot spread from one particle further than its instant neighbors, therefore, in the cumulative time-steps, the contact forces acting between all particles are established by their own interaction with the neighbor particle.

“The calculations are performed alternatively by applying Newton’s second law to the particles and the force-displacement law to the contacts” (Fu, 2005). The first equation identifies the movement of each particle within each contact, while the second law updates the contact force resulting from relative movement in every contact.

The main purpose of DEM is to sufficiently characterize a certain phenomenon; “it therefore requires the use of contact models that represent the characteristics of the simulated material as reliable as possible” (Montellano et al, 2011). However, DEM also needs that the values used for the numerical model to represent the properties of the real physical model. Consequently, the initial values which are acquired for the particles are established either by classic direct measurement, or by calibrating the existing simulation parameters so that, the behavior of the model represents that of the real situation. This

happens since there is no such method currently with which, the exact behavior of the granular matter to be replicated and thus, progressive calibration of the model based on observation of real model becomes important. A calculation cycle outline is given in Figure diagram A.2.

As seen in the diagram, calculation cycles require the repeated application of the law of motion to each particle, and a constant updating of wall positions. At the start of each time-step, the set of contacts is updated from the known particle and wall positions. The force-displacement law is then applied to each contact to update the contact forces based on the relative motion between the two entities at the contact and the contact constitutive model. Subsequently, the law of motion is applied to each particle to update its velocity and position according to the resulting force and moment stemming from the contact forces, as well as other forces acting on the particle (Itasca, 1999).

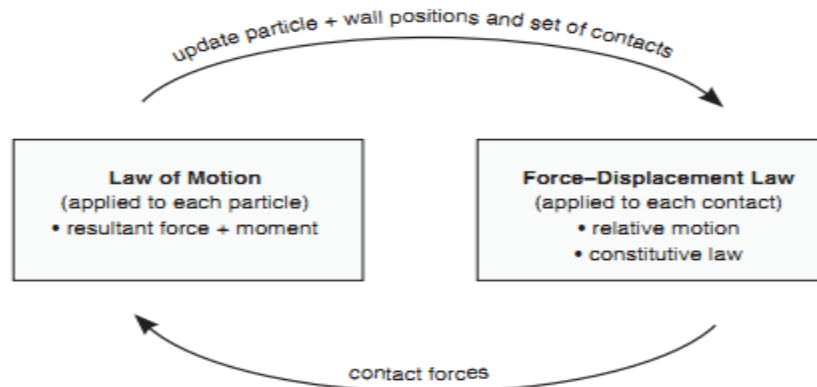


Figure A.2 Calculation cycle in DEM simulation (Itasca, 2011)

A.3 Force-Displacement Law

This law describes the relative displacement between two particles at the contact and the acting contact force on these particles. In Figures A.3 and A.4, Particle-particle and

particle-wall (or with any other fixed boundary in DEM) force diagrams are shown respectively. U^n is the overlap between the contacting entities, b , w and n_i represent ball and wall and normal unit vector of the contact respectively.

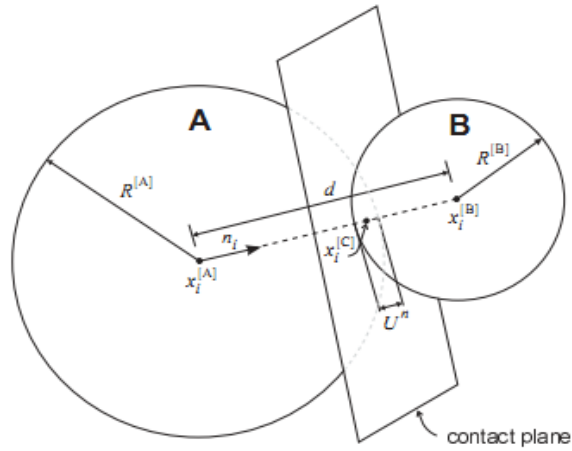


Figure A.3 Ball-Ball contact (Itasca, 2011)

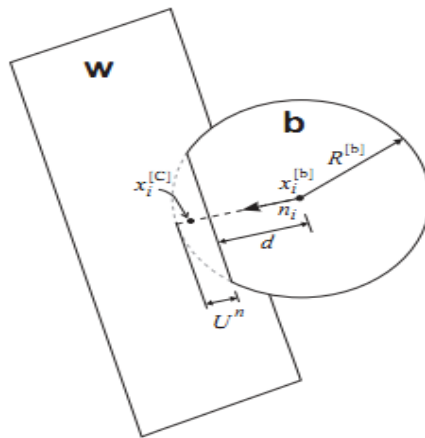


Figure A.4 Ball-Wall contacts (Itasca, 1999)

Where;

$$n_i = \frac{x_i^{[B]} - x_i^{[A]}}{d} \quad (\text{ball-ball})$$

$$d = |x_i^{[B]} - x_i^{[A]}| = \sqrt{(x_i^{[B]} - x_i^{[A]}) (x_i^{[B]} - x_i^{[A]})} \quad (\text{ball-ball})$$

Equation A.2 (Itasca, 1999)

U^n , which is the overlap, is the relative contact displacement in the normal direction is given by the expressions:

$$U^n = \begin{cases} R^{[A]} + R^{[B]} - d, & (\text{ball-ball}) \\ R^{[b]} - d, & (\text{ball-wall}) \end{cases} \quad \text{Equation A.3 (Itasca, 1999)}$$

And the position of the contact point is determined by expressions:

$$x_i^{[c]} = \begin{cases} x_i^{[A]} + \left(R^{[A]} - \frac{1}{2}U^n\right)n_i, & (\text{ball-ball}) \\ x_i^{[b]} + \left(R^{[b]} - \frac{1}{2}U^n\right)n_i, & (\text{ball-wall}) \end{cases} \quad \text{Equation A.4 (Itasca, 1999)}$$

F_i which is the forced between ball-ball or ball-wall could break down into a normal and shear component about the contact plane and, its normal component is given by expressions A.5 and A.6.

$$(a) \quad \dot{\gamma}_i = F_i^n + F_i^s, \quad (b) \quad F_i^n = K^n U^n n_i$$

Equation A.5 (a), and A.6 (b) (Itasca, 1999)

F_n and F_s indicate normal and shear components of F vector, respectively. K_n and K_s represent the normal and shear stiffness at the contact.

In a commonly utilized linear model for two entities in contact, A and B, normal and shear stiffness values are given by Equation A.7.

$$K_n = \frac{k_n^A k_n^B}{k_n^A + k_n^B} \cdot K_s = \frac{k_s^A k_s^B}{k_s^A + k_s^B}$$

Equation A.7 (Itasca, 1999)

A.4 Simplified Hertz-Mindlin Model

This model is a nonlinear contact formula between particles (unlike the more commonly used linear model). It was proposed by Mindlin in 1954. In order to work with this model, we need to provide the elastic constants, namely, shear modulus (G) and Poisson's ratio (ν) as inputs. The normal secant and shear tangent stiffness for this model are given as follows:

$$K^n = \left(\frac{2(G)\sqrt{2R}}{3(1-\nu)} \right) \sqrt{U^n}$$

$$k^s = \left(\frac{2(G)^2(3(1-\nu))\bar{R}^{1/3}}{2-\nu} \right) |F_i^n|^{1/3}$$

Equation A.8 (Itasca, 1999).

U^n is the overlap between spheres and F_i^n is the normal contact force.

A.5 Slip Model

In most of the DEM programs, a limit is set to the shear force value of F_{max}^s in the following formula (8.9) on the spheres dependent on the normal force applied on the sphere and the coefficient of friction μ .

$$F_{max}^s = \mu |F_1^n| \quad \text{Equation A.9 (Itasca, 1999)}$$

Therefore, when shear force rises above the maximum shear force assigned for the contact, the updated shear force is redefined as the maximum shear force.

$$\text{If } |F_1^s| \geq F_{max}^s, F_1^s = F_{max}^s \quad \text{Equation A.10 (Itasca, 1999)}$$

A.6 Rolling

When one desires to simulate the behavior of non-spherical particles with irregular shapes (for instance, sand grains), they should account for the resistance for free rolling that these particles show. We can observe an effect of rolling resistance in Figure A.5 .In the lack of spherically symmetric particle shapes. The ‘rolling resistance’ effect has to be added to the model later. A number of researchers (including Manchanda (2011)), felt a need to control the rolling of spherical particles to reproduce the stress-strain response observed in the simulation. However, rolling resistance models available in the literature today are very complicated to work with.

The rolling resistance is therefore stemmed from the deformation of the rolling part or wall and, it is a function of material of particles or the ground.

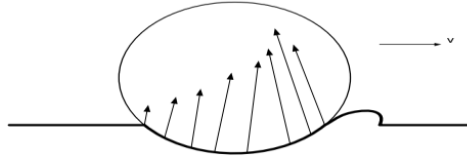


Figure A.5 Rolling resistance effect on particles (Preh and poisel, 2007).

A.7 Motion Law

As discussed earlier, the motion of a rigid component is established by the resulting force and moment vectors working upon it. This can be explained as the translational movement of a point on the component, along with rotational movement of the component itself. If we consider ω_i and ω'_I as angular velocity and angular acceleration respectively, the equation of motion can be given by two vectors; one vector is the resulting force against the translational movement, and the other one is the resulting moment of inertia of the rotational motion.

This means that we can express the translational motion in the vector form of: $\mathbf{F}_i = m (\ddot{\mathbf{x}} - \mathbf{g}_i)$ where, \mathbf{F}_i is the resultant some of all externally applied forces acting on the particle, m is the total mass of the particle, and \mathbf{g}_i is the body force acceleration vector (Itasca,1999). Equation of rotational motion for particles can be derived from Euler's equation; $\mathbf{M}_i = \mathbf{I} \omega'_i = (\frac{2}{5} m R^2) \omega'_I$, where \mathbf{I} is the principal moment of inertia of the particle and R is the radius of the spherical particle.

Most of the DEM software products operate on principle of spherical particle, so at this case, the calculation of moment of inertia for a spherical particle is adequate. Yet, many DEM packages let the users create their own super particles by combining two or more

spheres with different radius together so that they can sufficiently represent real world irregular particle shapes like wheat beans or rocks.

The package which is used for this study, *PFC3D* (Particle Flow 3D, Itasca), employs a Clump Logic and then solves the equation of motion, as well as force-displacement equations based on this logic. Once particles are added to a super particle (clump), the components of the said clump act as a rigid single particle with different geometry. Moreover, once a clump is created, then the component particles never break apart, no matter how much stress is applied on them, either normal or shear.

A.8 Time-step Establishment

The calculated solutions in DEM are stable on condition that the selected time-step will not go above the critical time-step. Thus, in DEM some methods are applied in order to estimate a critical time-step in the beginning of every cycle. We know that for a mass-spring system (in one dimension), with a mass of m , spring stiffness of k , the movement of the mass is governed by $-k x = m\ddot{x}$ and the critical time-step of this system is given by:

$t_{crit} = \frac{T}{\pi}$, where $T = 2\pi \sqrt{\frac{m}{k}}$. By applying these equations on a multi-mass-spring system,

the critical time-step for discrete element simulation is given by;

$$t_{crit} = \begin{cases} \sqrt{m/k^{tran}}, & \text{(translational motion)} \\ \sqrt{I/k^{rot}}, & \text{(rotational motion)} \end{cases} \quad \text{Equation A.11 (Itasca, 1999)}$$

Where, K^{tran} and K^{rot} are the translational and rotational stiffness, respectively.

These are some basic parameters needed for performing a discrete element simulation. In the Figure A.6, for better understanding of the forces and moments at each contact between two spherical particles, a simple depiction is given.

A.9 Damping System Model

Generally in most software packages, damping is applied in a DEM model for the energy produced by particle movements to be dispersed in order for the system to achieve a stable state in a shorter time span. Damping force is added to the equation of motion in order to damp the accelerated movement. This is the case with the *PFC3D* package which is used for this simulation study. “Damping works by decreasing the kinetic energy a certain number of times each simulation cycle” (Fu, 2005). Damping force is regulated by α in such a way that; $\alpha_{dc} = \pi D_f$ where, $D_f = \frac{\Delta W(i)}{W(i)} / 4 \pi$, α_{dc} is damping coefficient, D_f is a fraction of critical damping, $\Delta W(i)$ is the energy removed per cycle and, $W(i)$ is the mean kinetic energy at the instant of removal.

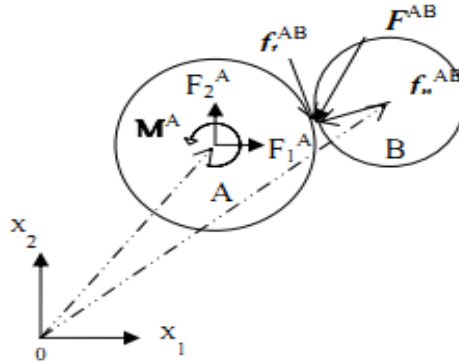


Figure A.6 Illustration of contact forces between two spheres (Itasca, 1999).

A.10 Contact Models

Most of the popular DEM simulation packages, including *PFC*, offer maximum of three models for the constitutive model contacts. These include;

- A stiffness model (principle contact model), mostly linear or, simplified Hertz-Mindlin
- A slip (frictional) model (optional)
- A bonding model (optional)

A.10.1 Linear Contact Model

This stiffness contact model associates the forces on the contact point and the resultant relative displacement in the normal and/ or shear directions. In Figure A.7, normal component of the stiffness model is illustrated.

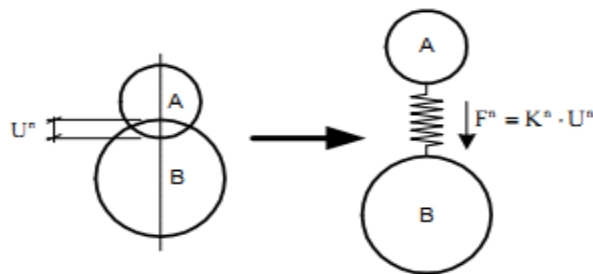


Figure A.7 Representation of normal component of stiffness as a spring-mass system in a linear contact model (Preh and Poisel, 2007).

The normal stiffness is secant stiffness because it corresponds to the normal force in normal displacement direction.

$$F_i^n = K^n \cdot U^n \cdot n_i \quad \text{Equation A.12 Normal spring force with nonlinear stiffness (Preh and Poisel, 2007).}$$

Additionally, in Figure A.8, the shear element of the stiffness model is shown.

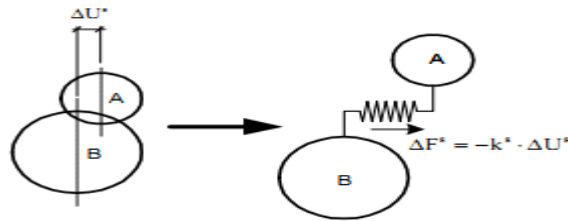


Figure A.8 Representation of shear component of stiffness model as a spring-mass system in a linear contact model (Preh and Poisel, 2007).

The shear stiffness is a tangent stiffness, as it corresponds to the increase of shear force to the increase of shear displacement (partial displacement, Δ)

$$\Delta F_i^s = -k^s \cdot \Delta U_i^s \quad \text{Equation A.13 Shear (tangential) spring force (Itasca, 1999).}$$

A.10.2 Bonds

A contact bond can be imagined as a pair of elastic springs (or a point of glue), with constant normal and shear stiffness acting at the contact point. These two springs have specified shear and tensile normal strengths; “however, the existence of a contact bond eliminates the slip possibility” (Itasca, 2011).

Figure A.9 shows a contact bond added between two balls with different radii.

contact bond

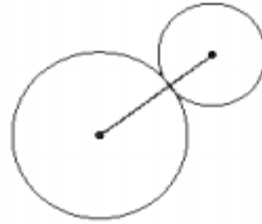


Figure A.9 This 'glue like' contact acts over a very small area in the contact point and does not show resistance to moment (Itasca, 1999).

In contrast, parallel bond consists of material which behaves like cementation between two particles. This type of contact has a radius less than those of the contacting particles. Figure A.10 illustrates this type of bond. The radius of the cementation should be an input to the model.

This bond adds extra material (deposited between two spheres in contact and, if normal and/ or shear stress surpass bond strength, it can break off.

parallel bond

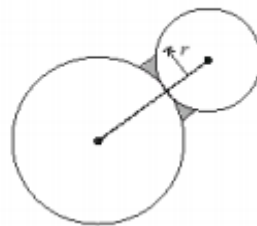


Figure A.10 This 'rigid, cementation' contact acts over large area in the contact point and shows resistance to moment as well (Itasca, 1999).

Appendix-B

CODES USED FOR SIMULATION MODELS (PARTIAL)

B.1 Models 1 and 2 (Center and side discharge of polyethylene plastic pellets) Codes

```
plot create W_master1
```

```
plot set back white cap size 25
```

```
plot add wall blue
```

```
plot add ball orange
```

```
plot add axes black
```

```
wall id=3 face (-.1,-.8,0) (.6,-.8,0) (.6,.8,0) (-.1,.8,0) kn=1e8 ks=1e5
```

```
wall id=4 face (-.1,-.05,0) (-.1,-.9,0) (1.7,-.9,0) (1.7,-.05,0) kn=1e8 ks=1e5
```

```
wall id=5 face (.9,-.8,0) (1.7,-.8,0) (1.7,.8,0) (.9,.8,0) kn=1e8 ks=1e5
```

```
wall id=6 face (1.7,.05,0) (1.7,.9,0) (-.1,.9,0) (-.1,.05,0) kn=1e8 ks=1e5
```

```
wall id=1 ty cy end1 .8 0 0 end2 .8 0 1 rad .8 .8 kn=1e8 edgecheck on
```

```
wall id=2 face (-.1,.80,1) (1.60,.8,1) (1.60,-.8,1) (-.1,-.80,1) kn=1e8
```

```
wall id=7 face (.3,-.17,0) (1.2,-.17,0) (1.2,.1,0) (.3,.1,0) kn=1e8
```

```
def ff_cylinder
```



```
ff_cylinder = 0

_brad = fc_arg(0)

_bx = fc_arg(1)

_by = fc_arg(2)

_bz = fc_arg(3)

_rad = sqrt((_bx-.8)^2 + _by^2)

rad_cz = .8

height = 1

if _rad + _brad > rad_cz then

    ff_cylinder = 1

end_if

end

def expand

rad_cz = .8

nrad_cz = -.8

d_cz = 1.6

height = 1
```

command

```
gen id 1 150000 rad 0.008 0.012 x 0 d_cz y nrad_cz rad_cz z 0 height &
```

```
filter ff_cylinder
```

```
prop dens 1210 kn=.5e6 ks=.5e6
```

```
end_command set gen_error off
```

command

```
gen id 150001 300000 rad 0.008 0.012 x 0 d_cz y nrad_cz rad_cz z 0 height &
```

```
filter ff_cylinder
```

```
prop dens 1210 kn=.5e6 ks=.5e6
```

```
end_command set gen_error off
```

command

```
gen id 300001 350000 rad 0.008 0.012 x 0 d_cz y nrad_cz rad_cz z 0 height &
```

```
filter ff_cylinder
```

```
prop dens 1210 kn=.5e6 ks=.5e6
```

```
end_command set gen_error off
```

end

```
set gen_error off
```

expand

def expand2

rad_cz = .8

nrad_cz= -.8

d_cz =1.6

height=1

command

gen id 350001 400000 rad 0.008 0.012 x 0 d_cz y nrad_cz rad_cz z 0 height &

filter ff_cylinder

prop dens 1210 kn=.5e6 ks=.5e6

end_command set gen_error off

command

gen id 400001 450000 rad 0.008 0.012 x 0 d_cz y nrad_cz rad_cz z 0 height &

filter ff_cylinder

prop dens 1210 kn=.5e6 ks=.5e6

end_command set gen_error off

command

```
gen id 450001 500000 rad 0.008 0.012 x 0 d_cz y nrad_cz rad_cz z 0 height &
```

```
filter ff_cylinder
```

```
prop dens 1210 kn=.5e6 ks=.5e6
```

```
end_command set gen_error off
```

```
end
```

```
set gen_error off
```

```
expand2
```

```
pause
```

```
hist ball xp .8 .1 .5 id=4
```

```
hist ball yp .8 .1 .5 id=5
```

```
hist ball zp .8 .1 .5 id=6
```

```
hist ball zvel .8 .1 .5 id=7
```

```
hist wall xforce id =1
```

```
hist wall zforce id=6
```

```
hist wall zforce id=7
```

```
hist ball zvel .2 .05 .7
```

```
hist ball zvel .8 .05 .7
```

hist ball zvel 1.3 .05 .7

hist ball zvel 1.2 .09 .6

set display history 1

hist write 1 Table 1

hist write 2 Table 2

hist write 6 Table 3

hist write 4 Table 4

hist write 5 Table 5

group clus1 range x 0 1.6 y -.8 .8 z 0 .2

group clus2 range x 0 1.6 y -.8 .8 z .2 .4

group clus3 range x 0 1.6 y -.8 .8 z .4 .6

group clus4 range x 0 1.6 y -.8 .8 z .6 .8

group clus5 range x 0 1.6 y -.8 .8 z .8 1

hist ball s11 .7 -.1 .2

hist ball s12 .7 -.1 .2

hist diagnostic muf

hist energy body

hist ball xp .8 .1 .5 id=4

hist ball yp .8 .1 .5 id=5

hist ball zp .8 .1 .5 id=6

hist ball zvel .8 .1 .5 id=7

hist wall xforce id =1

hist wall zforce id=6

set display history 1

hist write 1 Table 1

hist write 2 Table 2

hist write 6 Table 3

hist write 4 Table 4

hist write 5 Table 5

hist write 7 Table 6

group clus1 range x 0 1.6 y -.8 .8 z 0 .2

group clus2 range x 0 1.6 y -.8 .8 z .2 .4

group clus3 range x 0 1.6 y -.8 .8 z .4 .6

group clus4 range x 0 1.6 y -.8 .8 z .6 .8

group clus5 range x 0 1.6 y -.8 .8 z .8 1

hist ball s11 .7 -.1 .2

hist ball s12 .7 -.1 .2

hist diagnostic muf

hist energy body

damp default local 0.0

damp default viscous norm 0.4

measure id 1 x .3 y -.5 z .4 radius .1

measure id 2 x 1 y .1 z .5 radius .1

measure id 3 x .8 y 0 z .1 radius .1

measure id 4 x 0 y 0 z .3 radius .1

measure id 5 x 1.2 y .2 z .6 radius .35

hist id=8 measure poros id=2

hist id=9 measure poros id=1

hist id=10 measure poros id=3

hist id=11 measure ed23 id=1

hist id=12 measure s12 id=3

hist id=13 measure sliding_fraction id=2

hist id=14 measure poros id=5

hist ball zvel 1.6 .1 .5 id=138

hist ball xvel .8 .1 .5 id=139

hist ball yvel .8 .1 .5 id=140

(Partial) History Codes

hist ball zvel 0 .1 .5 id=141

hist ball zvel 0 -.1 .5 id=142

hist ball zvel 1 -.5 .5 id=143

hist ball zvel 1 -.13 .5 id=144

hist ball zvel .8 .1 .6 id=145

hist ball zvel .8 .1 .6 id=146

hist ball zvel 1.6 .8 .6 id=147

hist ball zvel 1.6 .8 .6 id=148

hist ball zvel .3 .3 .3 id=149

hist ball zvel .3 .8 .2 id=150

hist ball zvel .75 0 .65 id=151

hist ball zvel .75 0 .70 id=152

hist ball zvel .75 0 .1 id=153

hist ball zvel 0.1 0 .25 id=154

hist ball zvel .1 0 .45 id=155

hist ball zvel 0 -.06 .6 id=156

hist ball xp .88 .16 .29 id=157

hist ball yp .88 .16 .12 id=158

hist ball xp .88 .16 .59 id=159

hist ball yp 1.5 -.16 .3 id=160

hist ball xp 1.5 -.16 .4 id=161

hist ball yp .6 .6 .3 id=162

hist ball xp .6 .6 .6 id=163

hist ball yp .6 .6 .5 id=164

hist wall xforce id= 1

hist wall yforce id=1

hist wall zforce id=4

hist wall zforce id=1

hist ball xp .8 .1 .314 id=180

hist ball yp .8 .1 .314 id=190

hist ball zp .8 .1 .314 id=200

hist ball xp .8 .11 .2 id=21

hist ball yp .8 .11 .2 id=22

hist ball zp .8 .11 .2 id=23

hist ball xp .8 .1 .1 id=24

hist ball yp .8 .1 .1 id=25

hist ball zp .8 .1 .1 id=26

hist ball zp 1.2 0 .5 id=50

hist ball xp 1.2 .1 .2 id=51

hist ball yp 1.2 .1 .2 id=52..... Truncated

B.2 Model 3 (Corn discharge, center discharge)-Desired porosity 0.50 with radius multiplication method

```
plot create W_master
```

```
plot set back white cap size 25
```

```
plot add wall blue
```

```
plot add ball orange
```

```
plot add axes black
```

```
def ff_cylinder
```

```
ff_cylinder = 0
```

```
_brad = fc_arg(0)
```

```
_bx = fc_arg(1)
```

```
_by = fc_arg(2)
```

```
_bz = fc_arg(3)
```

```
_rad = sqrt((_bx-.8)^2 + _by^2)
```

```
rad_cy = .8
```

```
height = 1
```

```
if _rad + _brad > rad_cy then

    ff_cylinder = 1

end_if

if _bz + _brad > 1 then

    ff_cylinder=1

    end_if

end

def expand

    n_stiff = 4.5e5

    s_stiff = 4.5e5

    rad_cz = .8

    nrad_cz= -.8

    d_cz =1.6

    height = 1

    tot_vol = height * pi * rad_cz^2.0

    poros = 0.50 ; desired final porosity

    num = 15000 ; number of particles
```

rat = 1.5

mult = 1.6 ; initial radius multiplication factor

n0 = 1.0 - (1.0 - poros) / mult^3

r0 = (3.0*tot_vol*(1.0 - n0)/(4.0*pi*num))^(1.0/3.0)

rlo = 2.0 * r0 / (1.0 + rat)

rhi = rat * rlo

command

gen id 1 15000 rad rlo rhi x 0 d_cz y nrad_cz rad_cz z 0 height &

filter ff_cylinder

prop density 820 ks=s_stiff kn=n_stiff

end_command set gen_error off

get_poros

_mult = ((1.0 - poros) / (1.0 - pmeas))^(1.0/3.0)

command

initial radius mul _mult

wall id=1 ty cy end1 .8 0 0 end2 .8 0 1 rad .8 .8 kn=1e8 edgecheck on

wall id=2 face (-1.,.80,1) (1.60,.8,1) (1.60,-.8,1) (-1,-.80,1) kn=1e8

```
wall id=3 face (-.1,-.8,0) (.774,-.8,0) (.774,.8,0) (-.1,.8,0) kn=1e8

wall id=4 face (-.1,-.02,0) (-.1,-.8,0) (1.6,-.8,0) (1.6,-.02,0) kn=1e8

wall id=5 face (.826,-.8,0) (1.6,-.8,0) (1.6,.8,0) (.826,.8,0) kn=1e8

wall id=6 face (1.6,.02,0) (1.6,.8,0) (-.1,.8,0) (-.1,.02,0) kn=1e8

wall id=7 face (.6,-.1,0) (1,-.1,0) (1,.1,0) (.6,.1,0) kn=1e8

pause

    cycle 2000

    prop fric 0.3

    wall prop friction .20

set grav 0 0 -9.81

    cycle 1000

end_command

end

def get_poros

    sum = 0.0

    bp = ball_head

    loop while bp # null
```

```
sum = sum + (4.0/3.0) * pi * b_rad(bp)^3

bp = b_next(bp)

end_loop

pmeas = 1.0 - sum / tot_vol

end

set gen_error off

expand

get_poros

print pmeas

pause

hist ball xp .8 .1 .5 id=4

hist ball yp .8 .1 .5 id=5

hist ball zp .8 .1 .5 id=6

hist ball zvel .8 .1 .5 id=7

hist wall xforce id =1

hist wall zforce id=6

set display history 1
```

hist write 1 Table 1

hist write 2 Table 2

hist write 6 Table 3

hist write 4 Table 4

hist write 5 Table 5

hist write 7 Table 6

Appendix-C

CODES FOR NUMERICAL TRIAXIAL TESTS (PARTIAL)

```
SET random ; reset random-number generator

; -----

set gen_error off

def make_walls ; create walls: a cylinder and two plates

  extend = 0.1

  rad_cy = 0.5*width

  w_stiff= 1e8

  _z0 = -extend

  _z1 = height*(1.0 + extend)

  command

    wall type cylinder id=1 kn=w_stiff end1 0.0 0.0 _z0 end2 0.0 0.0 _z1 &

    rad rad_cy rad_cy

  end_command
```

```
_x0 = -rad_cy*(1.0 + extend)
```

```
_y0 = -rad_cy*(1.0 + extend)
```

```
_z0 = 0.0
```

```
_x1 = rad_cy*(1.0 + extend)
```

```
_y1 = -rad_cy*(1.0 + extend)
```

```
_z1 = 0.0
```

```
_x2 = rad_cy*(1.0 + extend)
```

```
_y2 = rad_cy*(1.0 + extend)
```

```
_z2 = 0.0
```

```
_x3 = -rad_cy*(1.0 + extend)
```

```
_y3 = rad_cy*(1.0 + extend)
```

```
_z3 = 0.0
```

```
command
```

```
  wall id=5 kn=w_stiff face (_x0,_y0,_z0) (_x1,_y1,_z1) (_x2,_y2,_z2) &
```

```
  (_x3,_y3,_z3)
```

```
end_command
```

```
_x0 = -rad_cy*(1.0 + extend)
```

```
_y0 = -rad_cy*(1.0 + extend)
```

```
_z0 = height
```

```
_x1 = -rad_cy*(1.0 + extend)
```

```
_y1 = rad_cy*(1.0 + extend)
```

```
_z1 = height
```

```
_x2 = rad_cy*(1.0 + extend)
```

```
_y2 = rad_cy*(1.0 + extend)
```

```
_z2 = height
```

```
_x3 = rad_cy*(1.0 + extend)
```

```
_y3 = -rad_cy*(1.0 + extend)
```

```
_z3 = height
```

```
command
```

```
wall id=6 kn=w_stiff face (_x0,_y0,_z0) (_x1,_y1,_z1) (_x2,_y2,_z2) &
```

```
(_x3,_y3,_z3)
```

```
end_command
```

```

end

;-----

def assemble ; assemble sample

s_stiff=0.0 ; initial stiffnesses

n_stiff=1e8

tot_vol = height * pi * rad_cy^2.0

rbar = 0.5 * (rlo + rhi)

num = int((1.0 - poros) * tot_vol / (4.0 / 3.0 * pi * rbar^3))

mult = 1.6 ; initial radius multiplication factor

rlo_0 = rlo / mult

rhi_0 = rhi / mult

command

gen id=1,num rad=rlo_0,rhi_0 x=-1.0,1.0 y=-1.0,1.0 z=0.0,height &

filter ff_cylinder

prop dens=820 ks=s_stiff kn=n_stiff

end_command

```

```
ii = out(string(num)+' particles were created')

sum = 0.0 ; get actual porosity

bp = ball_head

loop while bp # null

    sum = sum + 4.0 / 3.0 * pi * b_rad(bp)^3

    bp = b_next(bp)

end_loop

pmeas = 1.0 - sum / tot_vol

mult = ((1.0 - poros) / (1.0 - pmeas))^(1.0/3.0)

command

    ini rad mul mult

    cycle 1000

    prop ks=1e8 fric 0.20

    cycle 250

end_command

end

; -----
```

```
def cws ; change lateral wall stiffnesses

command

    wall type cylinder id 1 kn=w_stiff

end_command

end

; -----

def ff_cylinder

    ff_cylinder = 0

    _brad = fc_arg(0)

    _bx = fc_arg(1)

    _by = fc_arg(2)

    _bz = fc_arg(3)

    _rad = sqrt(_bx^2 + _by^2)

    if _rad + _brad > rad_cy then

        ff_cylinder = 1

    end_if

end
```

```
; -----  
  
macro zero 'ini xvel 0 yvel 0 zvel 0 xspin 0 yspin 0 zspin 0'  
  
SET height=4 width=2 rlo=0.035 rhi=0.07 poros=0.40  
  
make_walls  
  
assemble  
  
SET w_stiff= 1e8 ; make lateral wall stiffness=1/10 of ball stiffness  
  
cws  
  
cyc 500  
  
zero  
  
plot create assembly  
  
plot set back white  
  
plot set cap size 25  
  
plot set mag 1.25  
  
plot set rot 30 0 40  
  
plot add ball orange  
  
-----  
  
def get_ss ; determine average stress and strain at walls
```

```

new_rad = w_radend1(wadd1)

rdif = new_rad - rad_cy

zdif = w_z(wadd6) - w_z(wadd5)

new_height = height + zdif

wsrr = -w_radfob(wadd1) / (new_height * 2.0 * pi * new_rad)

wszz = 0.5*(w_zfob(wadd5) - w_zfob(wadd6)) / (pi * new_rad^2.0)

werr = 2.0 * rdif / (rad_cy + new_rad)

wezz = 2.0 * zdif / (height + new_height)

wevol = wezz + 2.0 * werr

end

; -----

def get_gain

alpha = 0.5

count = 0

avg_stiff = 0

cp = contact_head ; find avg. number of contacts on lateral walls

loop while cp # null

```



```
if c_gobj2(cp) = wadd1

    count = count + 1

    avg_stiff = avg_stiff + c_kn(cp)

end_if

cp = c_next(cp)

end_loop

avg_stiff = avg_stiff / count

gr = alpha * height * pi * rad_cy * 2.0 / (avg_stiff * count * tdel)

count = 0

avg_stiff = 0

cp = contact_head    ; find avg. number of contacts on top/bottom walls

loop while cp # null

    if c_gobj2(cp) = wadd5

        count = count + 1

        avg_stiff = avg_stiff + c_kn(cp)

    end_if

    if c_gobj2(cp) = wadd6
```

```
count = count + 1

avg_stiff = avg_stiff + c_kn(cp)

end_if

cp = c_next(cp)

end_loop

ncount = count / 2.0

avg_stiff = avg_stiff / count

gz = alpha * pi * rad_cy^2.0 / (avg_stiff * ncount * tdel)

end

; -----

def servo

while_stepping

get_ss

udr = gr * (wsrr - srrreq)

w_radvel(wadd1) = -udr

if z_servo = 1 ; switch stress servo on or off

udz = gz * (wszz - szzreq)
```

```
w_zvel(wadd5) = udz

w_zvel(wadd6) = -udz

end_if

end

; -----

def iterate

loop while 1 # 0

get_gain

if abs((wsrr - srrreq)/srrreq) < sig_tol then

if abs((wszz - szzreq)/szzreq) < sig_tol then

exit

end_if

end_if

command

cycle 100

end_command

end_loop
```

end

;-----

def wall_addr

wadd1 = find_wall(1)

wadd5 = find_wall(5)

wadd6 = find_wall(6)

end

wall_addr

zero

SET srrreq=-1e6 szzreq=-1e6 sig_tol=0.005 z_servo=1

iterate ; get all stresses to requested state

sav tt_str.SAV

return

def set_ini ; set initial strains

wezz_0 = wezz

wevol_0 = wevol

```
end

def conf

  devi = wszz - wsrr      ; deviatoric stress

  deax = wezz - wezz_0    ; axial strain

  devol = wevol - wevol_0 ; volumetric strain

  conf = wsrr             ; confining stress

end

; -----

def accel_platens

  _niter = _nsteps / _nchunks

  loop _chnk (1,_nchunks)

    if _close = 1 then

      _vel = _chnk*( _vfinal/_nchunks)

    else

      _vel = -_chnk*( _vfinal/_nchunks)

    end_if

  _mvel = -_vel
```

```
command

wall id 5 zvel= _vel

wall id 6 zvel= _mvel

cycle _niter

end_command

end_loop

end

set_ini

history id=1 conf

history id=2 devi

history id=3 deax

history id=4 devol

history id=11 werr

history id=12 wezz

SET hist_rep=50

SET z_servo=0

zero
```

```
sav tt_init.SAV ; ready for modulus and failure tests
```

```
return
```

```
res tt_init.sav
```

```
prop fric 10.0 s_bond=1e15 n_bond=1e15
```

```
set _vfinal= 0.1 _nsteps= 2000 _nchunks= 80
```

```
set _close = 1 ; load
```

```
accel_platens
```

```
cyc 2000
```

```
zero
```

```
set _close = 0 ; unload
```

```
accel_platens
```

```
cyc 2000
```

```
save triax_5.SAV
```

```
return
```

```
res tt_init.sav
```

```
prop fric=0.5
```

```
set _vfinal= 0.1 _nsteps= 2000 _nchunks= 80
```

```
set _close= 1 ; load

accel_platens

cyc 40000

zero

set _close= 0 ; unload

accel_platens

cyc 4000

zero

set _close= 1 ; load

accel_platens

cyc 20000

save triax_6.SAV

return

res tt_init.sav

prop fric=0.3 n_bond=1e5 s_bond=0.5e8

set _vfinal= 0.1 _nsteps= 2000 _nchunks= 80

set _close= 1 ; load
```


accel_platens

cyc 20000

zero

set _close= 0 ; unload

accel_platens

cyc 5000

zero

set _close= 1 ; load

accel_platens

cyc 40000

save triax_7.SAV

return

res tt_init.sav

prop fric=0.5 n_bond=1e5 s_bond=1e5

set _vfinal= 0.1 _nsteps= 2000 _nchunks= 80

set _close= 1 ; load

accel_platens

cyc 30000

zero

set _close= 0 ; unload

accel_platens

cyc 12000

zero

set _close= 1 ; load

accel_platens

cyc 37000

save triax_8.SAV

return